TIME-DEPENDENT GROWTH OF CERAMIC SUPPORTED NaA MEMBRANES – A MORPHOLOGICAL AND PERMEATION BASED STUDY

JACO ZAH
(B.Pharm., M.Sc.)

Thesis submitted in fulfilment of the requirements for the degree
Philosophiae Doctor
in Pharmaceutical Chemistry
at the School of Pharmacy of the North-West University

Promoter: Prof. H.M. Krieg
Co-promoter: Prof. J.C. Breytenbach

Potchefstroom
2006

Dedicated to my parents

LIST OF PUBLICATIONS

The scientific content in this thesis is based on the following papers:

1. J. Zah, H.M. Krieg, J.C. Breytenbach, Layer development and growth history of polycrystalline zeolite A membranes synthesised from a clear solution, Micropor. Mesopor. Mater. 93 (2006) 141.

2. J. Zah, H.M. Krieg, J.C. Breytenbach, Pervaporation and related properties of time-dependent growth layers of zeolite NaA on structured ceramic supports, J. Membr. Sci., *accepted for publication – article in press.*

3. J. Zah, H.M. Krieg, J.C. Breytenbach, Single gas permeation through thin layered zeolite NaA membranes: improved permeance through an unconventional, semicrystalline layer, J. Membr. Sci., *submitted.*

4. J. Zah, H.M. Krieg, J.C. Breytenbach, Enhanced selectivity of a zeolite A membrane by pretreating the alumina support with UV radiation, J. Membr. Sci., *submitted.*

ABSTRACT

Based on its ideal aperture size (4.1 Å) and hydrophilic framework, the NaA membrane possesses significant potential in the separation of many industrially important gaseous and liquid mixtures. In the local South African context, the foreseeable production of affordable, high-purity ethanol in the alternative fuel market exemplifies one such a possibility. However, there are still certain aspects to the composite NaA membrane that are not clearly understood. These include the time-dependent morphological and compositional development of the polycrystalline zeolite layer during its direct synthesis from a clear solution, and the subsequent relation between the intrinsically different layers thus obtained, and their (selective) permeation properties. In addition, the surface-chemical and structural influence of the support on membrane integrity and permeation resistance, respectively, requires further elucidation for the optimisation of selectivity and flux parameters. This project envisaged addressing these needs. Using a standard clear solution synthesis regime (Na_2O:Al_2O_3:SiO_2:H_2O = 49:1:5:980; 85 °C) and high-integrity α-Al_2O_3 supports, the aim was to improve the fundamental understanding of the composite NaA membrane as a whole, including structural and permeation related aspects, under the auspices of optimising and broadening the application potential of supported zeolite membranes in general.

Layer development. Membrane growth proceeded along two distinct morphological pathways over the duration of synthesis (1-4 h): an initial layer of semicrystalline, hemisphere-shaped grains (after 2 h) transforming into a fully crystalline layer with cubic morphology at the end of the growth process (4 h). A two-step growth rate trend was observed and could be correlated to the respective growth phases within the two underlying morphology types. The development of the hemisphere-shaped grains was associated with a period of accelerated growth during the first 2.5 h of synthesis (3.3×10^{-10} m.s^{-1}), followed by a period of slower growth for the formation of the cubic morphology (1.9×10^{-10} m.s^{-1}). Localised changes in supersaturation, combined with the possible effects of grain crowding, were offered as feasible explanations for the observed morphology and growth rate tendencies.

Single gas permeation. Single gas permeation of H_2, N_2 and SF_6 were measured at two temperatures (23 and 107 °C), specifically related to the semicrystalline (70 %; 2 h synthesis) and fully crystalline layers (100 %; 4 h synthesis). By comparing the permselectivity values with the respective Knudsen factors, it was shown that diffusion through the semicrystalline layer, at lower temperature, was predominantly based on molecular sieving (PS H_2/SF_6 = 63.8), which was much higher than the traditional membrane under the same conditions (PS H_2/SF_6 = 11.4). However, the opposite was observed at higher temperature – the H_2/SF_6 permselectivity of the crystalline layer (5.7) was somewhat higher than the first (5.2). Based on theoretical considerations, it was concluded that the crystal/amorphous interface in the semicrystalline membrane constituted a denser closure of the boundary interface, which could be attributed to a lower charge barrier presented by the amorphous phase (Si/Al > 1), but this integrity was lost at higher temperature due to thermal instability of the amorphous component. The results therefore suggested that interventions in the charge loading in the boundary phase, during synthesis, could provide a means for stricter control over the intercrystalline porosity in NaA membranes in general.

Pervaporation. Based on the outcomes of both the layer development and gas permeation studies, a comprehensive series of compositionally different NaA layers (t_c 2.0, 2.5, 3.0, 3.5 and 4.0 h) were tested in the pervaporative dehydration of water. Selected layers were also

synthesised on two structurally different supports, to investigate the role of the support microstructure and its resistance to mass flow. The separation performance of the layers on the first support (Φ_{pore} = 163 nm) were compared using a 95 wt.% EtOH feed at 45 °C. The selectivity (α_{WE}) depended strongly on the relative degree of crystallinity and the amount of amorphous material occluded in the intercrystalline pore regions. The highest selectivities were obtained with either low crystallinity combined with significant amorphous content (α_{WE} = 9 000 for the 2.0 h layer), or high crystallinity combined with a small amount of amorphous content (α_{WE} = 12 500 for the 3.5 h layer). This general trend was also observed for the respective layers synthesised on the second support (Φ_{pore} = 101 nm), but the α_{WE} values were much lower, ranging between 340 (for the 2.0 h layer) and 3 000 (for the 3.5 h layer). The difference was attributed to the increased dissolution of the second support, retarding the intergrowth of the zeolite layers. Despite the selectivity differences, the fluxes through each series of membranes on a specific support remained constant, showing that the support resistance to permeation was significantly high for both support types. The relative contributions to the total transmembrane resistance were calculated at ~60 % and ~70 % for the first and second support types respectively. The fugacity values at the zeolite/support interface of a given membrane (3.5 h synthesis on the second support) showed that the support resistance can limit the driving force achievable across the zeolite layer, even if the driving force across the composite membrane is increased.

Support surface chemistry. A supplementary study examined the influence of ultraviolet (UV) radiation on the α-Al_2O_3 support surface prior to synthesis, specifically in terms of the resultant effects on membrane integrity. Using pervaporation under similar conditions (95 wt.% EtOH; 45 °C) the selectivity values indicated a significant improvement in pervaporation performance of a given NaA layer (t_c 3.5 h, second support) after pre-exposing the support to UV radiation (α_{WE} = 25 500 for the pretreated membrane versus α_{WE} = 3 000 for the control). A simple hypothesis for the selectivity enhancement was described in terms of the UV-induced increase in the number of OH-groups on the α-Al_2O_3 surface, which improves the wettability of the support, particularly in the macroscopic defect sites. As a result, the initially formed precursor gel is spread uniformly over the surface, leading to a high integrity zeolite layer with reduced intercrystalline porosity. In essence, this investigation showed that UV radiation provides a simple, yet highly effective tool for optimising the physicochemical interaction between zeolite and support during synthesis, thereby increasing the selectivity performance of the ensuing NaA layer.

The aim of the project was met successfully by gaining new insights into the workings of the composite NaA membrane as a whole, including different structural and permeation related aspects. Future advances for the NaA membrane should be possible by finding condition-specific applications for the intrinsically different, time-dependent layers developed here, due to their high selectivity and permeance attributes under given conditions, or by applying the fundamental principles gained from their synthesis and permeation behaviour, to better suit existing applications. The generated data should also contribute to the further optimisation of supported zeolite membranes in general, both in terms of selectivity and permeance considerations.

UITTREKSEL

Die NaA-membraan hou vanweë die geskikte poriegrootte en hidrofiliese kristalraamwerk daarvan merkwaardige potensiaal in vir die skeiding van verskeie ekonomies belangrike gas- en vloeistofmengsels. Een voorsienbare toepassing in die plaaslike Suid-Afrikaanse konteks is die produksie van suiwer etanol vir die alternatiewe brandstofmark. Verskeie aspekte van die saamgestelde NaA-membraan word egter nog nie ten volle verstaan nie. Die belangrikste hiervan is die tydsafhanklike ontwikkeling van die morfologie en samestelling van die polikristallyne seolietlaag tydens die sintese daarvan vanuit 'n helder oplossing, asook die verhouding tussen die intrinsiek verskillende lae so verkry en hul (selektiewe) permeasie-eienskappe. Die invloed van die chemie en struktuur van die ondersteuner se oppervlak op die membraan se integriteit en permeasie-weerstand, onderskeidelik, noodsaak ook verdere studie, veral met die oog op die optimisering van die selektiwiteit en fluks. In die huidige projek is gepoog om hierdie leemtes aan te spreek. 'n Eksperimentele aanslag, gebaseer op die gebruik van 'n sinteseregime vanuit 'n helder oplossing (Na_2O:Al_2O_3:SiO_2:H_2O = 49:1:5:980; 85 °C) en hoë integriteit α-Al_2O_3-ondersteuners, is uitgevoer om die saamgestelde NaA-membraan in geheel, insluitend die strukturele en permeasie-aspekte, beter te verstaan. Sodoende kan 'n bydrae tot die toepassingsontwikkeling van ondersteunde seolietmembrane oor die algemeen gelewer word.

Laagontwikkeling. Die chronologiese groei van die seolietlaag (1-4 h) word gekenmerk deur twee verskillende morfologiese weë – 'n aanvanklike laag bestaande uit semikristallyne, halfmaanvormige kristalliete (na 2 h), gevolg deur 'n kristallyne laag bestaande uit kubusvormige kristalle aan die einde van die sintese (na 4 h). 'n Twee-stap groeitendens is waargeneem en kon met die onderskeie groeifases binne die twee morfologie tipes in verband gebring word. Die ontwikkeling van die halfmaanvormige kristalliete het tydens die versnelde groei gedurende die eerste 2.5 h van die sintese (3.3×10^{-10} m.s^{-1}) geskied, gevolg deur 'n periode van stadiger groei om die kubiese laag te vorm (1.9×10^{-10} m.s^{-1}). Gelokaliseerde veranderinge in die graad van oorversadiging binne die ontwikkelende membraan, asook die moontlike effekte van kristalophoping, word as sinvolle redes vir die waargenome tendense in morfologie en groeitempo aangevoer.

Enkelgaspermeasie. Die permeasie van H_2, N_2 en SF_6 as enkele gasse deur sowel die semikristallyne (70 %; 2 h-sintese) en kristallyne (100 %; 4 h-sintese) membrane is by twee verskillende temperature, 23 en 107 °C, gemeet. Deur die onderskeie ideale en Knudsen-selektiwiteite te vergelyk, is aangetoon dat diffusie deur die semikristallyne laag, by laer temperatuur, hoofsaaklik op molekulêre sifting berus: 'n *PS*-waarde van 63.8 vir H_2/SF_6, wat baie hoër is as dié van die kristallyne laag onder dieselfde kondisies (*PS* H_2/SF_6 = 11.4). By hoër temperatuur was die situasie egter omgekeer - die ideale H_2/SF_6-selektiwiteit van die kristallyne laag (5.7) was effens hoër as dié van die semikristallyne laag (5.2). Vanuit teoretiese oorwegings is afgelei dat die kristal/amorfe intervlak in die semikristallyne membraan vanweë 'n swakker ladingsversperring deur die amorfe komponent (Si/Al > 1) 'n digter grenssluiting vorm. Die amorfe komponent is egter termolabiel en hierdie integriteit gaan verlore by hoër temperatuur. Die resultate toon dus dat ingrepe in die ladingsversperrings binne die grensvlak, tydens membraansintese, moontlik tot beter beheer oor die interkristallyne porositeit van NaA-membrane oor die algemeen kan lei.

Pervaporasie. Op grond van die uitkomste wat in die studies van laagontwikkeling en gaspermeasie bereik is, is 'n volledige reeks van membraanlae, met verskillende intrinsieke

samestellings, gesintetiseer deur opeenvolgende sintesetye te gebruik (t_c 2.0, 2.5, 3.0, 3.5 en 4.0 h). Hierdie membrane is vergelyk deur hul pervaporasiegedrag in die ontwatering van 'n water/etanol-mengsel te toets. Sekere uitgesoekte seolietlae is ook op twee struktureel verskillende ondersteuners gesintetiseer om die invloed van die ondersteuner op die permeasie-weerstand te ondersoek. Die skeidingsgedrag van die lae op die eerste ondersteuner (Φ_{porie} = 163 nm) is onderling vergelyk deur 'n voermengsel van 95 % (m/m) EtOH by 45 °C te gebruik. Die waterselektiwiteit (α_{WE}) het goed met die relatiewe kristalliniteit en die hoeveelheid amorfe materiaal binne die interkristalgrense gekorreleer. Die hoogste selektiwiteit is deur óf 'n kombinasie van lae kristalliniteit met hoë amorfe inhoud (α_{WE} = 9 000 vir die 2.0 h laag) óf 'n kombinasie van hoë kristalliniteit met lae amorfe inhoud (α_{WE} = 12 500 vir die 3.5 h laag) verkry. Dieselfde algemene tendens is ook vir die seolietlae op die tweede ondersteuner (Φ_{porie} = 101 nm) waargeneem, maar die α_{WE}-waardes van laasgenoemde was heelwat laer – dit het tussen 340 (vir die 2.0 h laag) en 3 000 (vir die 3.5 h laag) gewissel. Die verskil hier word aan die hoër dissolusie van die tweede ondersteuner toegeskryf, wat die kontinuïteit van die seolietlae beïnvloed. Ten spyte van genoemde verskille in selektiwiteit het die fluks deur die membraanreekse op 'n spesifieke ondersteuner konstant gebly wat toon dat albei ondersteuners 'n betekenisvolle weerstand tot die totale permeasie bied. Die relatiewe bydrae tot die totale membraanweerstand is op ~60 % en ~70 % vir die eerste en tweede ondersteuners onderskeidelik bereken. Verdere berekening van die parsiële drukke by die seoliet/ondersteuner-intervlak (vir die 3.5 h-laag op die tweede ondersteuner) toon dat die ondersteuner se weerstand die dryfkrag oor die seolietlaag kan beperk, selfs al word 'n sterker dryfkrag oor die saamgestelde membraan aangelê.

Chemie van die oppervlak van die ondersteuner. In 'n aanvullende studie is die invloed van ultraviolet (UV)-straling op die α-Al_2O_3 ondersteuner se oppervlak, voor die sintesestap, ondersoek. Daar is hoofsaaklik gekyk na die moontlike effekte wat hierdie behandeling op die integriteit van 'n daaropvolgende gesintetiseerde membraan het (t_c 3.5 h, tweede ondersteuner). Deur soortgelyke pervaporasie-eksperimente te doen [95 % (m/m) EtOH by 45 °C], is gevind dat vooraf blootstelling aan UV-straling die selektiwiteit van pervaporasie merkwaardig verhoog - α_{WE} = 25 500 vir die voorafbehandelde membraan teenoor α_{WE} = 3 000 vir die onbehandelde membraan. 'n Eenvoudige hipotese is gestel vir die verklaring van die verhoogde selektiwiteit, naamlik dat die UV-straling die aantal OH-groepe op die ondersteuner se oppervlak verhoog. Dit lei tot die beter benatbaarheid van die ondersteuner deur die sintese-oplossing, veral in die makroskopiese defekte, sodat die aanvanklike gel-presipitaat eweredig oor die ondersteuner se oppervak vorm. Gevolglik word minder interkristallyne porieë gevorm en ontwikkel 'n membraan van hoë gehalte. Hierdie spesifieke ondersoek het getoon dat UV-straling 'n eenvoudige, dog hoogs doeltreffende manier bied om die fisies-chemiese interaksie tussen seoliet en ondersteuner tydens sintese te verbeter, om sodoende die selektiwiteit van die uiteindelike membraan te verhoog.

Die doel van die projek is dus bereik deur die fundamentele werking van die saamgestelde NaA-membraan toe te lig, met inbegrip van die tersaaklike aspekte van struktuur en permeasie. Verdere ontwikkeling van die NaA-membraan behoort moontlik te wees deur kondisie-spesifieke toepassingsmoontlikhede te vind vir die verskillende tydsafhanklike lae, aangesien hul ideale permeasie-eienskappe kondisie-gebonde is. Aanvullend hiertoe, behoort die nuwe insigte wat na vore gekom het ook sinvol gebruik te word om reeds bestaande membrane en hul toepassings in die algemeen te optimiseer.

TABLE OF CONTENTS

CHAPTER 1

INTRODUCTION

SUMMARY

Zeolite membranes show significant potential in the separation of many industrially important gaseous and liquid mixtures. In view of a global impetus in the search for alternative fuels, the NaA membrane is particularly suited for the production of affordable, high-purity ethanol, due to its ideal aperture size and hydrophilic nature. Unfortunately, these exact properties seem to hamper the successful use of the NaA membrane in dry gas and high temperature applications.

This chapter provides a basic overview of the economic importance of the NaA membrane and provides the motivation for further research into its synthesis and permeation related behaviour. A brief layout is given on the different subjects investigated in this thesis, including the morphological development of the membrane during synthesis, pervaporation and gas based separation phenomena.

1.1 BACKGROUND

1.1.1 GENERAL

Zeolite technology is a dynamically applied and rapidly expanding branch of separation science and catalysis. Due to their distinctive composition profiles, zeolites possess attractive properties for the large-scale reaction and separation of industrially important gaseous and liquid mixtures [1]. These properties include uniquely sized crystal porosities that allow for size and shape-*selective interaction, selective adsorption and diffusion* based behaviour, catalytic activity or neutrality and environmental stability. With specific relevance to the petrochemical industry, zeolites are indispensable in producing consumer goods and bulk chemicals such as gasoline, formaldehyde, ethanol and acetone. It is speculated that in certain first-world countries such as the Netherlands, not a single molecule of petroleum gas ends up in an engine ignition without having been exposed to a zeolite during some stage of its processing history. Another fitting example is the production of *p*-xylene from the reaction of benzene and methanol in zeolite HZSM-5 [2]. Affordable *p*-xylene is used for obtaining the polyethylenetelephthalate (PET) polymer, commonly seen as the plastic bottles from which we drink our soft drinks every day!

Currently however, commercial zeolites are mainly used in bulk mineral form, like granules, beads, pellets and extrudates, where the separation of gases for example, relies on the energy-demanding succession of temperature or pressure driven adsorption-desorption cycles [3]. To address the many practical and cost-related problems encountered in industry, research impetus is now shifting towards the development of supported zeolite membranes. In a membrane configuration, the specific catalytic, adsorption and diffusion related properties of the zeolite are retained, while the separation can be effected on a continuous, steady-state basis [4,5].

Due to a lack of mechanical stability of self-supported zeolite membranes, the most effective way of producing a high integrity membrane, is to synthesise a continuous layer of zeolite crystals on the surface of a mesoporous support. The use of ceramic carriers such as α-Al_2O_3, TiO_2 and ZrO_2 is preferred [6]. The combined properties of these inorganic composite membranes make them particularly attractive for separation under harsh conditions, compared to the traditionally employed polymeric membranes (Table 1.1).

Table 1.1: General advantages and disadvantages of inorganic (zeolite) membranes with respect to existing polymeric membranes [6]

Advantages	Disadvantages
Long-term stability at high temperatures	High capital cost
Resistance to harsh chemical environments	Brittleness
Resistance to high pressure drops	Low membrane surface area per module volume
Inertness to microbial degradation	Difficulty in achieving repeatable, high selectivities in large scale
Easy recovery after fouling	Generally low permeabilities
Easy catalytic activation	Difficult membrane-to-module sealing at high temperatures

It stands to reason that the capital cost for the large-scale application of zeolite membranes remains a decisive factor in implementing them commercially. Efforts are however ongoing to resolve these problems, since the long-term production benefits of such processes clearly outweigh the current shortcomings. A tentative solution to the need for efficacy, combined with affordability, might be not to replace the existing industrial structures for separation, such as adsorption and distillation columns, but to supplement them with membrane-based processes.

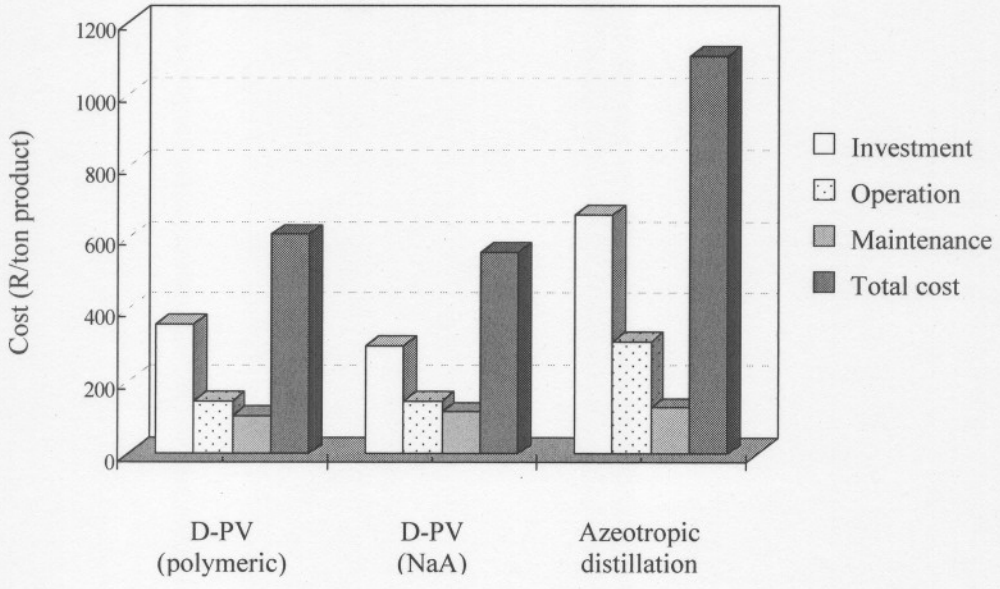

Figure 1.1: Projected cost analysis of azeotropic distillation, compared to hybrid systems where distillation was combined with polymeric [D-PV(polymeric)] and NaA zeolitic [D-PV(NaA)] pervaporation. Adapted from Van Hoof et al. [7].

A careful analysis on the viability of a distillation-pervaporation hybrid process for the azeotropic dehydration of *i*-propanol, and the investment costs associated with it, was recently reported by Van Hoof et al. [7] (Fig. 1.1). It involved a comparison of the traditional azeotropic distillation process with two hybrid systems – distillation combined with polymeric pervaporation (PERVAP® 2510, Sulzer Chemtech), and distillation combined with zeolitic pervaporation (ceramic based NaA, Mitsui & Co.), working at temperatures below 100 °C. From Fig. 1.1 it is evident that the hybrid system involving zeolitic pervaporation is the most attractive economic viability, with a theoretical saving of up to 49 % on total costs. In addition, this process projected a saving in energy costs of 48 %. Add the additional benefits previously mentioned, combine it with an environmentally friendly technology, and it becomes clear why the ceramic based NaA membranes were the first to come of age in the commercial pervaporation industry [8].

1.1.2 ZEOLITE NAA (LTA) MEMBRANES

The LTA crystal framework consists of alternating SiO_4 and AlO_4 tetrahedra in equal proportions (Si/Al = 1), leading to a negatively charged lattice structure. The charge imbalance is corrected by the intrinsic incorporation of cations during synthesis, affording the zeolite with strong hydrophilic properties. Since these counter-ions are mobile, zeolite A is highly susceptible to ion-exchange. The different ionic isoforms also exhibit different accessible aperture sizes to the three-dimensional pore network of the zeolite, changing from 3.2 Å in the potassium form (KA), to approximately 4.1 Å in the pure sodium form (NaA). The partially calcium-exchanged form (CaNaA) has the largest aperture of 4.6 Å. Understandably, this hydrophilic zeolite (particularly NaA) is ideally suited for the dehydration of water/organic mixtures and the drying of industrial gas streams. The micropore aperture is smaller than most organic molecules, but larger than water. The ionic Na^+-sites act as water-selective sorption and transport sites [9], increasing the relative diffusivity of water [10]. Also, NaA membranes prepared thus far contain non-zeolitic (intercrystalline) pore regions with hydrophilic silanol groups at the terminal crystal edges [11-13]. The excessively high separation factors achieved in particularly water/ethanol separation is therefore ascribed to the strong preferential adsorption of water in the zeolitic (intracrystalline) pores, as well as the rejection of ethanol molecules from the non-zeolitic pores by means of capillary water condensation.

1.2 MOTIVATION

Despite its commercial stature, there are still many aspects to the ceramic based NaA membrane that are poorly understood. These include the mechanisms of layer formation on the ceramic support surface during synthesis and the consequent influence of membrane morphology and composition on separation performance. A common denominator seems to be the uncontrollable nature (size) of the intercrystalline boundary phase, which appears to be an intrinsic property of the currently used membranes, considering their polycrystalline nature. Although the existence of these boundary "defects" is negligible in water-based separation at low temperature, it hampers the successful use of the membranes in dry gas and high temperature applications. In addition, the physical and chemical interaction between zeolite and support during synthesis, as well as the support's structural resistance to mass transfer of different permeants, seem to be rather underplayed in most studies dealing with zeolite based separation. This study envisages addressing some of these needs.

1.2.1 LAYER DEVELOPMENT (MORPHOLOGY)

The understanding of NaA layer growth remains limited to the generalised formation mechanisms for single crystals. Little is known about the nucleation step in the proximity of the support or about the crystallisation and intergrowth process during the initial stages of layer development. A more detailed understanding of these phenomena would improve the structural and morphological control of the synthesis process and could help researchers to optimise their efforts in achieving the desired membrane attributes.

1.2.2 GAS PHASE PERMEATION

One of the most important chemical processes in South Africa is related to the production of petrol from coal, by means of the Fisher-Tropsch synthesis reaction [$nCO + (2n+1)H_2 \leftrightarrow C_nH_{2n+2} + nH_2O$]. Due to its high affinity for water, the NaA membrane would be ideal for the continuous, *in situ* removal of water from reactor units, thereby increasing product yields and preventing catalyst deactivation [14]. Unfortunately, typical reaction temperatures are high (~350 °C) and the permeation of reactant gases (CO and H_2) through the intercrystalline pores can no longer be inhibited by the capillary condensation of water.

It has further been shown that the relative contribution of intercrystalline diffusion increases as the aluminium content of the zeolite layer increases [15,16]. It is therefore safe to say that certain thermodynamic limitations exist for the degree of intergrowth (continuity) in polycrystalline NaA layers. Clearly, new and alternative approaches to membrane preparation are needed to overcome the thermodynamic barriers, or at least to optimise the continuity of NaA layers within these natural boundaries of restricted intergrowth. An improved understanding of the origin of the intercrystalline boundary phase would facilitate more stringent control over the non-zeolitic permeation and increase the viability of the high temperature application of the NaA membrane.

1.2.3 PERVAPORATION

In view of a global energy revolution, recent developments in South Africa have been geared towards the fermentative production of ethanol from a common, annual overproduction of maize. A high and affordable turnover of high-purity ethanol is essential for the success of this alternative fuel industry, not to mention the foreseeable benefits to the chemical industry, for example the pharmaceutical industry, where ethanol is used as a solvent and reaction intermediary in the synthesis of many important drug entities.

The application value of the NaA membrane in this process is again embodied in its dehydration potential, which has been illustrated in Fig. 1.1, and is backed by its proven track record in water/ethanol pervaporation [8]. However, certain shortcomings still exist in the understanding of the pervaporation process as a whole, especially the role of support resistance. Since permeation through the support takes place under low pressure (vacuum) conditions, the flow is essentially governed by Knudsen diffusion and is bound to contribute substantially to the overall membrane resistance and selectivity. Only a limited amount of reference data on this subject is available, and more research could lead to the further optimisation of membrane productivity.

1.2.4 THE SUPPORT

The membranes used in this study were synthesised exclusively on α-Al_2O_3 (corundum) supports, due to its intrinsic stability attributes. All supports were produced in-house in a cylindrical form, since the cylinder shape lends itself to higher surface-to-volume reactor design. In addition, their mechanical strength is remarkable – the bursting pressure of a standard support tube (10 mm in diameter and 1 mm wall thickness) can be as high as 80 bar [6]. An important consideration,

though, is the favourable surface chemistry of the α-Al_2O_3 surface with regard to zeolite adhesion, especially when direct synthesis procedures are used. The terminal OH-groups at the oxide surface favour the interaction of the hydrophilic synthesis mixture with the support during the early stages of zeolitic membrane development, but also act as condensation anchors for growing zeolite crystals [17], thereby increasing the overall integrity of the membrane. However, the density (number) of these OH-groups on the surface is sensitive to the treatment history of the support prior to its use in zeolite synthesis. While ample literature is available on the general surface chemistry of α-Al_2O_3, the information on optimising these properties for enhanced membrane synthesis, is scarce.

1.3 AIM AND OBJECTIVES

The purpose of this study was to conduct a coherent series of investigations into the multivariate nature of the ceramic supported NaA membrane, with the objective of improving the fundamental understanding of mainly three aspects:

- the mechanisms governing the morphological development of a continuous, polycrystalline NaA layer on the support surface during synthesis from a clear solution;
- the relation between different structural and compositional isoforms of the NaA layers, and their selective properties during both gaseous and liquid based (pervaporation) permeation;
- the surface chemical and structural influence of the α-Al_2O_3 support on membrane integrity and permeation resistance respectively.

The obtained results should provide a platform for the further, commercially-driven optimisation of selectivity and flux parameters in not only the NaA based membrane, but also composite zeolite membranes in general.

1.4 OUTLINE OF THE THESIS

The thesis is presented in article format. Each of Chapters 2-5 represents the respective subjects covered in the motivation section above; as such they were prepared in standard scientific format and are able to stand independently. Within the context of this thesis, the general layout can be

summarised briefly from an overview of the different steps necessary for manufacturing and characterising a ceramic supported zeolite NaA membrane (Fig. 1.2).

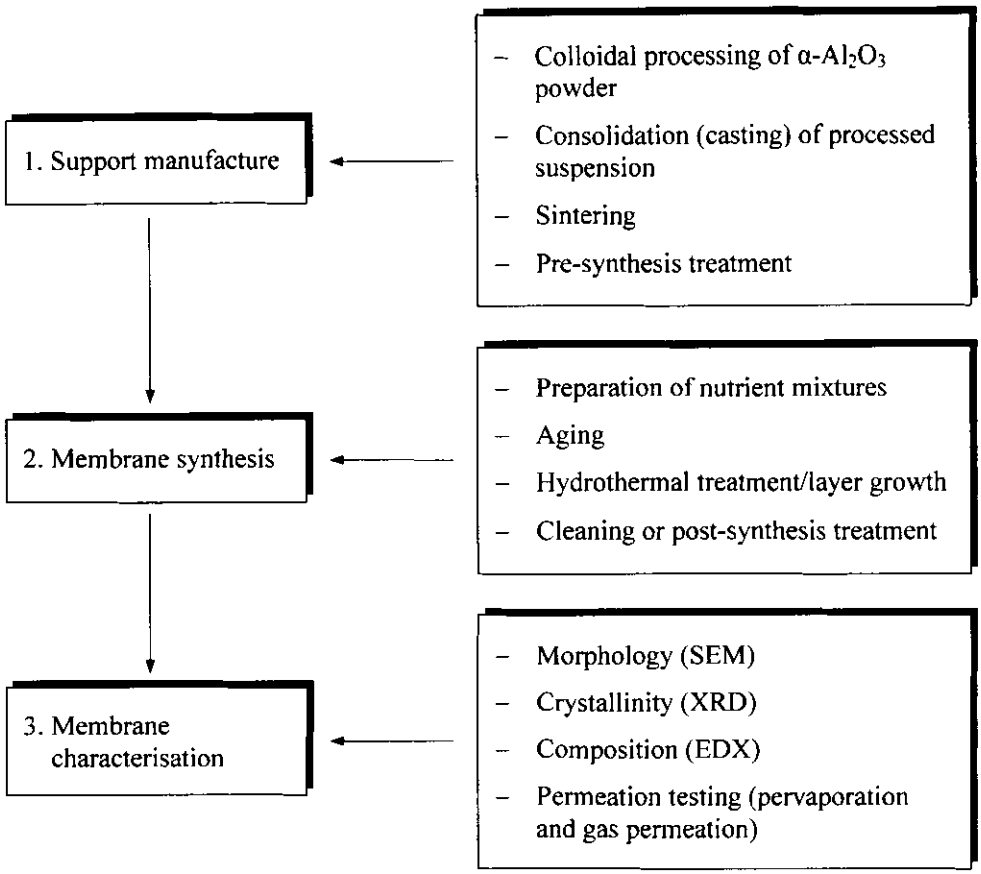

Figure 1.2: Basic process of producing a ceramic supported NaA membrane.

The main emphasis of the project was directed at steps 2 and 3. Regarding the synthesis of the NaA membranes, we applied a standard clear solution regime (Na_2O:Al_2O_3:SiO_2:H_2O = 49:1:5:980, at 85 °C) and studied the layer development chronologically (1.5-4.0 h). The layer growth was characterised by a series of morphological and compositional transitions over time and could be related to theoretical considerations on gel formation and supersaturation changes (**Chapter 2**). A fully crystalline membrane (Si/Al = 1) was formed after 4.0 h of synthesis; however, the intermediate layers showed promising potential as membranes themselves. The most predominant of these was the semicrystalline layer (70 %) obtained after only 2.0 h of synthesis.

The basic membrane capabilities of the 2.0 h layer were measured using single gas permeation at different temperatures and compared to that of the fully crystalline 4.0 h layer (**Chapter 3**). Remarkably, the semicrystalline layer exhibited superior ideal selectivities at lower temperature compared to both the experimental and literature presented crystalline membranes. The strong performance could be explained by the possible influence of the amorphous phase composition on the non-zeolitic boundary interface. This warranted further research into the properties of the other intermediate NaA layers (including synthesis times 2.5, 3.0 and 3.5 h).

Using pervaporation of a standard water/ethanol mixture, **Chapter 4** examined the relative selectivities of the other intermediate layers in comparison to the gas characterised 70 % and 100 % crystalline layers. Interesting trends were observed and could also be explained by the presence of amorphous material in the intercrystalline boundary phase.

Chapter 5 presents a supplementary study in which the surface chemistry of the α-Al_2O_3 support was modified with UV radiation prior to synthesis. A remarkable improvement was observed in the pervaporation selectivity of the ensuing membrane and was related to an improved interaction between the support and synthesis gel.

The research is concluded with a bird's-eye view on the pervaporation and dry gas performances of the different time-dependent NaA layers, relating to their structural and compositional differences, and an overview is given on the contrasting effects of the support's resistance in different modes of permeation. A general view is expressed on the complexity of the composite zeolite membrane as a whole and a few ideas are given for the future development of zeolite membranes in general (**Chapter 6**).

In both sections dealing with permeation (Chapters 3 and 4), the flow resistance of the ceramic support was investigated by calculating the specific permeant pressures at the zeolite/support interface. It was shown that a given support's resistance to flow was tolerable for gas phase separations under the applied conditions, but unacceptably high for pervaporation. Further optimisation of the permeability of the support structure is therefore necessary (step 1 in Fig.1.2). Although such optimisations were not specifically addressed in this volume of work, some preliminary work is given in **appendix A & B** to show that our efforts are ongoing to obtain a low-resistance, affordable alumina support in a single-step manufacturing process.

1.5 REFERENCES

[1] S. Sircar, A.L. Myers, Gas separation by zeolites, in S.M. Auerbach, K.A. Carrado, P.K. Dutta (Eds.), Handbook of Zeolite Science and Technology, Marcel Dekker Inc., New York, Basel, 2003, pp. 1063-1104.

[2] J.F. Haw, D.M. Marcus, Examples of organic reactions on zeolites: methanol to hydrocarbon catalysis, in S.M. Auerbach, K.A. Carrado, P.K. Dutta (Eds.), Handbook of Zeolite Science and Technology, Marcel Dekker Inc., New York, Basel, 2003, pp. 833-866.

[3] S. Nair, M. Tsapatsis, Synthesis and properties of zeolitic membranes, in S.M. Auerbach, K.A. Carrado, P.K. Dutta (Eds.), Handbook of Zeolite Science and Technology, Marcel Dekker Inc., New York, Basel, 2003, pp. 867-919.

[4] J. Caro, M. Noack, P. Kölsch, R. Schäfer, Zeolite membranes – state of their development and perspective, Micropor. Mesopor. Mater. 38 (2000) 3.

[5] A.S.T. Chiang, K. Chao, Membranes and films of zeolite and zeolite-like materials, J. Phys. Chem. Solids 62 (2001) 1899.

[6] M. Noack, J. Caro, Zeolite membranes, in F. Schüth, K.S.W. Sing, J. Weitkamp (Eds.), Handbook of Porous Solids Vol. 4, Wiley-VCH, Weinheim, 2002, pp. 2433-2507.

[7] V. van Hoof, L. van den Abeele, A. Buekenhoudt, C. Dotremont, R. Leysen, Economic comparison between azeotropic distillation and different hybrid systems combining distillation with pervaporation for the dehydration of isopropanol, Sep. Purif. Technol. 37 (2004) 33.

[8] Y. Morigami, M. Kondo, J. Abe, H. Kita, K. Okamoto, The first large-scale pervaporation plant using tubular-type module with zeolite NaA membrane, Sep. Purif. Tech. 25 (2001) 251.

[9] D. Shah, K. Kissick, A. Ghorpade, R. Hannah, D. Bhattacharyya, Pervaporation of alcohol-water and dimethylformamide-water mixtures using hydrophilic zeolite NaA membranes: mechanisms and experimental results, J. Membr. Sci. 179 (2000) 185.

[10] S. Furukawa, K. Goda, Y. Zhang, T. Nitta, Molecular simulation study on adsorption and diffusion behavior of ethanol/water molecules in NaA zeolite crystal, J. Chem. Eng. Jpn. 37 (2004) 67.

[11] M.A. Camblor, A. Corma, S. Iborra, S. Miquel, J. Primo, S. Valencia, Beta zeolite as a catalyst for the preparation of alkyl glucoside surfactants: the role of crystal size and hydrophobicity, J. Catal. 172 (1997) 76.

[12] H. Takaba, A. Koyama, S. Nakao, Dual ensemble Monte Carlo simulation of pervaporation of an ethanol/water binary mixture in silicalite membrane based on a Lennard-Jones interaction model, J. Phys. Chem. B 104 (2000) 6353.

[13] T. Sano, T. Kasuno, K. Takeda, S. Arazaki, Y. Kawakami, Sorption of water vapor on HZSM-5 type zeolites, Stud. Surf. Sci. Catal. 105 (1997) 1771.

[14] W. Zhu, L. Gora, A.W.C. van den Berg, F. Kapteijn, J.C. Jansen, J.A. Moulijn, Water vapour separation from permanent gases by a zeolite-4A membrane, J. Membr. Sci. 253 (2005) 57.

[15] M. Noack, P. Kölsch, J. Caro, M. Schneider, P. Toussaint, I. Sieber, MFI membranes of different Si/Al ratios for pervaporation and steam permeation, Micropor. Mesopor. Mater. 35-36 (2000) 253.

[16] M. Noack, P. Kölsch, V. Seefeld, P. Toussaint, G. Georgi, J. Caro, Influence of the Si/Al ratio on the permeation properties of MFI-membranes, Micropor. Mesopor. Mater. 79 (2005) 329.

[17] A.W.C. van den Berg, L. Gora, J.C. Jansen, T. Maschmeyer, Improvement of zeolite NaA nucleation sites on (001) rutile by means of UV-radiation, Micropor. Mesopor. Mater. 66 (2003) 303.

CHAPTER 2

LAYER DEVELOPMENT AND GROWTH HISTORY OF POLYCRYSTALLINE ZEOLITE A MEMBRANES SYNTHESISED FROM A CLEAR SOLUTION

ABSTRACT

A case study is presented on the specific layer growth history of an α-Al_2O_3 supported NaA zeolite membrane synthesised from a clear solution. Using a defined set of synthesis parameters, the layer development over time (1.0-4.0 h) was described in terms of morphology, growth rate and elemental composition. It was shown that membrane growth proceeds along two distinct morphological pathways over the duration of synthesis – an initial layer of semicrystalline, hemisphere-shaped grains transforming into a fully crystalline layer with cubic morphology at the end of the growth process. A two-step growth rate trend was observed and could be correlated to the respective growth phases within the two underlying morphology types. The development of the hemisphere-shaped grains was associated with a period of accelerated growth during the first 2.5 h of synthesis (3.3×10^{-10} m.s^{-1}), followed by a period of slower growth for the formation of the cubic morphology (1.9×10^{-10} m.s^{-1}). Localised changes in supersaturation, combined with the possible effects of grain crowding, were offered as feasible explanations for the observed morphology and growth rate tendencies. Following the elemental make-up of the developing membrane showed a gradual decrease in the Na/Si ratio with increasing crystallisation times, which was explained by the consumption of the amorphous content in the membrane as growth proceeds. The solid phase compositions (Na/Si ratio) could however not explain the observed morphology and growth rate changes.

Keywords: zeolite NaA, synthesis, membrane formation, morphology, growth rate

2.1 INTRODUCTION

Zeolite membrane technology has interested many scientists over the past decade. By applying the fundamental adsorptive, ion-exchange and catalytic properties [1] inherent to zeolitic materials, and merging them into a shape or size-selective membrane configuration, an abundance of industrial applications becomes possible. One example is the replacement of temperature-swing batch separation of hydrocarbons in the petrochemical industry with less energy-intensive, continuous membrane-based processes [2].

A typical zeolite membrane consists of a homogeneous layer of intergrown zeolite crystals synthesised on the surface of a porous support material such as Al_2O_3, TiO_2 or ZrO_2. Due to its hydrophilic nature and relative ease of preparation, zeolite A has been studied intensively in terms of hydrophilic/hydrophobic separations [3], especially in the pervaporative dehydration of water-alcohol mixtures [4,5]. Despite the successful commercialisation of supported NaA membranes [6], the fundamental understanding of membrane formation remains limited, and the production of effective NaA membranes still seems to rely on a synthesise-and-test lottery to find suitable membrane systems under given synthesis conditions. Conditions range from heterogeneous gel systems [7,8], clear solutions [9,10], pre-seeding techniques [11], centrifugally [12] or microwave-assisted crystallisation [13,14] and multistage hydrothermal treatments [15]. Although these widely differing approaches to membrane synthesis each have unique advantages, and attest to the flexibility of NaA crystallisation behaviour, the understanding of zeolite layer growth remains limited to the generalised formation mechanisms. A better understanding of the underlying formation events preceding the final membrane structure may enable researchers to simplify and optimise their efforts in achieving the desired membrane attributes. Even though ample information is available on the growth and crystallisation of NaA single crystals [16], the need exists for correlating these principles to individual membrane synthesis regimes.

To understand zeolite membrane formation, the critical processes of zeolite formation, such as nucleation and crystal growth, are usually considered [17]. Initially, molecular precursor species for nucleation and subsequent zeolite growth are generated from the supplied nutrient mixtures. Bearing in mind a continuous process of formation and dissolution of species, these precursors have to reach a certain threshold concentration before stable nuclei will survive and give rise to seeds that will grow into crystals [18]. As the precursor building blocks are consumed by the growing crystals, the pH and concentration equilibria in the remaining solution continuously changes, until a critical depletion of nutrients is reached and crystal growth stops. During

membrane synthesis, however, the additional effect of crystal immobility on the overall dynamics of crystallisation has to be considered.

The aim of this study was therefore to provide a mainly qualitative, observational account on the specific layer growth history of a supported NaA membrane, while relating these observations to well-established facts on the growth and development of zeolite A crystals in general. Uniform tubular supports of α-Al_2O_3 were used and the layer crystallisation was carefully followed over time.

2.2 EXPERIMENTAL

2.2.1 SUPPORT MANUFACTURE AND PREPARATION

Cylindrical α-alumina supports were manufactured in-house from a commercial α-alumina powder (AKP-15; Sumitomo Chemical Co. Ltd, Japan) by means of centrifugal casting. Using this technique a tubular alumina body was obtained by means of the accelerated differential settling of dispersed particles at the wall of a spinning cylindrical mould. The resulting cast consisted of a gradual particle size (and thus pore size) gradient along the radial axis, the smallest particles lining the inside surface of the tube. Since the starting powder had a narrow particle size distribution this effect was relatively small, but still efficient in generating a consistently smooth surface for zeolite deposition. Sintering the compact at 1050 °C provided enough stability while maintaining the open porous structure. The median pore diameter was 195 nm and porosity was 39.7 % (mercury intrusion; Autopore III, Micromeritics).

The sintered tubes, having an inner and outer diameter of 18.3 mm and 21.2 mm respectively, were cut to 60 mm in length and then sonicated for 10 minutes in a solution containing H_2O_2 (35 %) : NH_4OH (25 %) : H_2O in a volume-to-volume ratio of 1:1:5. This was done to remove all particle residues from the machining step and to clean possible handling contamination. Prior to synthesis the uniform supports were rinsed with deionised water, dried for 3 h at 140 °C and wrapped in Teflon tape to leave only the high integrity inside surface exposed to zeolite deposition.

2.2.2 ZEOLITE SYNTHESIS

The NaA layers were prepared in single stage syntheses by direct in situ crystallisation from a clear solution with a molar oxide ratio of $Na_2O:Al_2O_3:SiO_2:H_2O$ = 49:1:5:980 (adapted from the work of Van den Berg et al. [5]). Two reactant mixtures were prepared by respectively dissolving sodium metasilicate pentahydrate ($Na_2SiO_3 \cdot 5H_2O$: 28% Na_2O, 27% SiO_2; BDH, technical grade) and anhydrous sodium aluminate ($NaAlO_2$: 41% Na_2O, 54% Al_2O_3; Riedel-de Haën/Fluka) in freshly made sodium hydroxide solutions (Merck, analytical grade). The total amount of sodium was distributed in a ratio of 1:1.38 between the corresponding silicate and aluminate solutions while the water was divided evenly. The actual amounts of chemicals used for each mixture are shown in Table 2.1.

Table 2.1: Mixture compositions for NaA synthesis ($49Na_2O:1Al_2O_3:5SiO_2:980H_2O$)

Reactant mixture	$Na_2SiO_3 \cdot 5H_2O$ (g)	$NaAlO_2$ (g)	NaOH (g)	Deionised H_2O (g)
Silicate solution	2.628	-	3.481	20
Aluminate solution	-	0.452	4.807	20

After aging these separate solutions for approximately one hour they were combined by slow addition of the aluminate to the silicate solution under continued stirring, and aged further for one hour at room temperature [5]. Single supports were fitted tightly into a Teflon-lined tubular stainless steel autoclave and the latter filled to ~70 vol.% with the synthesis solution. Crystallisation proceeded under autogeneous pressure in an electronically controlled hot-air oven at 85 °C. Different time-lapse experiments were conducted, carefully reproducing hydrothermal conditions in all cases, but interrupting crystallisation at varying intervals to cover synthesis duration times from 1.0 to 4.0 h. To prevent the incorporation of suspended crystals into the membrane layers, the autoclave (and thus the support) was rotated around the horizontal axis at 25 r.p.m. for the duration of each thermal treatment. After synthesis the oven was switched off and the reactors allowed to cool down spontaneously over a period of approximately 3 h, under continued rotation. The slow cooling (~0.5 $°C.min^{-1}$) was necessary to accommodate the difference in thermal expansion coefficients for zeolite A (6.9×10^{-6} $°C^{-1}$ [19]) and α-alumina ($2\text{-}7 \times 10^{-6}$ $°C^{-1}$ [17]). The cooling step inevitably extended the crystallisation time for each layer, implying that the exact time increments given in this paper were slightly shorter than the

true crystallisation times. Care was however taken to keep the cooling cycles as uniform as possible for all syntheses.

The composites were removed from the remaining solution and neutralised by ultrasonic treatment in deionised water for one hour (6 × 10 min). In order to remove excessive amorphous material and expose the true crystalline morphology for each time-related membrane layer, selected samples were treated with a 0.3 M sodium hydroxide solution at 60 °C for one hour. The chosen NaOH concentration and exposure conditions were deemed sufficient for dissolving the aluminosilicate gel (amorphous phase) [20] at the layer surface, without meaningful dissolution of the crystalline zeolite surface itself [21]. After cleaning, the membranes were dried overnight at 120 °C, using a slow heating and cooling rate of ~1 °C.min^{-1}.

2.2.3 CHARACTERISATION

Zeolitic phase identification and relative crystallinity of the as–synthesised samples (before NaOH treatment) were determined by X-ray diffraction analysis (XRD; Siemens D-501). The diffractometer applied CuK_α radiation (λ_k = 1.5418 Å), operating at a tube voltage of 40 kV. Samples were rotated at 30 rpm. The step-size was 0.02° and scintillation was counted for 10 s per step. 2θ ranged from 4-50°.

Microstructure and morphology of growth layers were examined using scanning electron microscopy (SEM). Dried samples were mounted onto standard specimen stubs with double-sided carbon tape and coated with a ~20 nm thick Au/Pd (80/20) film using an Eiko Engineering IB-2 ion coater (at a sputtering rate of 5 nm.min^{-1}). Imaging was achieved under high vacuum at 15 kV acceleration voltage, using an FEI Quanta 200 ESEM instrument.

Compositional analysis on membrane cross-sections without prior Au/Pd coating was performed by means of energy-dispersive spectroscopy (EDS). Only those samples treated with NaOH were analysed, using an Oxford INCA 400 EDS system coupled to the electron microscope, floating at a magnification of 50 000 during an acquisition time of 100 s per sample.

2.3 RESULTS AND DISCUSSION

2.3.1 CRYSTALLINITY

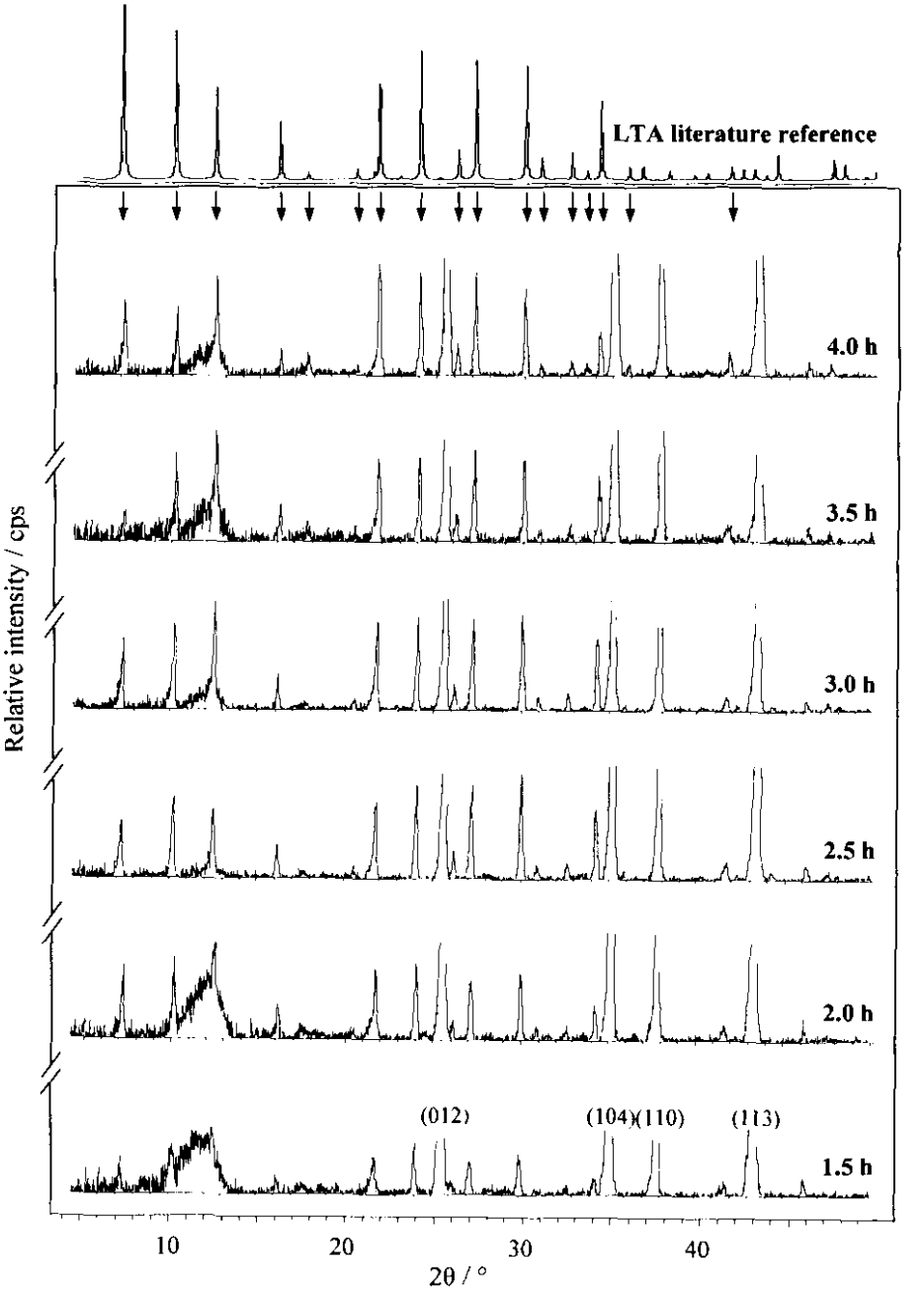

Figure 2.1: XRD patterns for the as-synthesised, consecutive membrane layers, showing that pure NaA reflections (indicated by arrows) are observable after 1.5 h of hydrothermal treatment. A reference diffractogram for hydrated zeolite LTA [22] is also included. The four indexed peaks at the bottom represent the α-Al_2O_3 support.

The XRD reflections for each time experiment are depicted in Fig. 2.1, showing that pure-phase NaA crystallinity appeared after a relatively short crystallisation time (t_c) of 1.5 h. The layer formed after t_c = 1.0 h (XRD not shown) was completely X-ray amorphous, implying that only zeolite NaA, without any other types of zeolites, developed from the amorphous aluminosilicate precursor layer. All growth layers, from t_c 1.5–4.0 h, contained NaA crystallites and crystals without any preferred orientation.

It was however evident that not all the membrane layers were completely crystalline. Assigning specific crystallinity values to each layer proved challenging, since each membrane sample used for analysis was limited in its amount of thin film zeolitic material. As a result, significant noise signals were observed in all XRD spectra, especially in the 2θ range below 15°. Nevertheless, using the four characteristic XRD peaks at 2θ = 21.7, 24, 27.2 and 30°, we estimated the crystallinity of the layer at t_c 1.5 h at ~35 %. This was done by assuming that the well-defined layer with flat cubic facets at the surface (at t_c 4.0 h) was 100 % crystalline (or very near). The peak-to-noise-height ratio for the 1.5 h layer was then calculated as a percentage of the corresponding ratio in the 4.0 h layer. No specific crystallinity values were assigned to the intermediate layers from t_c 2.0–3.5 h, but an increasing degree of crystallinity over time was presumed here.

2.3.2 LAYER GROWTH AND MORPHOLOGY

During an initial stage of delayed onset (induction time) the aging-matured precursor species in solution, consisting of alkali ions, aluminate, silicate and aluminosilicate monomers, dimers and oligomers, rearrange into amorphous gel particles [10,23,24]. According to Koegler et al. [25], the formation of this dormant gel phase might be partially attributed to the action of Na^+-ions in solution, weakening the electric double layer that stabilises the negatively charged solvated species of aluminate and silicate. Flocculation of the latter occurs and results in the formation of macromolecular colloids. These colloidal particles agglomerate [25], are brought to the support by Brownian motion and are then deposited onto the surface in a thin, amorphous gel film (Fig. 2.2 **A**).

The further development of the zeolite membrane depends on the formation of primary zeolite particles (nuclei). Early studies of zeolite nucleation considered different possible mechanisms for the formation of these nuclei, such as homogeneous nucleation in the liquid phase [26,27], heterogeneous nucleation at the interface of foreign particulate matter (the alumina support

surface in this case) [26,28], and secondary nucleation [26]. Various studies also dealt with nucleation in the gel phase itself [28-32], among whom Zhdanov [33] proposed the model of autocatalytic nucleation. The autocatalytic model basically includes only those nuclei formed in the gel matrix [28,31,32], from where they become active and start growing after their release from the dissolved part of the gel. Homogeneous and heterogeneous nucleation were initially thought to be possible additional sources of nuclei. Later on it was shown that homogeneous nucleation could be neglected [34], while recent evidence on the "gel memory effect" [35] indicated that all nuclei (at least for the low-silica zeolites) are formed by autocatalytic nucleation and that the number of nuclei formed by other mechanisms can be neglected.

We thus assume that all nuclei necessary for the growth of the NaA membrane were formed within the matrix of the gel film, due to the high supersaturation of nutrients in the gel [10,36-38]. The induction time for membrane growth is therefore associated with the formation of the gel film, the formation of nuclei within the film, and the exposure of viable nuclei to the surrounding solution as the gel phase starts to dissolve during continued hydrothermal treatment [16].

The nucleation event is followed by the appearance of small crystallites (<100 nm) that are grouped together in hemisphere-shaped clusters (Fig. 2.2 **B1**). Each cluster can be seen as a closely packed arrangement of crystallites embedded in an amorphous gel droplet, where adjacent droplets roughly match the ceramic support's surface contours (i.e. the surface roughness). Within each cluster, the crystallites grow from nutrients that are provided by the progressively dissolving gel. Fig. 2.2 **B** further shows a narrow distribution (concentration) of crystallites at the surface of each cluster. This observation corroborates the predictions made by Gonthier and Thompson [39,40], who assumed an empirical narrow distribution of dormant nuclei near the outer surfaces of the initial gel particles.

Removal of the excess amorphous phase (Fig. 2.2 **B2**) reveals that the bases of the clusters are firmly attached to the support and that individual crystallites have reached a size where surrounding neighbours become impingent upon each other. Subsequently they begin to merge together by means of an intergrowth mechanism.

Fig. 2.3 **A** (t_c = 2.0 h) shows that this merging process, or densification, takes place not only within individual clusters, but also between tightly-knit neighbouring clusters to produce larger, tripod-intersected hemisphere-shaped grains. Some pinholes (the intercrystalline voids encircled

in Fig. 2.3) are still visible and their origin can be traced back to voids between the original clusters seen in Fig. 2.2 **B**.

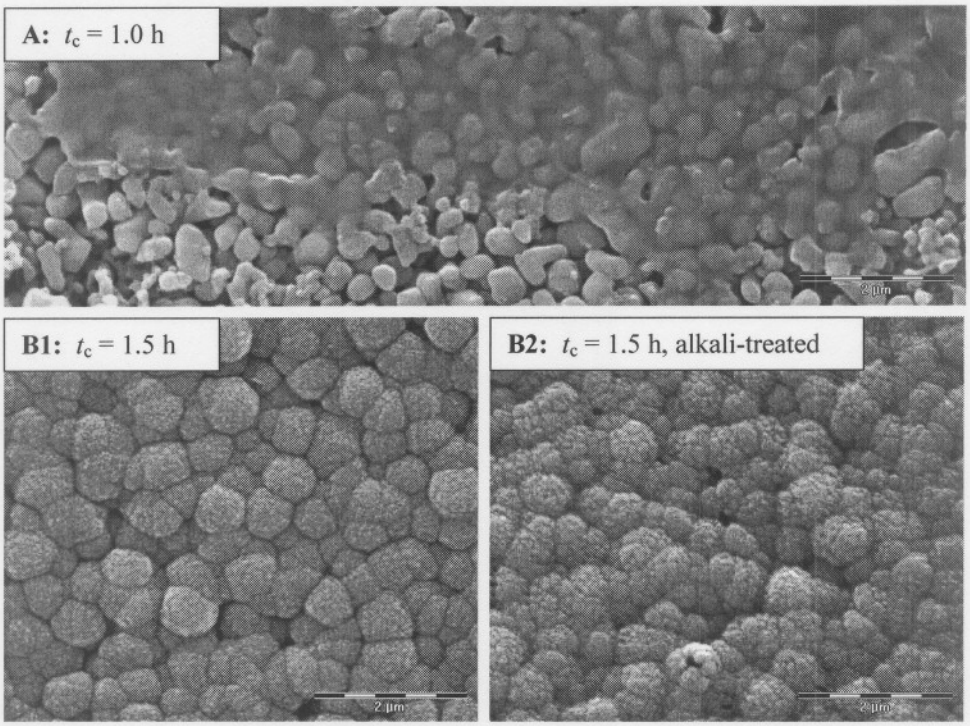

Figure 2.2: Top view SEM imaging of NaA layer development as a function of crystallisation time, t_c. Firstly an amorphous gel layer is deposited on the support surface (**A**), followed by the build-up of semi-crystalline clusters (**B1**, **B2**). Note the growing crystallites, seen as white specs, within each hemisphere-shaped cluster.

Since the growth rates of crystallites within the clusters are assumed equal, it seems logical that groups of clusters in close proximity of each other will intergrow first, followed by the bridging of gaps between the respectively formed grains. In other words, the size of each of the ensuing hemisphere-like grains (Fig. 2.3 **A**) is determined by the amount of clusters originally incorporated in their formation. The grain boundaries will develop where the original cluster groups were separated by voids or geometrical indentations inherited from the curvature between the ceramic support particles. However, such a translation of support microstructure into membrane surface would dictate the grain sizes only within certain confines, due to the thermodynamic limitations that control grain growth [41]. Although these thermodynamic limitations are beyond the scope of this investigation, the key explanation seems to be an increase

in electrostatic repulsion between neighbouring grains as they grow, especially in highly negatively-charged framework type zeolites such as LTA [42]. The surface charge between contiguous grains of a certain size presents an interfacial energy barrier that obstructs the complete intergrowth of grains and leads to the formation of intercrystalline grain boundaries.

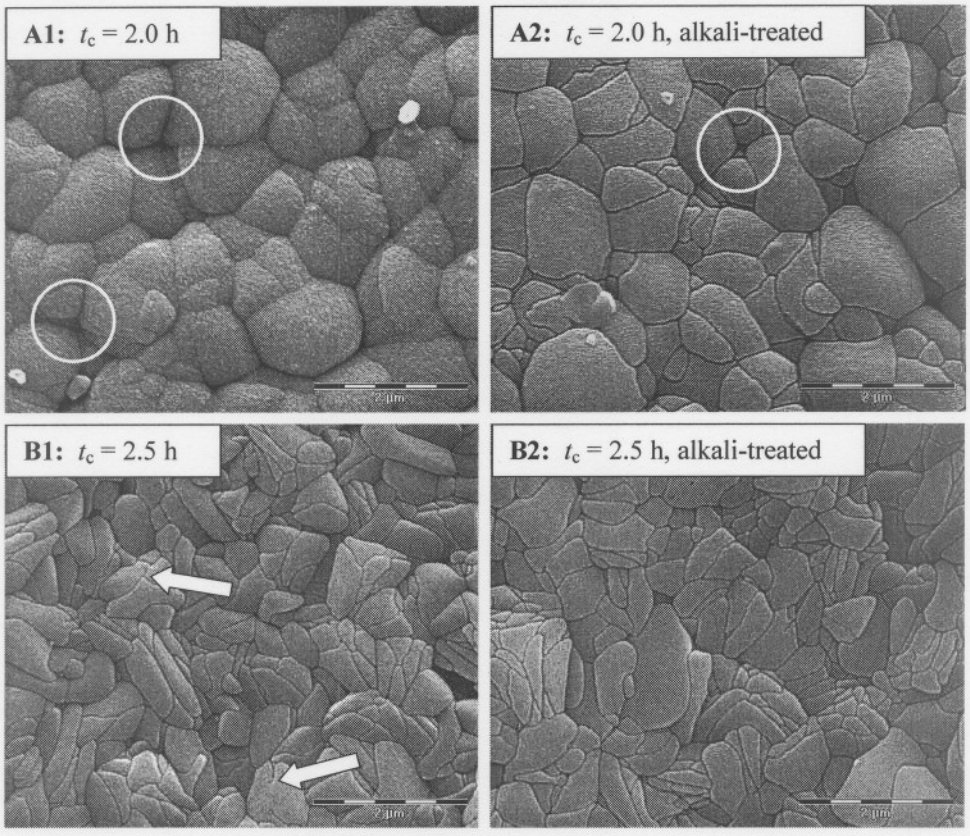

Figure 2.3: Layer development as a function of crystallisation time, t_c = 2.0 h (**A**) and 2.5 h (**B**). Cluster intergrowth leads to hemisphere-shaped grains (**A1**). The white circles indicate areas of poor intergrowth, i.e. pinholes. After 2.5 h the crystal morphology changes as notches appear (**B1**, shown by arrows) with grains developing additional growth planes.

It is evident from the difference between Fig. 2.3 **A1** and **A2** that an amorphous layer still covers the crystallising bases of the grains. Since the layer thickness has increased, the nutrients from the originally deposited gel layer in Fig. 2.2 **A** must have been consumed at this stage. It is therefore suggested that amorphous precursor material (gel), containing dormant nuclei, is continuously assimilated at the growing surfaces during these first stages of crystallisation (t_c 1.0-2.0 h).

Further growth of the membrane is characterised by a sudden change in the layer morphology after 2.5 h (Fig. 2.3 **B**). Each of the hemisphere-shaped grains has now developed notches at their perimeters, which subsequently propagate across the individual grain surfaces to form additional crystal faces. Comparing Fig. 2.3 **B1** and **B2** also indicates that the accumulation of amorphous material at the layer surface has now significantly decreased (also compare Fig. 2.4 **A1** and **A2**). This means that the morphology change coincided with a drop in nutrient concentrations, since the gel was associated with a high supersaturation of nutrients. In addition, the preceding grains in Fig. 2.3 **A** were exceedingly crowded, resulting in an increase in the lateral forces that they exerted on each other. It is therefore also possible that these lateral forces could have contributed to the notching of the crystallising grains. Still, the contribution of grain crowding to the morphology transformation is assumed to be, at most, complementary to that of the decreased nutrient concentrations.

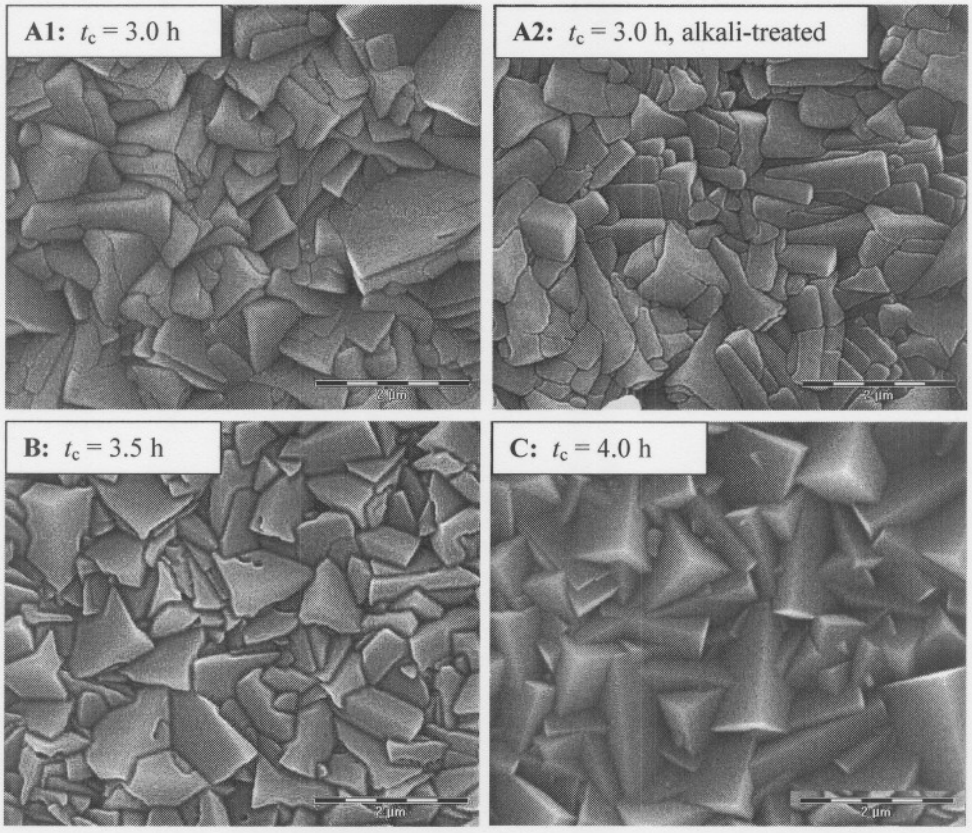

Figure 2.4: Layer morphology as a function of crystallisation time, t_c (continued). The additional growth planes on each grain line up (**A**) and eventually fuse together (**B**) into low-index, cubic facets at the end of crystallisation (**C**).

The final stages of membrane development are shown in Fig. 2.4. The additional crystal planes formed at the beginning of the morphology transformation increase in size and eventually fuse together again to form the low-index crystal faces seen in Fig. 2.4 **B**. The crystal edges also become well-defined and the crystallisation process ends in the well-known cubic morphology.

2.3.3 GROWTH RATE AND ELEMENTAL ANALYSIS

The growth profile of zeolitic films in general follows the same trend as that of single crystals from gels or clear solutions [43,44]. After nucleation, the film thickness increases linearly during crystallisation and reaches an asymptotically constant value at the end of the crystallisation process, where the concentration of precursor species in solution nears the solubility of the zeolite under those specific synthesis conditions. Unfortunately this generalisation is usually not clearly related to the intrinsic intergrowth mechanisms or morphological changes that occur within the stabilising membrane layer during the crystallisation process. It has to be kept in mind that zeolite growth on a molecular scale remains a kinetic balance between hydrolysis and condensation of viable precursor species with the crystal surface.

It is by now well-accepted that both crystal growth and dissolution take place via a layer-by-layer mechanism and atomic force microscopy (AFM) studies [45-48] have related the height of these layers to the dimensions of the sodalite cage, the tertiary building unit for zeolite A. From the current description on layer development it appears that the kinetic formation and dissolution equilibria are constantly changing during the membrane growth process, due to localised supersaturation variations and grain crowding.

Studying the NaA film thickness over time (Fig. 2.5) revealed that the increase in layer thickness was not linearly correlated to the full duration of synthesis and, judging from the data trend, it seemed that a nominal decrease in the growth rate occurred after ~2.5 h of hydrothermal treatment. Considering the induction time of ~1.0 h, the rate change occurred about halfway into crystallisation and the overall increase in thickness could be better represented by two independent linear trends over the whole crystallisation period (t_c 1.0–4.0 h).

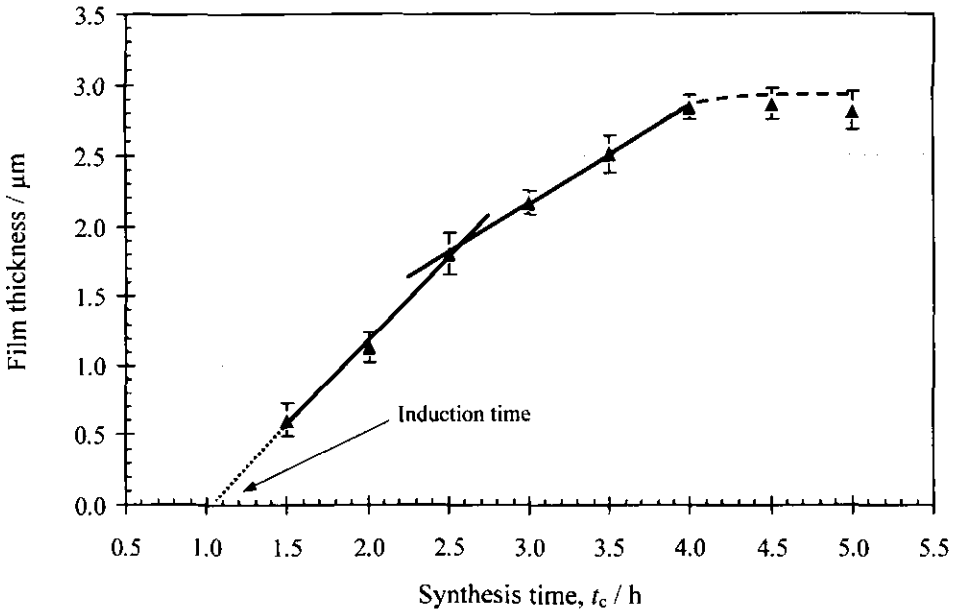

Figure 2.5: *Film thickness, averaged from 10 scattered measurements each, as a function of* crystallisation time, t_c.

The initial period of accelerated growth (3.3×10^{-10} m.s^{-1}), up to $t_c = 2.5$ h, took place under the supersaturation conditions determined by the solubility of the amorphous aluminosilicate precursor and the formed zeolite A. (The initial concentrations of Al and Si in the liquid phase probably dropped slightly during the formation of the amorphous gel, after which they probably remained constant up to $t_c = 2.5$ h.) The "breakpoint" in the growth (crystallisation) process occurred when the entire amorphous phase at the surface had been dissolved and further growth, at a lowered constant rate of 1.9×10^{-10} m.s^{-1}, was facilitated by a decrease in the liquid phase concentrations of both Al and Si. The growth process ended (i.e. the growth rate was zero and the layer thickness constant) when the concentrations of Al and Si in the liquid phase reached the values characteristic for the solubility of zeolite A formed under the given conditions.

Similarities between NaA membrane growth and single crystal synthesis could also be found in the elemental composition of the layers at different stages of growth, as determined by EDS. Due to interference from the α-Al_2O_3 support, Al-results deviated unacceptably, and membrane analyses were restricted to the composition of Na and Si, which was expressed as the Na/Si atomic percentage ratio (Fig. 2.6). Considering that the intermittent layers (t_c 1.5-3.5 h) were

only partially crystalline, even after removal of the excessive amorphous aluminosilicate at the surface, Fig. 2.6 provides information on the composition of this essential amorphous component of the solid phase at different stages of crystallisation. This is possible because the composition of the crystalline part in each layer remained constant with Na/Si = 1. In addition, the Na/Al ratio in the solid phase is known to be very close to unity, not only in the crystalline part, but also in the amorphous component [33,49]. (The reason is that each Na^+ ion compensates a negative charge caused by the incorporation of a tri-valent Al atom in place of a tetra-valent Si atom in the aluminosilicate structure.) The Na/Si ratio in the solid phase is therefore a direct indication of the corresponding Al/Si ratio.

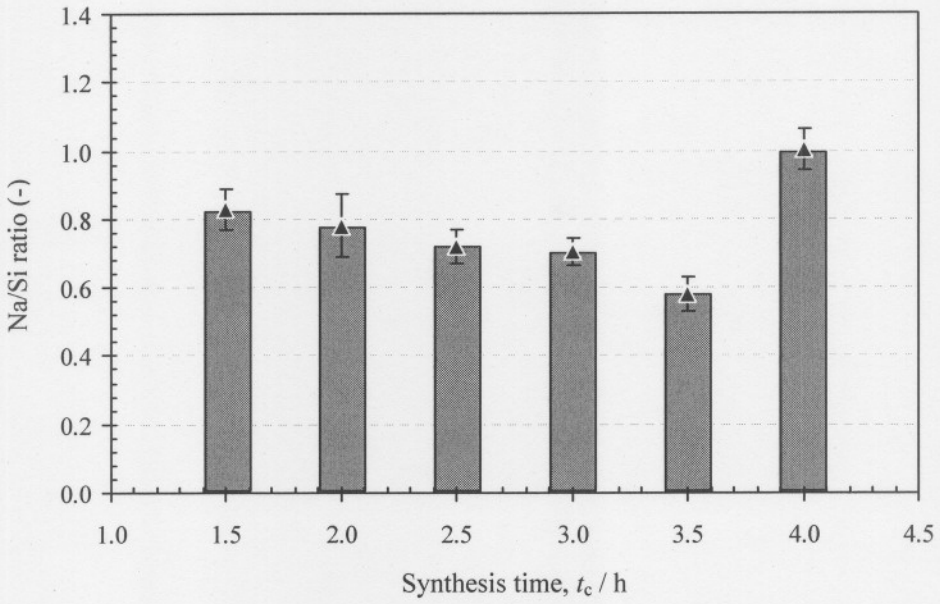

Figure 2.6: Na/Si atomic % ratio as a function of synthesis time. Floating EDS analyses were done at layer cross-sections under high magnification (50 000×). Error bars indicate standard deviations from the average of 3 measurements each.

Following the trend in Fig. 2.6 implies, firstly, a shortage of Na^+ ions (and thus Al-anions) with regard to silicate species in the amorphous solid phase during the main part of crystallisation (t_c 1.5-3.5 h) and secondly, a gradual decrease in this relative amount of Na^+ and Al-ions as layer growth proceeds. Equimolar amounts of constituents (Na:Al:Si = 1:1:1) are only present in the fully crystalline membrane after 4.0 h.

Different studies dealing with free crystal synthesis have shown that the Si/Al ratio in the amorphous component is usually higher than 1 [49-52]. In other words, the Na/Si ratio (and therefore the Al/Si ratio) in the amorphous part of the aluminosilicate structure is usually <1. The decrease in the Na/Si ratio over time is then simply caused by the reduction in the amount of amorphous content as it is consumed in equal amounts of Na, Al and Si by the crystalline component, i.e. the Na/Si ratio in the remaining amorphous component gradually decreases. The change in the membrane compositions depicted in Fig. 2.6 therefore agrees completely with the fundamentals of NaA crystallisation in general.

Unfortunately the solid phase compositions could not explain the observed growth rate change as discussed previously. In a perceptive kinetic study by Bosnar et al. [53] it was shown that only Na^+ ions, in conjunction with aluminate and silicate anions, from solution, take part in the surface reaction of growing NaA crystals. This observation was explained by means of Lindner and Lechert's assumption [54] that only monomeric silicate (≡Si-O$^-$, ≡Si-OH) and aluminate [$Al(OH)_4^-$] species are responsible for crystal growth by, inter alia, nucleophilic attack on aluminate centres at the zeolite surface,

$$[\text{Zeo}{\equiv}\text{Al}{-}\text{OH}]^-\,\text{Na}^+ \;+\; {}^-\text{O}{-}\text{Si}{\equiv} \;\rightleftharpoons\; [\text{Zeo}{\equiv}\text{Al}{-}\text{O}{-}\text{Si}{\equiv}]^-\,\text{Na}^+ \;+\; \text{OH}^-$$

and incorporation of aluminium as a nucleophilic substitution reaction between deprotonated silanol groups on the surface and solvated aluminate species,

$$\text{Zeo}{\equiv}\text{Si}{-}\text{O}^-\,\text{Na}^+ \;+\; \text{Al(OH)}_4^- \;\rightleftharpoons\; [\text{Zeo}{\equiv}\text{Si}{-}\text{O}{-}\text{Al(OH)}_3]^-\,\text{Na}^+ \;+\; \text{OH}^-$$

The driving force, and thus the growth rate, for the development of the NaA layer is therefore not determined by the (amorphous) solid phase concentrations of Na, Al and Si, but rather by the liquid phase concentrations of these components during different stages of growth. For example, simple calculation based on the composition of the reaction mixture shows that the Na^+ content in the liquid phase remains almost constant (2.375×10^{-1} mol at $t_c = 0$ h and about 2.348×10^{-1} mol when approximately 50 % of aluminium and the corresponding amount of silicon have been spent for the formation of the solid phase). This means that the Na/Si ratio in the liquid phase increased from about 19.2 at $t_c = 0$ h, to about 24.4 when 50 % of the aluminium has been spent for the formation of the membrane layer. Clearly there exists no resemblance between the liquid and solid phase ratios of Na, Al and Si respectively, explaining why the observed two-step trend in the growth rate could not be related to the solid phase compositions. More experimental work is needed to determine the liquid phase concentrations of each component during membrane

development, and their exact kinetic relation to the observed morphological and growth rate changes.

2.4 CONCLUSIONS

Zeolite NaA layers were synthesised from a clear solution by direct in situ crystallisation on uniform α-Al_2O_3 supports. A descriptive account was given on the structural membrane development over time, culminating in a dense polycrystalline membrane after 4.0 h. The average film thickness, as well as the Na/Si elemental composition of the respective layers, was followed as a function of crystallisation time (1.5-4.0 h).

It was shown that membrane growth for NaA, under the given synthesis conditions, proceeded along two distinctive morphological pathways: a homogeneous layer of semicrystalline, hemisphere-shaped grains after 2.0 h, followed by the well-known cubic morphology after 4.0 h. Formation of the first layer type could be explained in terms of the supersaturation of nutrients in the associated gel material. Transition into the second morphology type coincided with a suggested decrease in nutrient concentrations, while grain crowding within the structural membrane confines probably contributed to this transformation.

Membrane growth did not proceed linearly along the full duration of synthesis, but followed two independent linear trends, an initial period of accelerated growth (3.3×10^{-10} $m.s^{-1}$), followed by growth at a constant lowered rate of 1.9×10^{-10} $m.s^{-1}$. The decline in growth rate after 2.5 h was correlated to the morphology transformation and therefore mainly attributed to the supersaturation changes. Elemental analysis indicated a decrease in the Na/Si ratio over time and reflected on the composition of the amorphous component in the intermittent layers. The solid phase compositions could however not explain the observed morphology and growth rate tendencies. Further work is needed on the liquid phase concentrations of Na, Al and Si species to resolve the mechanisms regulating the growth process of the membrane.

This study on a NaA composite membrane demonstrates that in membrane syntheses, where the grain population is high, layer growth is characterised by subtle morphological transitions that are not as evident in single crystal synthesis.

2.5 ACKNOWLEDGEMENTS

The authors are indebted to Prof. J.C. Jansen (TU Delft, The Netherlands) for his expert advice and guidance on the synthesis procedures, without which this study would not have been possible. We also wish to thank Dr. L. Tiedt (NWU, South Africa) for his meticulous accuracy in taking the SEM images, and Dr. S. Verryn (UP, South Africa) for the XRD analyses. The financial assistance of the Department of Labour (DoL), South Africa, towards this research is hereby acknowledged. Opinions expressed and conclusions arrived at, are those of the authors and are not necessarily to be attributed to the DoL.

2.6 REFERENCES

[1] J.C. Jansen, J.H. Koegler, H. van Bekkum, H.P.A. Calis, C.M. van den Bleek, F. Kapteijn, J.A. Moulijn, E.R. Geus, N. van der Puil, Zeolitic coatings and their potential use in catalysis, Micropor. Mesopor. Mater. 21 (1998) 213.

[2] S. Nair, M. Tsapatsis, Synthesis and properties of zeolitic membranes, in S.M. Auerbach, K.A. Carrado, P.K. Dutta (Eds.), Handbook of Zeolite Science and Technology, Marcel Dekker Inc., New York, Basel, 2003, pp. 867-919.

[3] M. Kazemimoghadam, A. Pak, T. Mohammadi, Dehydration of water/1-1-dimethylhydrazine mixtures by zeolite membranes, Micropor. Mesopor. Mater. 70 (2004) 127.

[4] K. Okamoto, H. Kita, K. Horii, K. Tanaka, M. Kondo, Zeolite NaA membrane: preparation, single-gas permeation, and pervaporation and vapor permeation of water/organic liquid mixtures, Ind. Eng. Chem. Res. 40 (2001) 163.

[5] A.W.C. van den Berg, L. Gora, J.C. Jansen, M. Makkee, Th. Maschmeyer, Zeolite A membranes synthesized on a UV-irradiated TiO_2 coated metal support: the high pervaporation performance, J. Membr. Sci. 224 (2003) 29.

[6] Y. Morigami, M. Kondo, J. Abe, H. Kita, K. Okamoto, The first large-scale pervaporation plant using tubular-type module with zeolite NaA membrane, Sep. Purif. Tech. 25 (2001) 251.

[7] K. Aoki, K. Kusakabe, S. Morooka, Separation of gases with an A-type zeolite membrane, Ind. Eng. Chem. Res. 39 (2000) 2245.

[8] X. Xu, W. Yang, J. Liu, X. Chen, L. Lin, N. Stroh, H. Brunner, Synthesis and gas permeation properties of an NaA zeolite membrane, Chem. Commun. (2000) 603.

[9] L.C. Boudreau, M. Tsapatsis, A highly oriented thin film of zeolite A, Chem. Mater. 9 (1997) 1705.

[10] L. Gora, K. Sterletzky, R.W. Thompson, G.D.J. Phillies, Study of the crystallization of zeolite NaA by quasi-elastic light-scattering spectroscopy and electron microscopy, Zeolites 18 (1997) 119.

[11] X. Xu, W. Yang, J. Liu, L. Lin, Synthesis and perfection evaluation of NaA zeolite membrane, Sep. Purif. Tech. 25 (2001) 475.

[12] F. Tiscareño-Lechuga, C. Téllez, M. Menéndez, J. Santamaría, A novel device for preparing zeolite-A membranes under a centrifugal force field, J. Membr. Sci. 212 (2003) 135.

[13] L. Bonaccorsi, E. Proverbio, Microwave assisted crystallization of zeolite A from dense gels, J. Cryst. Growth 247 (2003) 555.

[14] Y. Han, H. Ma, S. Qiu, F-S. Xiao, Preparation of zeolite A membranes by microwave heating, Micropor. Mesopor. Mater. 30 (1999) 321.

[15] X. Xu, W. Yang, J. Liu, L. Lin, N. Stroh, H. Brunner, Synthesis of NaA zeolite membrane on a ceramic hollow fiber, J. Membr. Sci. 229 (2004) 81.

[16] B. Subotić, J. Bronić, Theoretical and practical aspects of zeolite crystal growth, in S.M. Auerbach, K.A. Carrado, P.K. Dutta (Eds.), Handbook of Zeolite Science and Technology, Marcel Dekker Inc., New York, Basel, 2003, pp. 129-203.

[17] M. Noack, J. Caro, Zeolite membranes, in F. Schüth, K.S.W. Sing, J. Weitkamp (Eds.), Handbook of Porous Solids Vol. 4, Wiley-VCH, Weinheim, 2002, pp. 2433-2507.

[18] F. Schüth, GIT-Spezial (1996) 12, in F. Schüth, K.S.W. Sing, J. Weitkamp (Eds.), Handbook of Porous Solids Vol. 4, Wiley-VCH, Weinheim, 2002, p. 2456.

[19] D.W. Breck, Zeolite Molecular Sieves, Wiley, New York, 1974.

[20] T. Antonić, A. Cizmek, B. Subotić, Dissolution of amorphous aluminosilicate zeolite precursors in alkaline solutions. 2. Mechanism of the dissolution, J. Chem. Soc. Faraday Trans. 90 (1994) 1973.

[21] A. Cizmek, L. Komunjer, B. Subotić, M. Siroki, S. Roncevic, Kinetics of zeolite dissolution. Part 1. Dissolution of zeolite A in hot sodium hydroxide, Zeolites 11 (1991) 258.

[22] M.M.J. Treacy, J.B. Higgins, Collection of Simulated XRD Powder Patterns for Zeolites, 4th ed., Elsevier, Amsterdam, 2001.

[23] P.W.J.G. Wijnen, T.P.M. Beelen, R.A. van Santen, Silica-gels from aqueous silicate solutions – combined Si-29 NMR and small-angle X-ray-scattering spectroscopic study, in H.E. Bergna (Ed.), The Colloid Chemistry of Silica, Adv. Chem. Ser. No. 234, American Chemical Society, Washington, DC, 1994, pp. 517-531.

[24] W.H. Doktor, H.F. van Garderen, T.P.M. Beelen, R.A. van Santen, W. Bras, Homogeneous versus heterogeneous zeolite nucleation, Angew. Chem. Int. Ed. Engl. 34 (1995) 73.

[25] J.H. Koegler, H. van Bekkum, J.C. Jansen, Growth model of oriented crystals of zeolite Si-ZSM-5, Zeolites 19 (1997) 262.

[26] E.F. Freund, Mechanism of the crystallization of zeolite X, J. Cryst. Growth 34 (1976) 11.

[27] R.W. Thompson, M.J. Huber, Analysis of the growth of molecular sieve zeolite NaA in a batch precipitation system, J. Cryst. Growth 56 (1982) 711.

[28] B. Subotić, A. Groavac, Kinetic analysis of autocatalytic nucleation during crystallization of zeolites, in: B. Držaj, S. Hočevar, S. Pejovnik (Eds.), Zeolites: Synthesis, Structure, Technology and Application, Studies in Surface Science and Catalysis, Vol. 24, Elsevier, Amsterdam, 1985, pp. 199-206.

[29] S.P. Zhdanov, N.N. Samulevitch, Nucleation and crystal growth of zeolites in crystallizing alumino-silicate gels, in: L.V.C. Rees (Ed.), Proceedings of the 5th International Zeolite Conference, Heyden, London-Philadelphia-Rheine, 1981, p. 75.

[30] P.K. Dutta, D.C. Shieh, M.J. Puri, J. Phys. Chem. 91 (1987) 2332.

[31] J. Bronić, B. Subotić, I. Smit, L.A. Despotovic, Influence of gel ageing on zeolite nucleation processes, in P.J. Grobet, W.J. Mortier, E.F. Vansant, G. Schulz-Ekloff (Eds.), Innovation in Zeolite Materials Science, Elsevier, Amsterdam, 1988, p. 107.

[32] B. Subotić, Influence of autocatalytic nucleation on zeolite crystallization processes, in: M.L. Occelli, H.E. Robson (Eds.), Zeolite Synthesis, American Chemical Society Symposium Series No. 398, American Chemical Society, Washington, DC, 1989, p. 110.

[33] S.P. Zhdanov, Some problems of zeolite crystallization, in E.M. Flanigen, L.B. Sand (Eds.), Molecular Sieve Zeolites – I, Adv. Chem. Ser. No. 101, American Chemical Society, Washington, DC, 1971, p. 20.

[34] J. Bronić, B. Subotić, Role of homogeneous nucleation in the formation of primary zeolite particles, Micropor. Mater. 4 (1995) 239.

[35] T. Antonić-Jelić, S. Bosnar, J. Bronić, B. Subotić, M. Škreblin, Micropor. Mesopor. Mater. 64 (2003) 21.

[36] Y. Yan, S.R. Chaudhuri, A. Sarkar, Chem. Mater. 8 (1996) 473.

[37] L. Gora, K. Streletzky, R.W. Thompson, G.D.J. Phillies, Study of the effects of initial-bred nuclei on zeolite NaA crystallization by quasi-elastic light scattering spectroscopy and electron microscopy, Zeolites 19 (1997) 98.

[38] S. Mintova, N.H. Olson, V. Valtchev, T. Bein, Science 283 (1999) 958.

[39] S. Gonthier, R.W. Thompson, Effects of seeding on zeolite crystallisation, and the growth behavior of seeds, in: J.C. Jansen, M. Stöker, H.G. Karge, J. Weitkamp (Eds.), Advanced Zeolite Science and Applications, Studies in Surface Science and Catalysis, Vol. 85, Elsevier, Amsterdam, 1994, p 43.

[40] C. Falamaki, M. Edrissi, M. Sohrabi, Studies on the crystallization kinetics of zeolite ZSM-5 with 1,6-hexanediol as a structure-directing agent, Zeolites 19 (1997) 2.

[41] R.W. Thompson, Recent advances in the understanding of zeolite synthesis, in: H.G. Karge, J. Weitkamp (Eds.), Molecular Sieves, Vol. 1, Springer-Verlag, Berlin, 1998, pp. 1-33.

[42] B. Oonkhanond, M.E. Mullins, Electrical double-layer effects on the deposition of zeolite A on surfaces, J. Colloid Interface Sci. 284 (2005) 210.

[43] M. Lassinantti, J. Hedlund, J. Sterte, Faujasite-type films synthesized by seeding, Micropor. Mesopor. Mater. 38 (2000) 25.

[44] A. Gouzinis, M. Tsapatsis, On the preferred orientation and microstructural manipulation of molecular sieve films prepared by secondary growth, Chem. Mater. 10 (1998) 2497.

[45] M.W. Anderson, J.R. Agger, N. Hanif, O. Terasaki, Growth models in microporous materials, Micropor. Mesopor. Mater. 48 (2001) 1.

[46] J.R. Agger, N. Pervaiz, A.K. Cheetham, M.W. Anderson, Crystallization in zeolite A studied by atomic force microscopy, J. Am. Chem. Soc. 120 (1998) 10754.

[47] S. Sugiyama, S. Yamamoto, O. Matsuoka, H. Nozoye, J. Yu, G. Zhu, S. Qiu, O. Terasaki, AFM observation of double 4-rings on zeolite LTA crystals surface, Micropor. Mesopor. Mater. 28 (1999) 1.

[48] S. Sugiyama, O. Matsuoka, S. Yamamoto, Surface structures of zeolites studied by atomic force microscopy, Micropor. Mesopor. Mater. 48 (2001) 103.

[49] I. Krznarić, T. Antonić, B. Subotić, Physical chemistry of aluminosilicate gels. 1. Influence of batch concentration on chemical composition of the gels, Zeolites 19 (1997) 29.

[50] I. Krznarić, T. Antonić, B. Subotić, Physical chemistry of aluminosilicate gels. Part 2. Influence of the batch molar ratio SiO_2/Al_2O_3 on chemical composition of the gels, Micropor. Mesopor. Mater. 20 (1998) 161.

[51] I. Krznarić, T. Antonić, B. Subotić, V. Babić-Ivančić, Results of thermal and hydrothermal treatment of the aluminosilicate gels prepared at different batch concentrations, Thermochimica Acta 317 (1998) 73.

[52] I. Krzanrić, B. Subotić, Physical chemistry of aluminosilicate gels. Part 3. Influence of batch alkalinity on the chemical composition of gels, Micropor. Mesopor. Mater. 28 (1999) 415.

[53] S. Bosnar, T. Antonić, J. Bronić, B. Subotić, Mechanism and kinetics of the growth of zeolite microcrystals. Part 2: influence of sodium ions concentration in the liquid phase on the growth kinetics of zeolite A microcrystals, Micropor. Mesopor. Mater. 76 (2004) 157.

[54] T. Lindner, H. Lechert, Influence of fluoride on the crystallization kinetics of zeolite NaY, Zeolites 14 (1994) 582.

CHAPTER 3

SINGLE GAS PERMEATION THROUGH THIN LAYERED ZEOLITE NaA MEMBRANES: IMPROVED PERMEANCE THROUGH AN UNCONVENTIONAL, SEMICRYSTALLINE LAYER

ABSTRACT

The successful application of zeolite A membranes in the industrial market has thus far been restricted to the pervaporative dehydration of solvent streams in the pharmaceutical and engineering industries. Their application in gas separation processes remains elusive, largely due to the existence of uncontrollable, intercrystalline diffusion pathways in the boundary regions of neighbouring crystals.

In this study the gas permeation characteristics of an unconventional, semicrystalline (70 %) zeolite NaA layer, where the boundary phase is filled with amorphous aluminosilicate, was examined and compared to a traditional polycrystalline membrane. To this end, we used single gas permeation of H_2, N_2 and SF_6 at two temperatures. In general, the permeances of all gases through the conventional layer increased in response to temperature, indicating a governing contribution of activated (gaseous) diffusion over the temperature interval tested. Typical permeances of H_2 were in the order of 4.8×10^{-7} (23 °C) to 6.5×10^{-7} $mol.m^{-2}.s^{-1}.Pa^{-1}$ (107 °C). For the semicrystalline layer, the same trends were observed for N_2 and SF_6, while the permeance of H_2 decreased sharply from 8.7×10^{-7} (23 °C) to about 3.9×10^{-7} $mol.m^{-2}.s^{-1}.Pa^{-1}$ at 107 °C. This was attributed to the expansion of the crystal/amorphous interface at higher temperature.

By comparing the permselectivity values with the respective Knudsen factors, it was shown that diffusion through the semicrystalline layer, at lower temperature, was predominantly based on molecular sieving ($PS\ H_2/SF_6 = 63.8$), which yielded much higher selectivities than the traditional membrane under the same conditions ($PS\ H_2/SF_6 = 11.4$). However, at higher temperature the H_2/SF_6 permselectivity of the crystalline layer (5.7) was somewhat higher than that of the semicrystalline membrane (5.2).

Based on theoretical considerations, it was concluded that the crystal/amorphous interface in the semicrystalline membrane constituted a denser closure of the boundary interface, which could be attributed to a lower charge barrier presented by the amorphous phase (Si/Al > 1), but this integrity was lost at higher temperature due to the thermal instability of the amorphous material. The results therefore suggest that interventions in the charge loading in the boundary phase, during synthesis, could provide a means for stricter control over the intercrystalline porosity in NaA membranes in general.

Keywords: zeolite NaA membrane, single gas, permeance, intercrystalline boundary, semicrystalline

NOMENCLATURE

d	molecule jump distance	m
E	activation energy	$J.mol^{-1}$
g	geometrical factor	(-)
ΔH_{ads}	Henry's law heat of adsorption	$J.mol^{-1}$
J_i	flux or transmission rate of component *i*	$mol.m^{-2}.s^{-1}$
M_i	molar weight of component *i*	$kg.mol^{-1}$
P_B	permeability	$mol.m.m^{-2}.s^{-1}.Pa^{-1}$
PS	ideal or permselectivity	(-)
p	(partial) pressure	Pa
R	universal gas constant	$= 8.314\ J.K^{-1}.mol^{-1}$
r_p	pore radius	m
T	absolute temperature	K

Greek letters

Π	permeance	$mol.m^{-2}.s^{-1}.Pa^{-1}$
Φ_k	kinetic diameter	Å
α_{Kn}	Knudsen selectivity	(-)
β	Poiseuille flow component	$mol.m^{-2}.s^{-1}.Pa^{-2}$
δ	layer thickness	m
ε	fractional porosity	(-)
η	gas viscosity	Pa.s
μ	tortuosity	(-)
$\bar{v}$	molecular velocity	$m.s^{-1}$

Subscripts

mem	composite membrane (zeolite + support)
zs	zeolite/support interface
Kn	Knudsen
Pois	Poiseuille
fs	feed side of the support
d	downstream
fm	feed side of the composite membrane
g	(activated) gaseous diffusion
total	total permeance through the zeolite layer
intercrys	intercrystalline diffusion

3.1 INTRODUCTION

Zeolite membranes have potential in separating mixtures that are difficult to isolate with traditional techniques, such as distillation, extraction, crystallisation or selective sorption. Specifically in pervaporation applications, zeolite membranes offer distinct advantages in the separation of close-boiling mixtures, azeotropes and thermally sensitive compounds [1]. Pertaining to gas phase separations, the unique crystallographic and physical properties offered by zeolitic membranes are desirable in many industrially important separation processes. Examples are the isolation of N_2 and O_2 from air, air pollution control, removal of trace contaminants like H_2S and SO_2 in obtaining ultrapure gas streams, the production of H_2 from steam/methane reforming, and the separation of aromatic and *n/i*-isomers in the petrochemical industry [2].

A promising candidate for membrane application is the hydrophilic A-type (LTA) zeolite. Due to its high aluminium content and the subsequent susceptibility to ion-exchange, the accessible unit cell aperture for this zeolite type can be altered from 3.2 Å (in the potassium form, KA), to 4.1 Å (NaA) or even 4.6 Å (NaCaA) [3]. It stands to reason why LTA membranes have already been successfully commercialised in the pervaporative dehydration of aqueous solvent streams [4]. Not only is the aperture diameter small enough to allow the selective permeation of water molecules, while rejecting most organic compounds, but the highly polar nature of the zeolite also promotes the separation of aqueous mixtures based on selective sorption and diffusion differences [5]. Using NaA layers on different support types, separation factors in excess of 2.5×10^4 have been reported for the pervaporation of water/alcohol mixtures at 45 °C [6-8]. Testing binary mixtures of Fischer-Tropsch gases, Zhu et al. [9] achieved a vapour-based H_2O/H_2 selectivity of 309 at 30 °C. These remarkable separations have been ascribed to the strong affinity and elevated diffusivity of water in the zeolitic pores, but also the blocking of intercrystalline pores by the capillary condensation of water at low temperature.

Although the small pore network is also attractive for the separation of many small-sized gas molecules, dry gas separation on NaA membranes remains limited. Accounting for the yet-to-be-improved reproducibility of batch membrane syntheses, average selectivities for binary gas mixtures reported to date hardly exceeds the respective Knudsen diffusion ratios [10-12]. The general explanation lies in accentuated permeation along the non-zeolitic voids and grain boundaries which are activated upon drying the impermeable hydrated membrane [13].

In general, it has been shown that the relative contribution of intercrystalline diffusion increases as the aluminium content of the zeolite layer increases [10,14-16]. It seems that the intercrystalline porosity in a NaA membrane (Si/Al = 1) is an intrinsic property of the zeolite itself, and it is therefore safe to say that certain thermodynamic limitations exist which restrict the degree of intergrowth (continuity) in polycrystalline NaA layers. (While these limitations probably originate from the charge loading on the surface and in the bulk of the zeolite crystal structure, another possible cause will be discussed in this paper.) This intercrystalline porosity explains the poor repeatability in the preparation of these membranes and why different synthesis techniques, such as seeding, microwave synthesis and multilayer methods, on average, produce membranes with relatively poor gas separation capabilities. It is clear that new and alternative approaches to membrane preparation are needed to overcome the thermodynamic barriers, or at least to optimise the continuity of NaA layers within these natural boundaries of restricted intergrowth. One such an approach is to investigate alternative isoforms of the same zeolite, such as metastable, semicrystalline layers. Although the synthesis of such layers has been described in literature [13,17], their permeation properties remain elusive.

Traditionally, NaA crystals have been distinguished by their well-recognised cubic morphology, as reflected by both single crystal and membrane layer syntheses [3,18]. Using direct synthesis from a clear aluminosilicate solution, we recently published a paper on the underlying crystallisation events taking place during the single-step synthesis of a NaA layer on the surface of a high integrity alumina support. For a fixed set of synthesis parameters (precursor composition and crystallisation temperature), it was illustrated that a crystalline layer of intergrown cubic morphology, obtained after 4 h, was preceded by a series of intergrowth mechanisms between adjacent groupings of spherical crystallites. By following the growth tendencies over time, we found that a thin, continuous layer of hemispheric grains had formed after only 2 h of synthesis. The formation of this layer was related to elevated degrees of supersaturation during the initial stages of growth. Although it represented an intermediate, metastable configuration of semicrystalline grains, which ultimately transformed into the cubic morphology under extended crystallisation times, it showed certain promising characteristics for membrane applications. The small size of the grains (~1 μm) resulted in a very thin zeolite layer (1.7-2.4 μm for a double layer), which would provide a high zeolite surface area-to-volume ratio for promoting separation at high permeation fluxes. Furthermore, the irregular shape of the grains led to tripod-shaped intersections between neighbouring grains, which would theoretically enhance the continuity, and therefore selectivity, of the membrane [19].

The aim of this study was therefore to prepare two intrinsically different NaA layers and compare their gas permeation properties. To point out the relative contributions of intercrystalline transport in each membrane, we performed single gas permeation measurements at two different temperatures. The results indicated significantly higher permeation rates, as well as higher ideal selectivities, for the unconventional semicrystalline layer. According, it suggests that interventions in the underlying crystallinity (and therefore composition) of the zeolite layer could provide a means to improve gas separation phenomena in NaA membranes.

3.2 EXPERIMENTAL

3.2.1 MEMBRANE PREPARATION

Cylindrical membrane supports were manufactured in-house from a high purity commercial α-Al_2O_3 powder (AKP-15; Sumitomo Chemical Company Ltd., Japan), having a narrow particle size distribution around an average of 0.61 μm. Firstly a colloidal suspension (40 wt.%) was prepared by stabilising the particles with ammonium polymethacrylate (Darvan C; R.T. Vanderbilt Company, Inc, Norwalk, USA) in a pH-adjusted aqueous medium. The suspended particles were then cast into a tubular shape using a centrifugal deposition technique [20-23]. A noteworthy advantage of this technique is the different velocities at which different-sized particles in the suspension settle down. Despite the narrow size distribution of the original suspension, a small fraction of particles will inevitably fall below the bulk average. These very small particles are then isolated by the centrifugal force field and deposited into a high integrity top layer on the inside surface of the resulting cast, producing an asymmetrical support structure in a single step.

After drying, the green supports were sintered at 1200 °C to consolidate the particles while keeping the open porosity structure intact. Average pore diameters for the supports were measured at 163 ± 8 nm, while porosity values for consecutively prepared tubes were also highly reproducible at 34 ± 1 %.

The sintered tubes were cut to 60 mm in length and then sonicated for 10 min in a solution comprising H_2O_2 (35%):NH_4OH (25%):H_2O in a volume-to-volume ratio of 1:1:5. This was done to remove all particle residues that resulted from the machining step and to clean handling contamination. Prior to synthesis all supports were thoroughly rinsed with water, dried for 3 h at

140 °C and wrapped in Teflon tape to leave only the inside surface (tube side) exposed to zeolite deposition.

Two reactant mixtures were prepared by respectively dissolving sodium metasilicate pentahydrate ($Na_2SiO_3 \cdot 5H_2O$; BDH, technical grade) and anhydrous sodium aluminate ($NaAlO_2$: 41% Na_2O, 54% Al_2O_3; Riedel-de Haën/Fluka) in freshly made sodium hydroxide solutions (NaOH pellets; Merck, analytical grade, in deionised water). These separate solutions were aged for approximately 1 h at room temperature before slowly adding the aluminate to the silicate solution under continued stirring. The combined mixture (clear solution) comprised the following molar oxide composition:

$$48.9\ Na_2O{:}1\ Al_2O_3{:}5.08\ SiO_2{:}979.2\ H_2O$$

The final solution was aged for a total of 1 h at room temperature, of which 30 min was directly on the support under rotating conditions. This was to ensure that the support surface was adequately wetted with the synthesis solution. Note that no external heat was supplied during this time.

Layer crystallisation proceeded under autogeneous pressure in a Teflon-lined steel autoclave at 85 °C, using conventional heating in an electronically controlled hot-air oven. The two morphologically discrete NaA membranes were obtained by varying the duration of synthesis, i.e. a homogeneous layer of hemisphere-shaped grains after 2 h, (type A) and a facetted crystal layer with the typical cubic morphology after 4 h (type B). For each type, we prepared two membranes independently to determine repeatability. To enhance continuity of the membranes, we applied two-stage syntheses (double zeolite layers) in all cases. For the second layers we used the exact same procedure, except that all synthesis solutions were aged externally. After synthesis, the composite membranes were extensively rinsed with deionised water in an ultrasonic water bath (4 × 6 min) to remove the remainder of the synthesis solution, but also to clear any excessive zeolite growth from the membrane surface.

3.2.2 MEMBRANE CHARACTERISATION

3.2.2.1 Morphology and crystallinity

Topological features, thicknesses and a qualitative estimate of the continuity of the membrane layers were determined by scanning electron microscopy (SEM). Dried samples were coated

with a ~20 nm thick coating of Au/Pd (80/20) and in vacuo images were generated using an FEI Quanta 200 ESEM instrument. The layer thickness of each membrane was taken as the average of ten scattered measurements.

X-ray diffraction analysis was used to confirm the identity, purity and orientation of grains/crystallites in the zeolite phase. To this end we used a Siemens D-501 diffractometer, applying CuK_α radiation (λ_k = 1.5418 Å) under a tube voltage of 40 kV. Samples were rotated at 30 rpm. The step size was 0.02° and scintillation was counted for 10 s/step, covering a 2θ range between 4° and 50°. The relative peak intensities were used to estimate the crystallinity of the zeolite layers.

3.2.2.2 Elemental analysis

In addition to the XRD assessments, we also determined the elemental make-up (Si/Al ratio) of each morphology type to confirm our crystallinity estimations. Uncoated membrane fragments were embedded in a resin matrix from where polished cross-sections were prepared. Samples were analysed by energy-dispersive X-ray spectrometry (EDX) on a Jeol Superprobe 733 instrument, under 4 kV of electron acceleration voltage and a 12 nA beam current. The lateral resolution for the measurements was about 1 μm for a matrix with a density of ~2 $g.cm^{-3}$. Al was calibrated on corundum, Na on albite and Si on quartz. The oxygen content was calculated by stoichiometry, assuming that Al was present as Al_2O_3, Na as Na_2O and Si as SiO_2. The estimated detection limit was 0.5-1 wt.%.

3.2.2.3 Single gas permeation

Single gas permeation values were measured for H_2, N_2 and SF_6 (all > 99.96 % in purity, from Afrox, SA), using the continuous flow method (CFM) [24]. The CFM provides a simple and expedient measure of gas flow where the driving force for permeation is a constant pressure difference (Δp) across the membrane. In contrast to the Wicke-Kallenbach method, no sweep gas is used in the CFM, to eliminate the possibility of counter-diffusion of the sweep gas from the permeate to the feed side of the membrane [25].

The membranes were sealed into a gas-tight permeation module in a dead-end configuration (**3**, Fig. 3.1). The module was positioned in an electronic oven (**4**) and the temperature was

controlled by a relay-connected thermocouple which was placed near the feed/membrane interface. Experiments were done at 23 and 107 °C. Gases were fed to the tube (zeolite) side of membranes at a Δp of 1.00 ± 0.02 bar, as monitored by a differential pressure gauge (**5**, DELTA-trans digital; WIKA). The permeate flow was measured by a downstream soap-film flow meter (**6**) under local atmospheric conditions (0.87 bar).

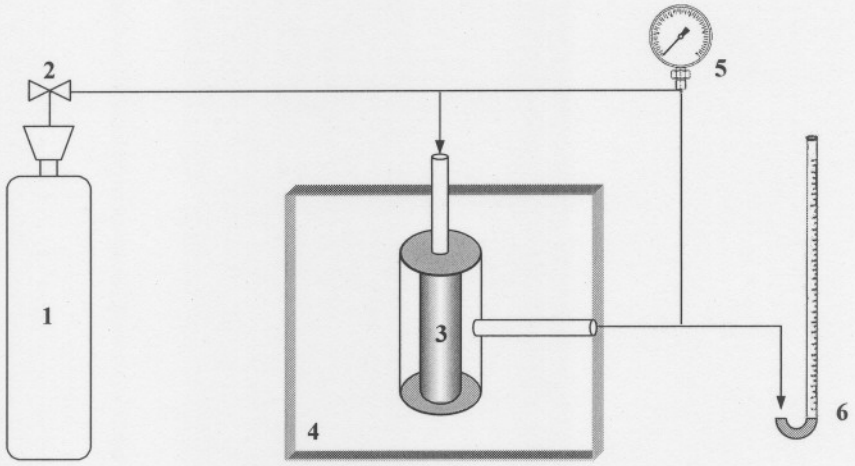

Figure 3.1: Simple experimental set-up for the continuous-flow measurement of single gas permeation (transmembrane Δp = 1 bar).

Note that the as-synthesised membranes were practically impermeable to all gases at room temperature and were therefore dried beforehand for 24 h at 70 °C under low vacuum (0.140 bar). For each gas under consideration, the membranes were initially purged for at least 5 h under measurement conditions to allow for steady-state permeation.

The permeation flux (J_i, in mol.m^{-2}.s^{-1}) in each experiment was recorded as an average of 10 measurements over a period of 30 min. The total membrane permeance (Π_{mem}, in mol.m^{-2}.s^{-1}.Pa^{-1}) was defined as the flux divided by the pressure difference applied across the membrane. The standard deviation within each set of measurements was less than 1 %, confirming steady-state levels. However, the deviation between the two similar, but independently prepared membranes, was higher – approximately 20 % and 15 % for the type A and type B membranes respectively. The reported values for each membrane type are given as the average of the two membranes in each group.

The ideal or permselectivity ($PS_{i/j}$) for gas i over gas j was defined as the single-component permeance ratio, under the given measurement conditions. The membrane performances were evaluated qualitatively by comparing these permselectivities to the respective Knudsen selectivities (α_{Kn}), where

$$\alpha_{Kn}\left(\frac{i}{j}\right) = \sqrt{\frac{M_j}{M_i}} \quad , \qquad (...3.1)$$

with M denoting the molar weight (in $kg.mol^{-1}$) of the gas.

3.3 RESULTS AND DISCUSSION

3.3.1 MORPHOLOGY, CRYSTALLINITY AND COMPOSITION

A detailed morphological discussion on both membrane types was recently presented by Zah et al. [17]. We will therefore only highlight the most important structural features. From the cross-sectional view (Fig. 3.2) is it clear that both membranes were firmly bound to the support surface, with limited penetration of the zeolitic phase into the underlying pores of the support. Despite their modest thicknesses (especially for the type A membrane), both membranes seemed to consist of a continuous layer.

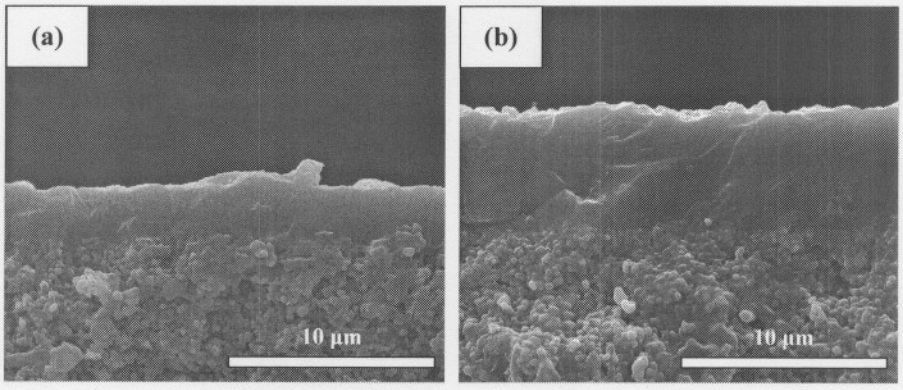

Figure 3.2: Cross-sectional SEM view of membrane type A (**a**) and type B (**b**). Average thicknesses were 1.7-2.4 µm and 5.6-6.3 µm respectively.

The XRD reflections (not shown) indicated that both membranes contained crystalline zeolite NaA, without any preferred orientation of the crystals/crystallites. No contaminating phases, such as hydroxysodalite, zeolite X or zeolite P [4,26], could be detected. Based on spectral analyses, growth rate tendencies, as well as the elemental compositions of the two respective membranes, the metastable type A membrane was found to be ~70 % crystalline, while type B represented a fully crystalline NaA membrane [17].

From the top view perspective of the two membrane layers (Fig. 3.3), it is clear that the hemispheric grains in membrane A were, in fact, not fully intergrown, but rather separated by a boundary phase of amorphous gel (Fig. 3.3**a**). According to the crystallinity estimates, the hemispheric grains themselves were not completely crystalline either. Membrane A could therefore be conceptualised as a closely packed arrangement of NaA grains embedded in an amorphous gel matrix, where the intercrystalline slits are filled with amorphous material. In contrast, the crystals in membrane B seemed to be fully intergrown, and the boundary phase consisted only of the interface between adjacent crystals (Fig. 3.3**b**).

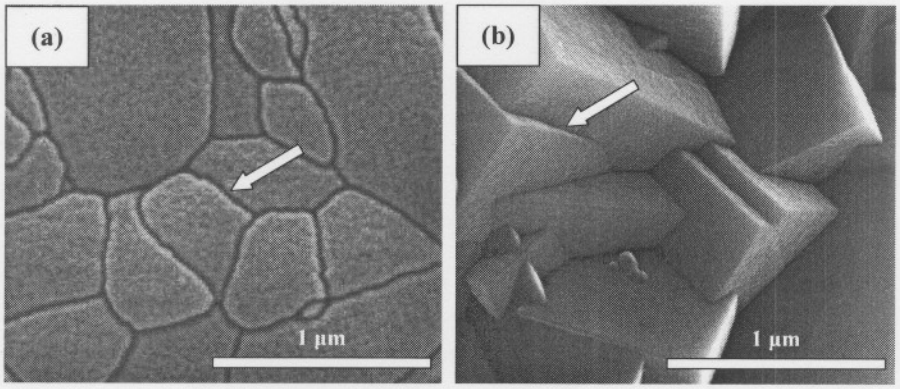

Figure 3.3: High resolution top view images of membrane type A (**a**) and type B (**b**). Arrows indicate the respective boundary phases in each membrane.

A typical, cross-sectional analysis of the Si/Al composition for the semicrystalline type A membrane is given in Fig. 3.4. Considering that the crystalline component of the membrane has a fixed composition (Si/Al = 1), Fig. 3.4 shows that the amorphous component in this membrane was enriched in silicon (i.e. Si/Al > 1). This fact has been previously recorded in literature [27-30], and resembles an attenuated degree of charge distribution in membrane A, because the

excess of Si-tetrahedra in the membrane matrix do not require Na counter-ions to balance their framework charge. For membrane B (not shown) the Si/Al ratio was found to be 1, confirming complete crystallinity. The possible influence of these differences on the permeation properties of the membrane will be discussed in section 3.3.2.3.

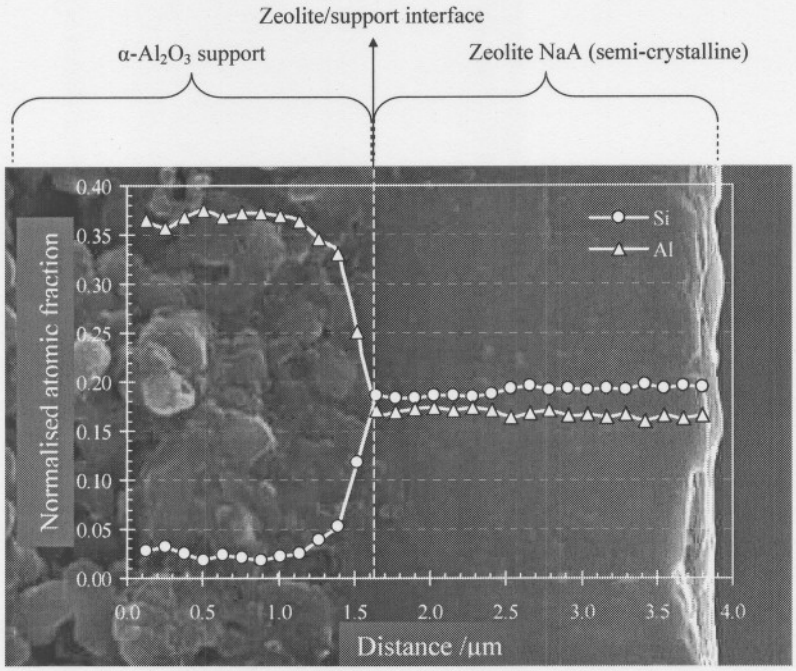

Figure 3.4: Si/Al elemental composition as a function of distance across the semicrystalline type A membrane.

3.3.2 SINGLE GAS PERMEATION

3.3.2.1 Support correction

The flow through the composite membrane is a combination of flow through the top zeolite layer and flow through the support structure. Due to the support resistance, the effective pressure gradient over the zeolite layer will be somewhat smaller than the applied gradient across the composite. To correct the total permeance for the true zeolite layer permeance, the pressure at the zeolite/support interface (p_{zs}) has to be known, which can be calculated if the permeation characteristics of the support are known [31].

The support permeance consists of both Knudsen and Poiseuille flow contributions, due to the relatively large pore sizes, according to:

$$\Pi_{support} = \Pi_{Kn} + \Pi_{Pois} \qquad (...3.2)$$

The Knudsen permeance (Π_{Kn}, in mol.m^{-2}.s^{-1}.Pa^{-1}) is given by [32]:

$$\Pi_{Kn} = \frac{2.g_{Kn}.\bar{v}_i.r_p}{3RT\delta} \qquad \text{with} \quad \bar{v} = \sqrt{\frac{8RT}{\pi.M}} \quad \text{and} \quad g_{Kn} = \varepsilon.\mu_K \qquad (...3.3)$$

where g_{Kn} is a geometrical factor equal to the product of the support porosity ε (-) and reciprocal Knudsen tortuosity ($\mu_K = 1/\tau$). $\bar{v}$ is the average molecular velocity (in m.s^{-1}), r_p is the support pore radius (m), R is the universal gas constant (= 8.314 J.K^{-1}.mol^{-1}), T the absolute temperature (K), δ is the support thickness (m) and M the molar weight (kg.mol^{-1}) of the permeating gas.

The Poiseuille permeance (Π_{Pois}) can be described mathematically as [32]:

$$\Pi_{Pois} = \beta \cdot \bar{p} \qquad \text{where } \beta = \frac{1}{RT} \cdot \frac{g_{Pois}}{\delta} \cdot \frac{r_p^2}{8\eta} \quad \text{with} \quad g_{Pois} = \varepsilon.\mu_P \qquad (...3.4)$$

where $\bar{p}$ is the average pressure across the support, $(p_{fs} + p_d)/2$, in Pa; β the Poiseuille flow component (in mol.m^{-2}.s^{-1}.Pa^{-2}) and η denotes the gas viscosity (in Pa.s). The geometrical factor for Poiseuille flow g_{Pois} is slightly different from that in Eq. 3.3, because the tortuosity factor differs for the two permeation mechanisms. Note that, in contrast to Knudsen flow, the Poiseuille permeance is linearly dependent on the pressure over the support. By measuring the support permeance as a function of average pressure, the value of g_{Pois} can be determined from the slope of the straight line. To this end, we used the flow of N_2 at room temperature (results not shown). For a given pressure regime, the value of g_{Kn} could then be calculated according to Eq. 3.2. Since both these constants were now known, the relevant values for Π_{Kn} and β could be estimated for the other permeation gases, at different temperatures, by substituting the appropriate mass and viscosity values into Eqs. 3.3 and 3.4. According to De Lange et al. [33], the accuracy of this extrapolation technique lies between 5-10 %.

Using the above data, the pressure at the zeolite/support interface for each experiment in the current investigation was calculated by [34]:

$$p_{zs} = \frac{-\Pi_{Kn} + \left[\Pi_{Kn}{}^2 + \beta\left(\beta.p_d^2 + 2.\Pi_{Kn}.p_d + 2.J\right)\right]^{0.5}}{\beta} \qquad (...3.5)$$

where p_d is the experimental downstream pressure. Eq. 3.5 is based on the fact that the experimental flux through the composite membrane, at steady state, is equal to the flux through the zeolite and the flux through the support. The corrected zeolite layer permeance was thus obtained by simply dividing the composite's flux by the pressure drop over the zeolite, i.e. $J/(p_{fm} - p_{zs})$. The actual support permeance in each experiment was calculated in a similar fashion to determine the contribution of the support resistance to the total transmembrane resistance. These values are shown for the fully crystalline type B membrane in Table 3.1. The support correction is crucial, especially at the higher temperature (107 °C), because the support permeance decreases with temperature, which influences the driving force (pressure drop) across the selective zeolite layer.

Table 3.1: Respective Knudsen and Poiseuille permeances of the probe gases through the support, including the support resistance to flow, as determined for the type B membrane

Temperature (°C)	Π_{Kn} (10^{-6} mol.m^{-2}.s^{-1}.Pa^{-1})			Π_{Pois} (10^{-7} mol.m^{-2}.s^{-1}.Pa^{-1})			Total support resistance[a] (%)		
	H_2	N_2	SF_6	H_2	N_2	SF_6	H_2	N_2	SF_6
23	9.05	2.42	1.06	7.86	3.93	4.58	4.6	3.4	2.7
107	7.99	2.14	0.94	5.19	2.61	2.94	7.1	9.8	8.4

[a] Calculated from the fraction $(p_{zs} - p_d)/(p_{fm} - p_d)$

The corrected zeolite permeances will be used exclusively in the following section for comparing the performances of the two membrane types.

3.3.2.2 Zeolitic permeation: type A versus type B

In general, the permeance through a perfect zeolite NaA layer would consist of both activated surface and activated gaseous permeance contributions. The degree to which each of these mechanistic permeation pathways would contribute to the total permeance would depend mainly on the adsorptive and diffusional behaviour of the probe gas within the pore matrix, as well as the permeation temperature, since temperature influences both the adsorption coverage and

diffusivity. At higher temperatures, the diffusivity increases, which enhances the permeance. At the same time, the adsorption coverage on the zeolite should decrease, which has a negative influence on permeance. Usually the activation energy of diffusion is higher than the heat of adsorption, meaning that the effect of increased diffusivity overrules the loss in adsorption, so that the overall permeance will increase. Only when the activation energy of diffusion is smaller than the heat of adsorption, the permeance is expected to show a local maximum with temperature, after which it will drop with further increasing temperature [31]. Such a scenario is thus mainly applicable to strongly adsorbable gases and conditions where the adsorbate loadings (for Langmuirian adsorption) on the zeolite are high.

Table 3.2: Microphysical properties for the probe gases, which may affect their interaction potential with the polar NaA framework[a]

Component	Kinetic diameter, Φ_k (Å)	ΔH_{ads}[b] (kJ.mol^{-1})	Polarisability (10^{-25} cm^3)	Dipole moment (10^{-18} esu cm)	Quadrupole moment (10^{-26} esu cm^2)
H_2	2.89	-9.91	8.0	0	0.66
N_2	3.64-3.80	-16.4	17.6	0	1.52
SF_6	5.13	(-)	65.4	0	0.00

[a] Data extracted from Sircar & Myers [2], unless stated otherwise

[b] Calculated from Henry's Law constants generated by Akten et al. [35]

The microphysical properties for the experimental gases are shown in Table 3.2. Since the window aperture of zeolite NaA is 4.1 Å, only H_2 and N_2 should be able to migrate through the membrane, while SF_6 (control gas) is rejected. Both H_2 and N_2 are weak adsorbates on zeolite A - the heats of adsorption are approximately -10 kJ.mol^{-1} and -16 kJ.mol^{-1} respectively. Furthermore, the adsorption of both gases under the applied conditions falls within the lower ranges of the Henry regime [35], implying very low loadings.

Based on these considerations, the zeolitic permeances in the current investigation are assumed to consist mainly of activated gaseous diffusion (Π_g), where [9,36]:

$$\Pi_g = \frac{1}{RT} \cdot \frac{g}{\delta} \cdot d \cdot \sqrt{\frac{8RT}{\pi M}} \cdot \exp\frac{-E_g}{RT}, \qquad (...3.6)$$

with E_g the activation energy for gaseous diffusion. For pure zeolitic transport, the permeances of H_2 and N_2 are therefore expected to increase with temperature. Real zeolite membranes,

however, contain a certain degree of non-zeolitic (intercrystalline) pathways parallel to the direction of transport.

The total experimental permeance is thus a summation of the zeolitic and intercrystalline permeances:

$$\Pi_{total} = \Pi_g + \Pi_{intercrys} \qquad (...3.7)$$

Depending on the slit size of the intercrystalline regions, the non-zeolitic transport may be governed by contributions of activated transport (small pores similar to zeolitic pores), but also Knudsen and Poiseuille flow mechanisms as described by Eqs. 3.3 and 3.4 (for larger pores and defects). Fig. 3.5 shows the experimental permeance as a function of temperature for the two membranes.

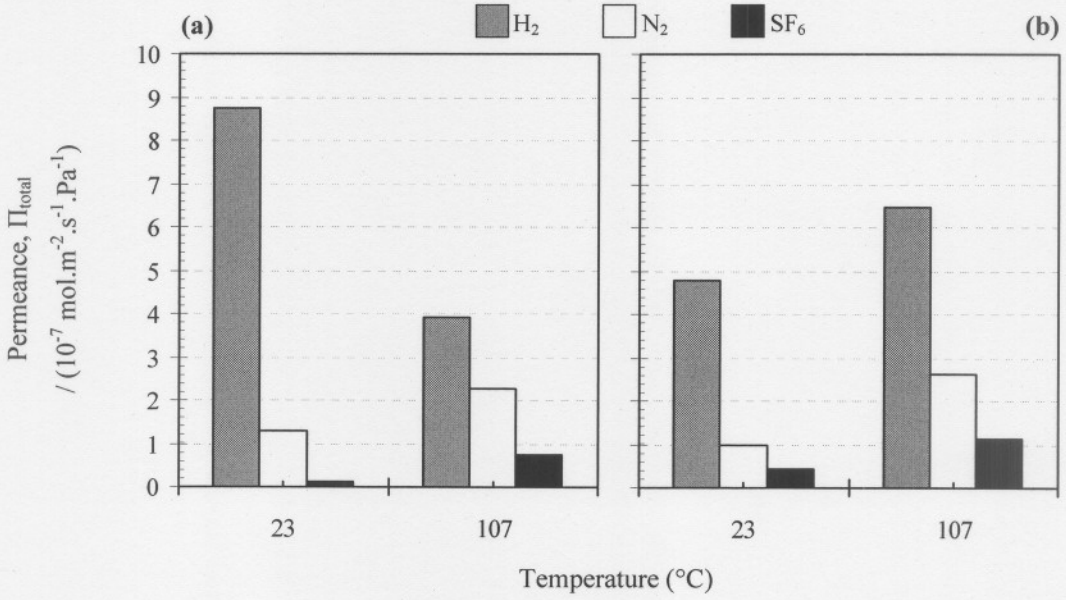

Figure 3.5: Single gas permeances for H_2, N_2 and SF_6, as a function of temperature, for membrane type A **(a)** and type B **(b)**.

Both membrane types exhibited higher permeances to H_2 than to either N_2 or SF_6 – an obvious observation in view of the kinetic diameter and mass of the probe gases. The permeance of SF_6 in all instances signified the existence of non-zeolitic pores. For both membranes, these permeances increased with temperature, indicating that the (intercrystalline) transport of SF_6 was

mainly controlled by an activated diffusion mechanism. The same observation was made for the permeance of N_2, also for both membranes; it does not imply that activated diffusion was the only flow mechanism present for these gases, only that it probably constituted the governing part of the total membrane permeance. The situation for H_2 was somewhat different. For membrane B, the temperature-related increase in permeance suggested the same prevalence of activated gaseous diffusion over the applied temperature range, but for membrane A, the H_2 permeance dropped at 107 °C. The flow of hydrogen was therefore dominated, at least at 107 °C, by non-activated diffusion (Knudsen and/or Poiseuille) where the permeance is inversely dependent on temperature (Eqs. 3.3 and 3.4).

To further elucidate the differences between the two membrane types, Fig. 3.6 illustrates the respective permeabilities (P_B). The permeability is obtained by multiplying the permeance with the membrane thickness, and thus represents an intrinsic material property of the membrane layer. Obviously the same trends should be valid as for the mentioned permeances, but the permeability provides a platform for the direct comparison of the exact values in each instance.

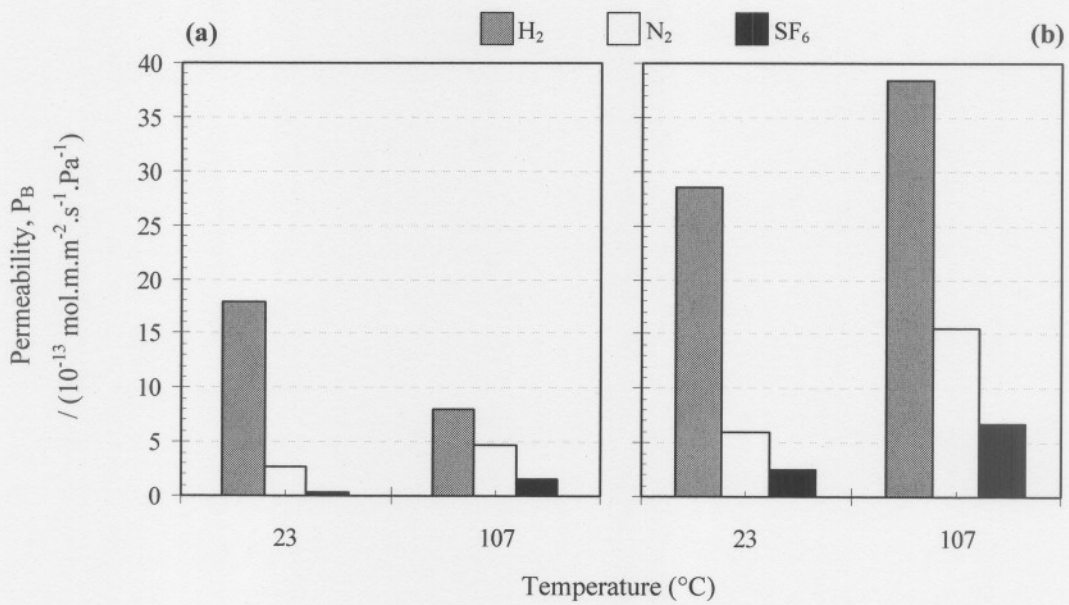

Figure 3.6: Single gas permeabilities for H_2, N_2 and SF_6, as a function of permeation temperature, for membrane type A **(a)** and type B **(b)**.

In general, the permeabilities for all gases were lower in the type A membrane than at the corresponding temperatures in the type B membrane. It suggests that the amorphous component

in the A-type layer has an inhibitory effect on the permeation of all gases, irrespective of the underlying flow mechanisms. Understandably so, since the microporosity of the first type should be in line with its crystallinity, which is ~70 %. In theory one would thus expect the permeability values for the two membranes, at a given temperature, to scale with the same 0.7 factor. Experimentally this was not observed, which can be explained by the non-zeolitic permeation at a given temperature contributing to different degrees to the total flow (Eq. 3.7).

The marginal permeability of SF_6 at 23 °C, for the type A membrane, implies that the intercrystalline slits were smaller in size than in the type B membrane at the same temperature. The permselectivity values confirmed this (Fig. 3.7). The H_2/N_2 selectivity for the type A membrane at 23 °C was 6.7, meaningfully higher than the corresponding α_{Kn} value of 3.74, while the H_2/SF_6 selectivity was 63.8, which was much higher than the α_{Kn} of 8.54, confirming that permeation was largely based on activated zeolitic diffusion (molecular sieving). The corresponding selectivity values for the type B membrane at 23 °C were only incrementally higher than the α_{Kn} values, showing a larger contribution of intercrystalline flow here. The indication is therefore that the crystal/amorphous material interface (type A) forms a tighter junction than the crystal/crystal interface in membrane B.

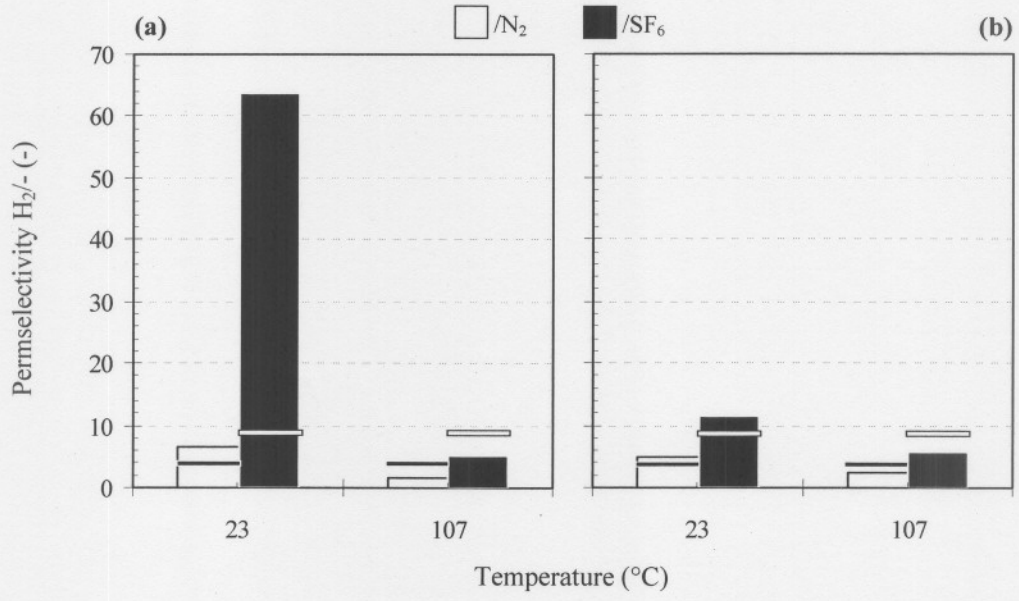

Figure 3.7: Permselectivity for H_2/N_2 and H_2/SF_6, for membranes A **(a)** and B **(b)**, at 23 °C and 107 °C. The respective Knudsen selectivity values are indicated as cross bars.

At the higher temperature of 107 °C the permselectivities for both membranes were lower than the Knudsen factors, implying a stronger contribution of Poiseuille flow at this temperature. The relative selectivities for the different membranes showed an inverse tendency to that found at 23 °C. Both the H_2/N_2 and the H_2/SF_6 selectivities were lower for the type A membrane – approximately 1.73 and 5.16 respectively, compared to the 2.47 and 5.69 values for the type B membrane. These results suggest that the intercrystalline slits in the first membrane have expanded at higher temperature, to a size larger than those in the B-type membrane under the same conditions. Also, by comparing the selectivity drop for membrane B from 23 to 107 °C, a similar expansion of the intercrystalline pores was observed, although to a smaller extent than for membrane A. In summary, it would be fair to assume that the expanded intercrystalline pores in membrane A (at 107 °C) were still small enough to allow for the predominant activated diffusion of both N_2 and SF_6 over the temperature interval tested here, since their permeabilities increased, but at the same time large enough to reduce the permeability of H_2 due to non-zeolitic diffusion mechanisms. Due to the limited data, the exact size of the intercrystalline pores, and the specific magnitude of the different flow regimes within them, remains a subject for future research.

The effect of increased intercrystalline transport at higher temperature was also previously observed for a supported silicalite-1 membrane [37], and attributed to the dissimilar expansion of the support and the zeolite layers at high temperature. The explanation seems relevant for the current NaA membranes as well. The thermal expansion coefficient of α-alumina ranges between $2\text{-}7 \times 10^{-6}$ °C^{-1} [24], while NaA expands at about 6.9×10^{-6} °C^{-1} [38]. Since the semicrystalline type A membrane can be perceived as a packing of NaA crystals in an amorphous gel matrix [17], it would explain the higher flexibility of the non-zeolitic pores in this membrane – the crystal/amorphous gel junction yielded more easily under the thermal stress than the rigid crystal/crystal junctions in the fully crystalline type B membrane. Although a complete stability study was not done, the performance of the semicrystalline layer started to deteriorate after two consecutive cycles of heating/cooling between 23 and 107 °C, suggesting that the thermally-induced expansion of the crystal/amorphous interface was irreversible. The fully crystalline type B layer, on the other hand, returned to its original state after the same temperature cycle. It implies that any amorphous content in the zeolite layer, despite its initial benefit to the permeation performance, reduces the thermo-mechanical stability of the membrane.

Table 3.3: Literature survey for single gas permeation through NaA composite membranes, under relatively similar conditions

Support	Remarks	T (°C)	Π_{mem} (10^{-7} mol.m^{-2}.s^{-1}.Pa^{-1})			PS (-)		Reference
			H_2	N_2	SF_6	H_2/N_2 (3.74)[a]	H_2/SF_6 (8.54)[b]	
α-Al_2O_3	Unseeded; clear solution (2 h synthesis)	23	8.017	1.253	0.136	6.4	59.1	This study
α-Al_2O_3	Unseeded; clear solution (4 h synthesis)	23	4.566	0.962	0.408	4.8	11.2	This study
α-Al_2O_3	Seeded; synthesis gel	25	2.860	0.120	-	23.9	106.0[c]	[39,40]
α-Al_2O_3	Seeded, clear solution	25	1.020	0.152	-	6.7	19.1[d]	[26]
α-Al_2O_3	Unseeded; clear solution (2 h synthesis)	107	3.745	2.071	0.715	1.8	5.2	This study
α-Al_2O_3	Unseeded; clear solution (4 h synthesis)	107	5.997	2.354	1.038	2.6	5.8	This study
α-Al_2O_3	Seeded; synthesis gel	105	0.100	0.025	0.009	4.0	10.7	[6]
α-Al_2O_3	Seeded; synthesis gel	105	0.425	0.115	0.043	3.7	9.8	[6]

[a,b] Respective α_{Kn} values
[c,d] H_2/n-C_4H_{10}

3.3.2.3 Polycrystalline zeolite A membranes and intercrystalline porosity

Table 3.3 presents the permeance and selectivity values for the two membranes types, compared to other data reported for NaA membranes tested under similar conditions. Note that these values reflect the non-corrected performance of each composite membrane and are therefore somewhat lower than those of the actual zeolite layers, due to support resistance. In addition, a direct comparison between the values from different laboratories should be exercised with care, because different experimental procedures were employed by the authors in characterising their membranes. Either way, Table 3.3 serves to show that our membranes compare well to those published so far, especially the fully crystalline type B layer with its traditional cubic morphology. The current results, however, indicate that the permeation properties of the semicrystalline type A membrane are superior at lower temperatures (also considering the high permeance values). Unfortunately it fails to compete with the traditional layers at higher temperatures, due to the lack of thermal stability.

Taking the general repeatability of the various synthesis procedures into account, the average performance of the NaA membranes still falls short of that described for the well-known MFI membranes [41], where a standard H_2/SF_6 permselectivity of 43 can be used as a benchmark for membrane quality. It seems that the uncontrolled intercrystalline porosity in the NaA membranes is a common factor, irrespective of the different preparation approaches used.

The intergrowth between neighbouring zeolite crystals during membrane synthesis is strongly associated with the surface charge barrier between them. Using the DLVO theory, Oonkhanond & Mullins [42] have shown that the nett repulsion between two zeolite A crystals is approximately four times higher than between two ZSM-5 crystals, due to differences in the repulsion forces at the electrical double-layer. Since these (electrostatic) repulsion forces are related to the underlying aluminium content in each crystal, it is understandable that the polycrystalline NaA layers (Si/Al = 1) posses intrinsically larger intercrystalline slits than the ZSM-5 layers (Si/Al >> 1). Even for ZSM-5 layers with varying aluminium content, the results of Noack et al. [15] suggest a stronger degree of intergrowth (continuity) as the aluminium content in the zeolite layer decreases. Furthermore, the magnitude of the intercrystalline repulsion increases with increasing particle size [42], which could partially explain the differences in separation results reported for differently prepared zeolite A membranes. Based on this interpretation, the enhanced performance of the semicrystalline type A membrane in this study could be attributed to two factors:

- The interface between the crystalline and amorphous phases in the membrane constitutes a lower repulsion energy, because the amorphous component has a lower aluminium content (Si/Al > 1), and this contributes to a denser closure of the non-zeolitic boundaries.

- The crystal/crystal interfaces that do exist in the membrane are also in closer contact than in the type B membrane, due to the smaller crystal sizes. Our previous study on the growth history of these polycrystalline membranes supports this statement, where it was shown that nano-sized crystallites (< 100 nm) that formed during the early stages of synthesis, seem to coalesce perfectly to form larger grains (~1 μm), while no further intergrowth was observed beyond those larger grain sizes [17]. For the fully crystalline type B membrane (with crystal sizes around 2 μm), it is therefore likely that the charge barrier between neighbouring crystals is simply too high to allow for the complete closure of the boundary interface during the final stages of membrane synthesis.

As a final remark, we would like to consider an interesting study by Feibelman [43], investigating the dissipation of water between two, near-contacting hydrophilic surfaces. By employing the Navier-Stokes equations, it was demonstrated that water forms a nano-scale hydration layer on the surface of each hydrophilic solid and when the separation distance between the two surfaces is around 5 nm and smaller, the viscosity of this "interphase" water layer, at room temperature, is approximately 10^7-10^8 times higher than that of bulk water! The hydration layer thus creates a repulsive force that keeps the two surfaces apart. In analogy, it is highly possible that a similar situation occurs during the synthesis of a NaA membrane. The increased viscosity of water in the boundary phases between adjacent crystals would not only contribute to the electrostatic repulsion described above, but also inhibit the diffusion of nutrient species for growth in these intercrystalline slit areas, thereby establishing a fixed, "intrinsic" degree of intercrystalline porosity in the final membrane. Remarkably enough, the exact opposite phenomenon is expected to take place between two hydrophobic surfaces in near-contact with each other [43], where water is readily displaced and the surfaces are then predicted to mutually attract. This theory might explain why true, repeatable molecular sieving properties have thus far only been observed for the hydrophobic silicalite-1 type membranes.

3.4 CONCLUSIONS

The permeation properties of two structurally different zeolite NaA layers were investigated, using single gas measurements of H_2, N_2 and SF_6 at 23 and 107 °C. The first layer (type A) was approximately 70 % crystalline and consisted of hemisphere-shaped zeolite grains embedded into an amorphous aluminosilicate gel matrix. The second layer (100 % crystalline) consisted of the traditional, tightly-knit cubic morphology.

For membrane B, the permeances of all gases increased as a function of temperature, indicating a prevalence of activated (gaseous) diffusion over the temperature interval tested. Typical permeance values for H_2 ranged from 4.8×10^{-7} (23 °C) to 6.5×10^{-7} $mol.m^{-2}.s^{-1}.Pa^{-1}$ (107 °C). The respective ideal selectivities indicated, however, that a sizeable fraction of the total permeance was regulated by flow regimes through non-zeolitic, intercrystalline regions, especially at the higher temperature. The temperature effect was attributed to the expansion of the crystal/crystal interface at 107 °C.

For membrane A, the same increasing tendency of permeance with temperature was observed for N_2 and SF_6. In contrast, the permeance of H_2 decreased sharply from 8.7×10^{-7} (23 °C) to about 3.9×10^{-7} $mol.m^{-2}.s^{-1}.Pa^{-1}$ at 107 °C. Comparison of the Knudsen and selectivity factors showed that the initial permeance of H_2 at 23 °C was strongly regulated by molecular sieving (*PS* $H_2/SF_6 = 63.8$), while Knudsen and Poiseuille flow mechanisms was predominant at higher temperature (*PS* $H_2/SF_6 = 5.2$). It indicated a similar expansion of the intercrystalline boundaries as observed for membrane B, but to a larger extent. The expanded boundaries in membrane A (at 107 °C) were therefore still small enough to allow for the predominant activated diffusion of both N_2 and SF_6 over the temperature interval tested, since their permeabilities increased, but at the same time large enough to reduce the permeability of H_2 due to non-zeolitic diffusion mechanisms.

The difference in the performances of the two membranes was explained by theoretical considerations. Based on possible electrostatic and hydration repulsion forces, it was suggested that the crystal/amorphous interface in the semicrystalline type A membrane constitutes a denser closure of the boundary interface, which could be attributed to a lower charge barrier presented by the amorphous phase (Si/Al > 1). However, despite its initial benefit to the permeation performance, it compromised the thermal stability of the membrane.

3.5 ACKNOWLEDGEMENTS

The financial assistance of the Department of Labour (DoL), South Africa, towards this research is hereby acknowledged. Opinions expressed and conclusions arrived at, are those of the authors and are not necessarily to be attributed to the DoL. The authors wish to thank Dr. L. Tiedt (NWU, South Africa) for the SEM images, Dr. S. Verryn (UP, South Africa) for the XRD analyses and Dr. C. Reinke (Mineralogy, Mintek) for the EPMA data. We also thank Mr J. Kroeze (Technical Advisory - SST, NWU, South Africa) for preparing the membrane reactors and the permeation setup.

3.6 REFERENCES

[1] T. C. Bowen, R. D. Noble, J. L. Falconer, Fundamentals and applications of pervaporation through zeolite membranes, J. Membr. Sci. 245 (2004) 1.

[2] S. Sircar, A.L. Myers, Gas separation by zeolites, in S.M. Auerbach, K.A. Carrado, P.K. Dutta (Eds.), Handbook of Zeolite Science and Technology, Marcel Dekker Inc., New York, Basel, 2003, pp. 1063-1104.

[3] J.C. Jansen, D. Kashchiev, A. Erdem-Senatalar, Preparation of coatings of molecular sieve crystals for catalysis and separation, in J.C. Jansen, M. Stöker, H.G. Karge, J. Weitkamp (Eds.), Advanced Zeolite Science and Applications, Stud. Surf. Sci. Catal. Vol. 85, Elsevier, Amsterdam, 1994, pp. 215-250.

[4] Y. Morigami, M. Kondo, J. Abe, H. Kita, K. Okamoto, The first large-scale pervaporation plant using tubular-type module with zeolite NaA membrane, Sep. Purif. Tech. 25 (2001) 251.

[5] S. Furukawa, K. Goda, Y. Zhang, T. Nitta, Molecular simulation study on adsorption and diffusion behavior of ethanol/water molecules in NaA zeolite crystal, J. Chem. Eng. Jpn. 37 (2004) 67.

[6] J. Zah, H.M. Krieg, J.C. Breytenbach, Pervaporation and related properties of time-dependent growth layers of zeolite NaA on structured ceramic supports, J. Membr. Sci., *accepted for publication.*

[7] K. Okamoto, H. Kita, K. Horii, K. Tanaka, M. Kondo, Zeolite NaA membrane: preparation, single-gas permeation, and pervaporation and vapour permeation of water/organic liquid mixtures, Ind. Eng. Chem. Res. 40 (2001) 163.

[8] A.W.C. van den Berg, L. Gora, J.C. Jansen, M. Makkee, Th. Maschmeyer, Zeolite A membranes synthesized on a UV-irradiated TiO_2 coated metal support: the high pervaporation performance, J. Membr. Sci. 224 (2003) 29.

[9] W. Zhu, L. Gora, A.W.C. van den Berg, F. Kapteijn, J.C. Jansen, J.A. Moulijn, Water vapour separation from permanent gases by a zeolite-4A membrane, J. Membr. Sci. 253 (2005) 57.

[10] K. Aoki, K. Kusakabe, S. Morooka, Gas permeation properties of A-type zeolite membrane formed on porous substrate by hydrothermal synthesis, J. Membr. Sci. 141 (1998) 197.

[11] K. Aoki, K. Kusakabe, S. Morooka, Separation of gases with an A-type zeolite membrane, Ind. Eng. Chem. Res. 39 (2000) 2245.

[12] X. Chen, W. Yang, J. Liu, L. Lin, Synthesis of zeolite NaA membranes with high permeance under microwave radiation on mesoporous-layer-modified macroporous substrates for gas separation, J. Membr. Sci. 255 (2005) 201.

[13] S. Nair, M. Tsapatsis, Synthesis and properties of zeolitic membranes, in S.M. Auerbach, K.A. Carrado, P.K. Dutta (Eds.), Handbook of Zeolite Science and Technology, Marcel Dekker Inc., New York, Basel, 2003, pp. 867-919.

[14] T. Sano, S. Ejiri, K. Yamada, Y. Kawakami, H. Yanagishita, Separation of acetic acid-water mixtures by pervaporation through silicalite membrane, J. Membr. Sci. 123 (1997) 225.

[15] M. Noack, P. Kölsch, J. Caro, M. Schneider, P. Toussaint, I. Sieber, MFI membranes of different Si/Al ratios for pervaporation and steam permeation, Micropor. Mesopor. Mater. 35-36 (2000) 253.

[16] M. Noack, P. Kölsch, V. Seefeld, P. Toussaint, G. Georgi, J. Caro, Influence of the Si/Al ratio on the permeation properties of MFI-membranes, Micropor. Mesopor. Mater. 79 (2005) 329.

[17] J. Zah, H.M. Krieg, J.C. Breytenbach, Layer development and growth history of polycrystalline zeolite A membranes synthesised from a clear solution, Micropor. Mesopor. Mater. 93 (2006) 141.

[18] S. Dumrul, S. Bazzana, J. Warzywoda, R.R. Biederman, A. Sacco Jr., Imaging of crystal growth-induced fine surface features in zeolite A by atomic force microscopy, Micropor. Mesopor. Mater. 54 (2002) 79.

[19] J.C. Jansen, J.H. Koegler, H. van Bekkum, H.P.A. Calis, C.M. van den Bleek, F. Kapteijn, J.A. Moulijn, E.R. Geus, N. van der Puil, Zeolitic coatings and their potential use in catalysis, Micropor. Mesopor. Mater. 21 (1998) 213.

[20] A. Nijmeijer, C. Huiskes, N.G.M. Sibelt, H. Kruidhof, H. Verweij, Centrifugal casting of tubular membrane supports, Am. Ceram. Soc. Bull. 77 (1998) 95.

[21] G.C. Steenkamp, H.W.J.P. Neomagus, H.M. Krieg, K. Keizer, Centrifugal casting of ceramic membrane tubes and the coating with chitosan, Sep. Purif. Technol. 25 (2001) 407.

[22] P.M. Biesheuvel, V. Breedveld, A.P. Higler, H. Verweij, Graded membrane supports produced by centrifugal casting of a slightly polydisperse suspension, Chem. Eng. Sci. 56 (2001) 3517.

[23] K. Kim, S. Cho, K. Yoon, J. Kim, J. Ha, D. Chun, Centrifugal casting of alumina tube for membrane application, J. Membr. Sci. 199 (2002) 69.

[24] M. Noack, J. Caro, Zeolite membranes, in F. Schüth, K.S.W. Sing, J. Weitkamp (Eds.), Handbook of Porous Solids Vol. 4, Wiley-VCH, Weinheim, 2002, pp. 2433-2507.

[25] J. van de Graaf, F. Kapteijn, J.A. Moulijn, Methodological and operational aspects of permeation measurements on silicalite-1 membranes, J. Membr. Sci. 144 (1998) 87.

[26] X. Xu, W. Yang, J. Liu, L. Lin, Synthesis of NaA zeolite membranes from clear solution, Micropor. Mesopor. Mater. 43 (2001) 299.

[27] I. Krznarić, T. Antonić, B. Subotić, Physical chemistry of aluminosilicate gels. 1. Influence of batch concentration on chemical composition of the gels, Zeolites 19 (1997) 29.

[28] I. Krznarić, T. Antonić, B. Subotić, Physical chemistry of aluminosilicate gels. Part 2. Influence of the batch molar ratio SiO_2/Al_2O_3 on chemical composition of the gels, Micropor. Mesopor. Mater. 20 (1998) 161.

[29] I. Krznarić, T. Antonić, B. Subotić, V. Babić-Ivančić, Results of thermal and hydrothermal treatment of the aluminosilicate gels prepared at different batch concentrations, Thermochimica Acta 317 (1998) 73.

[30] I. Krzanrić, B. Subotić, Physical chemistry of aluminosilicate gels. Part 3. Influence of batch alkalinity on the chemical composition of gels, Micropor. Mesopor. Mater. 28 (1999) 415.

[31] R.S.A. de Lange, K. Keizer, A.J. Burggraaf, Analysis and theory of gas transport in microporous sol-gel derived ceramic membranes, J. Membr. Sci. 104 (1995) 81.

[32] R.J.R. Uhlhorn, A.J. Burggraaf, Gas separations with inorganic membranes, in R.R. Bhave (Ed.), Inorganic Membranes: Synthesis, Characteristics and Applications, Van Nostrand Reinhold, New York, 1991, pp. 155-176.

[33] R.S.A. de Lange, J.H.A. Hekkink, K. Keizer, A.J. Burggraaf, Formation and characterization of supported microporous ceramic membranes prepared by sol-gel modification techniques, J. Membr. Sci. 99 (1995) 57.

[34] Y.S. Lin, A.J. Burggraaf, Preparation and characterization of high-temperature thermally stable alumina composite membrane, J. Am. Ceram. Soc. 74 (1991) 219.

[35] E.D. Akten, R. Siriwardane, D.S. Sholl, Monte Carlo simulation of single- and binary-component adsorption of CO_2, N_2 and H_2 in zeolite Na-4A, Energy Fuels 17 (2003) 977.

[36] W.J.W. Bakker, L.J.P. van den Broeke, F. Kapteijn, J.A. Moulijn, Temperature dependence of one-component permeation through a silicalite-1 membrane, AIChE J. 43 (1997) 2203.

[37] N. Nishiyama, L. Gora, V. Teplyakov, F. Kapteijn, J.A. Moulijn, Evaluation of reproducible high flux silicalite-1 membranes: gas permeation and separation characterization, Sep. Purif. Technol. 22-23 (2001) 295.

[38] D.W. Breck, Zeolite Molecular Sieves, Wiley, New York, 1974.

[39] X. Xu, W. Yang, J. Liu, X. Chen, L. Lin, N. Stroh, H. Brunner, Synthesis and gas permeation of an NaA zeolite membrane, Chem. Comm. (2000) 603.

[40] X. Xu, Y. Bao, C. Song, W. Yang, J. Liu, L. Lin, Synthesis, characterization and single gas permeation properties of NaA zeolite membrane, J. Membr. Sci. 249 (2005) 51.

[41] M. Noack, P. Kölsch, R. Schäfer, P. Toussaint, I. Sieber, J. Caro, Preparation of MFI membranes of enlarged area with high reproducibility, Micropor. Mesopor. Mater. 49 (2002) 25.

[42] B. Oonkhanond, M.E. Mullins, Electrical double-layer effects on the deposition of zeolite A on surfaces, J. Colloid Interface Sci. 284 (2005) 210.

[43] P.J. Feibelman, Effect of high-viscosity interphases on drainage between hydrophilic surfaces, Langmuir 20 (2004)1239.

CHAPTER 4

PERVAPORATION AND RELATED PROPERTIES OF TIME-DEPENDENT GROWTH LAYERS OF ZEOLITE NaA ON STRUCTURED CERAMIC SUPPORTS

ABSTRACT

A fundamental description is given on the H_2O/EtOH pervaporation behaviour of morphologically different layers of zeolite NaA. Five unique NaA layers were prepared under similar conditions (Na_2O:Al_2O_3:SiO_2:H_2O = 49:1:5:980; 85 °C), but varying crystallisation times (2.0-4.0 h). Selected layers were also synthesised on two structurally different Al_2O_3 supports, to investigate the role of the support microstructure and its resistance to mass flow.

The separation performances of the layers on the first support, with an average pore diameter of 163 nm, were compared using a 95 wt.% EtOH feed at 45 °C. The selectivity (α_{WE}) depended strongly on the relative degree of crystallinity and the amount of amorphous material occluded in the intercrystalline pore regions. The highest selectivities were obtained with either low crystallinity combined with significant amorphous content (α_{WE} = 9 000 for the 2.0 h layer), or high crystallinity combined with a small amount of amorphous content (α_{WE} = 12 500 for the 3.5 h layer). This general trend was also observed for the respective layers synthesised on the second support (101 nm pore diameter), but the α_{WE} values were much lower, ranging between 340 (for the 2.0 h layer) and 3 000 (for the 3.5 h layer). The difference was attributed to the increased dissolution of the second support, retarding the intergrowth of the zeolite layers.

Despite the selectivity differences, the fluxes through each series of membranes on a specific support remained constant, showing that the support resistance to permeation was significantly high for both support types. The relative contributions to the total transmembrane resistance were calculated at ~60 % and ~70 % for the first and second support types respectively. The fugacity values at the zeolite/support interface of a given membrane (3.5 h synthesis on the second support) showed that the support resistance can limit the driving force achievable across the zeolite layer, even if the driving force across the composite membrane is increased.

Keywords: zeolite NaA membrane, pervaporation, permeability, support resistance, driving force

NOMENCLATURE

a_i	activity of component *i* in the feed	(-)
D_i	diffusion coefficient for component *i*	($cm^2.s^{-1}$)
D_{Kn}	Knudsen diffusivity	($cm^2.s^{-1}$)
f_i^f	fugacity of component *i* in the liquid feed	(kPa)
f / f^f	relative fugacity (i.e. fugacity normalised as a fraction of the feed fugacity)	(-)
$-\Delta H_{ads}$	enthalpy of adsorption	($kJ.mol^{-1}$)
J_i	molar flux of component *i*	($mol.m^{-2}.h^{-1}$)
k_B	Boltzmann constant	(1.38×10^{-16} $g.cm^2.s^{-2}.K^{-1}$)
l_S	support layer thickness	(mm)
l_Z	zeolite layer thickness	(μm)
M_i	molecular weight (molar weight divided by Avogadro's constant)	(g)
P_{Bi}	permeability coefficient for component *i*, related to the zeolite layer thickness	($mol.m.m^{-2}.s^{-1}.Pa^{-1}$)
p_i	partial pressure for component *i*	(kPa)
p_i°	saturated vapour pressure for component *i*	(kPa)
p^p	permeate total pressure	(kPa)
p_i^{zs}	partial pressure (fugacity) for component *i* at the zeolite/support interface	(kPa)
Q	total mass pervaporation flux	($kg.m^{-2}.h^{-1}$)
R	universal gas constant	(8.314 $J.K^{-1}.mol^{-1}$)
S_i	solubility coefficient for component *i*	($mol.m^{-3}.Pa^{-1}$)
t_c	synthesis (crystallisation) time	(h)
T	absolute temperature	(K)
μ_i	chemical potential of component *i*	($kJ.mol^{-1}$)
μ_i°	chemical potential of 1 mole of component *i*	($kJ.mol^{-1}$)
x_i	mole fraction of component *i* in the liquid feed	(-)
z_i	mole fraction of component *i* in the vapour permeate	(-)

Greek letters

$\alpha_{w,E}$	selectivity (separation factor) for H_2O/EtOH liquid mixtures	(-)
γ_i	activity coefficient for component *i* in the liquid phase	(-)
ε	fractional porosity of the support layer	(-)
Φ_k	molecular kinetic diameter	(nm)
Φ_{pore}	pore diameter	(nm)

Superscripts

f	feed
p	permeate
v	vapour
zs	zeolite/support

Subscripts

E	ethanol (EtOH)
pv	pervaporation
s	support
sinter	sintering
w	water (H_2O)
z	zeolite

Note that the parameter units given here are those generally used throughout the text, but they cannot necessarily be substituted directly into the equations given under section 4.2 (Theory). Some unit conversions might be necessary.

4.1 INTRODUCTION

The first method for producing a supported zeolite membrane was patented in 1987 [1], marking the advent of an exciting new field in membrane science. A remarkable number of publications related to the development of such supported membranes (composites) ensued, including selective layers of framework types MFI (ZSM-5 and its siliceous counterpart silicalite-1), FAU (zeolites X and Y) and LTA (zeolite A) [2-11]. These studies mainly centred on the synthesis and gas permeation properties of differently prepared membranes and meaningful progress has been made in understanding not only the growth of the zeolite layers [12], but also the gas-phase transport and separation phenomena across them [13].

The fundamental understanding of liquid based separations (pervaporation) remains somewhat neglected – an ironic fact in face of the recent commercialisation of the hydrophilic NaA membranes in pervaporative solvent dehydration [14]. It shows that the development of these pervaporation membranes has been mainly empirical, without a lucid understanding of the basic processes taking place during mixture pervaporation across a supported NaA membrane. These processes (mainly adsorption and diffusion) regulate the selective transport through both the zeolite and the support layers, and depend on the intrinsic material properties of the zeolite layer (morphology, crystallinity and permeability) and the structural properties of the support (pore size and porosity). In addition, the driving force for each component in the separation mixture is a key factor in determining the overall permeation flux through the composite membrane.

In a recent publication regarding the growth of NaA layers on the surface of a porous alumina support [15], we illustrated that morphologically different membrane layers could be isolated by interrupting the growth process at consecutive time intervals across the crystallisation period. The current study presents a structured investigation of pervaporation through these time-dependent, thin layered zeolite A membranes. The observations were explained in terms of the basic principles of driving force, adsorption and diffusion. A standard H_2O/EtOH mixture (95 wt.% EtOH) was used under fixed conditions of temperature and pressure to examine the intrinsic differences between the layers in terms of selectivity and flux. Two structurally different supports were used to show how the membrane attributes for a given layer can depend on the stability of the alumina surface. Under conditions of increasing temperature, it was also shown that the support resistance can significantly influence the driving force for transport across a specific zeolite layer.

4.2 THEORY – PERVAPORATION TRANSPORT

In pervaporation, the transport route for any molecule traveling from the zeolite to the support side of the composite membrane comprises different steps. First it has to pass through the bulk of the feed solution, by means of convective transport, to the feed/zeolite interface. Here it adsorbs on the surface and in the pores of the zeolite layer, followed by directional diffusion through the zeolitic layer. This diffusion process can occur via both intra- and intercrystalline pore regions of the zeolite layer. At the zeolite/support interface, each molecule then has to desorb from the zeolite surface and evaporate into the vapour phase, driven by the permeate side vacuum. The permeation route is completed after the molecule has penetrated through the support pores, leaving the composite membrane at the downstream side.

4.2.1 ZEOLITE-MEDIATED TRANSPORT

Apart from molecular sieving, where the zeolite pores differentiate between permeating molecules on the basis of size exclusion, the mechanism for separation of mixtures by real zeolite membranes depends strongly on adsorption and diffusion differences between different types of molecules interacting with the zeolite framework [16].

At temperatures normally associated with pervaporation (T_{pv} < 70 °C), molecules diffuse along zeolitic pores by jumping between adsorption sites at the wall of the zeolite framework (i.e. surface diffusion) [17,18]. Molecules with a larger enthalpy of adsorption, $-\Delta H_{ads}$, will adsorb preferentially compared to other, weaker interacting components. In a component mixture this phenomenon is known as adsorption selectivity, and it is highly significant for the pervaporative separation of H_2O/EtOH mixtures on hydrophilic zeolites like NaA. The reason being that the adsorption selectivity can be directly related to the separation selectivity (α_{WE}) of the membrane towards these components [19]. The $-\Delta H_{ads}$ for H_2O on NaA is approximately 100 kJ.mol^{-1} [20], while for EtOH it is estimated below 85 kJ.mol^{-1} [21]. Selective adsorption of H_2O will therefore diminish the available zeolite coverage space for interaction with EtOH molecules. Moreover, H_2O is a smaller molecule and the saturated adsorption capacity of NaA is much higher for H_2O (15×10^{-3} mol.g^{-1} zeolite [22]) than for EtOH (4×10^{-3} mol.g^{-1} zeolite [23]). As a cumulative effect of these factors, H_2O then also condenses inside the intercrystalline pore regions, further blocking the entry of EtOH molecules into the membrane and thus increasing H_2O selectivity.

Surface diffusion along the pore wall is an activated process, because the molecules need energy to overcome the potential wells presented at each adsorption site, and thus a driving force is required for diffusion from the feed to the permeate side of the zeolite layer. The driving force for a single component *i* depends on its chemical potential (μ_i), where

$$\mu_i = \mu_i^\circ + RT \ln a_i \tag{4.1}$$

with μ_i° being the chemical potential of 1 mole of pure substance at temperature *T*, and a_i denoting the activity for *i*. The activity of each component can be expressed as its relative vapour pressure,

$$a_i = \frac{p_i}{p_i^\circ} \tag{4.2}$$

where p_i is the partial vapour pressure and p_i° the saturated vapour pressure at temperature *T*. In pervaporation though, temperatures are relatively low and the feed mixture is in a liquid phase. Since liquids are nearly incompressible, the pressure residing over the feed liquid has little effect on the driving force for adsorption on the zeolite. The activity is therefore rather related to the concentration (mole fraction) of component *i* in the liquid feed mixture and can alternatively be given by

$$a_i = x_i \gamma_i \tag{4.3}$$

with x_i representing the mole fraction and γ_i the activity coefficient. If we now define the driving force for adsorption of component *i* from the liquid feed onto the zeolite as its feed fugacity (f_i^{f}) [24], where

$$f_i^{\mathrm{f}} = a_i p_i^\circ \tag{4.4}$$

we obtain, from Eq. 4.2-4.4, that:

$$f_i^{\mathrm{f}} = p_i = x_i \gamma_i p_i^\circ \tag{4.5}$$

Note that Eq. 4.5 expresses the feed fugacity as a linear function of the saturated vapour pressure p_i°, implying that, at a constant activity value ($x_i \gamma_i$), the fugacity increases when the saturated vapour pressure increases (with an increase in temperature, for example). The feed fugacity in

pervaporation is therefore a thermodynamic measure of the tendency of a given component to leave the liquid phase [24]. Mass transfer for that component can then only take place in two directions – the gas phase residing over the feed solution, or adsorption onto the zeolite. If the transfer into the gas phase is properly controlled so that the mole fraction of that component in the liquid phase remains essentially unchanged, mass transfer is then mainly directed toward adsorption on the zeolite.

In relation to the solution-diffusion model, used to describe transport through polymeric membranes, the transmembrane permeability of component i (P_{Bi}) is a function of both the diffusivity (D) and solubility (S) of that component in the corresponding membrane material:

$$P_{Bi} = D_i S_i \tag{4.6}$$

Wijmans and Baker [25,26] have shown that the transmembrane flux for component i (J_i) through the polymer can then be written, in analogy to gas permeation, as:

$$J_i = \frac{P_{Bi}}{lz}\left(p_i^{f} - p_i^{v}\right) \tag{4.7}$$

Here the factor terms p_i^{f} and p_i^{v} would denote the partial pressures in the feed and permeate respectively, while lz is the active membrane thickness. Further refinement in terms of pervaporation, gives [25]

$$J_i = \frac{P_{Bi}}{lz}\left(x_i \gamma_i p_i^{\circ} - z_i p^{p}\right) \tag{4.8}$$

where z_i represents the permeate mole fraction of i, and p^{p} the total permeate pressure. Note how Eq. 4.8 uses the fugacity gradient (the parenthetical term on the right-hand side) across the polymeric membrane as driving force for permeation. The feed-side fugacity ($x_i \gamma_i p_i^{\circ}$) is related to the liquid concentration (mole fraction) and temperature as discussed earlier. Fugacity on the permeate side depends on the vacuum pressure and is simply given by the product of the mole fraction and total permeate pressure (i.e. $z_i p^{p}$), because ideal gas conditions are assumed here.

In contrast to the solution-diffusion model though, pervaporation through a zeolite membrane obeys an adsorption-diffusion mechanism. The solubility parameter in Eq. 4.6, if related to zeolitic pervaporation, can be visualised in terms of the zeolite-specific adsorption coefficient.

Such an adsorption coefficient would be understudied by the specific enthalpy of adsorption and the saturation capacity, dependent on molecular size, of the zeolite for that component. Together with a zeolite-specific diffusivity parameter, the component permeability $P_{B,i}$ (Eq. 4.6) would thus become relevant to zeolitic pervaporation.

It is imperative to realise however, that the flux-driving force dependence in Eq. 4.8 is based on certain simplifying assumptions, such as a constant diffusivity coefficient and Henry type (linear) adsorption behaviour. It is known that diffusion coefficients are coverage-dependent [27] and thus concentration dependent. Also, zeolitic adsorption follows Langmuirian-type behaviour [28]. These effects are even more dominant at the near-saturated coverage conditions prevailing during pervaporation [24]. For this reason there are more comprehensive modeling approaches available to describe zeolitic transport. One example is the extension of the dusty gas model to describe the surface diffusion of species on the zeolite in terms of variable coverage and saturation conditions, using the Maxwell-Stefan equations [29-31]. However, the simple predictive treatment discussed here (Eq. 4.8), is useful when comparing the pervaporation performance of different membranes under fixed conditions of temperature and feed concentration.

4.2.2 TRANSPORT THROUGH THE SUPPORT

Permeate flow through the support is governed by its pore size, and for pervaporation through small pore layers (Φ_{pore} < 400 nm) this flow falls mainly within the Knudsen regime [18,32]. Knudsen diffusion occurs when molecules collide more often with the pore wall than with each other and this form of mass transfer resistance increases when the pore diameter decreases. Considering a pure component water flux of 50 $mol.m^{-2}.h^{-1}$ (~1.0 $kg.m^{-2}.h^{-1}$), Bowen et al. [18] demonstrated that for pervaporation through a 400 nm pore diameter support, about 90 % of the flow could be attributed to Knudsen diffusion. (The remainder of flow was accounted for by Poisseuille flow.) At similar fluxes through a 200 nm support however, Knudsen diffusion contributed to more than 97 % of the total flow through the support, clearly showing that support resistance can have a recognisable effect on the permeate flow.

Since the permeate is in the vapour phase, the actual pressure drop for Knudsen diffusion over the support layer can be estimated by [18]:

$$J_i = \frac{\varepsilon D_{Kn}}{l_s RT}\left(p_i^{zs} - z_i p^{p}\right) \tag{4.9}$$

Here ε denotes the fractional support porosity, p_i^{zs} is the partial vapour pressure (fugacity) for component i at the zeolite/support interface and l_s is the thickness of the support layer. D_{Kn} is the Knudsen diffusivity and can be calculated by [33]

$$D_{Kn} = \frac{\Phi_{pore}}{3}\sqrt{\frac{2k_B T}{M_i}} \tag{4.10}$$

with Φ_{pore} being the support pore diameter, k_B the Boltzmann constant and M_i the molecular mass (molar weight divided by Avogadro's number). Since the flux J_i through the composite membrane, at steady state permeation, is equal to the flux through the support, the fugacity at the zeolite/support interface of a given component can easily be calculated by measuring the total transmembrane flux, as well as the permeate composition.

4.3 EXPERIMENTAL

4.3.1 SUPPORT MANUFACTURE AND PREPARATION

Tubular supports were made in-house from colloidally processed α-Al_2O_3 suspensions by means of centrifugal casting. This technique (depicted in Fig. 4.1) allows the differential settling of suspension particles at the wall of an axisymmetrically spinning cylindrical mould. The centrifugal force field dictates the rate at which different sized particles settle down (force $\propto$ particle size) and depending on the particle size distribution in the original suspension, the finest particles always line the inside surface of the radially deposited cast. Even in suspensions with narrow particle size distributions, the technique always produces an asymmetrical support cast with a highly regular and smooth inside surface. This cast is then dried and sintered at elevated temperature to provide the necessary mechanical strength. Further details on the procedure can be obtained from Refs. [34-37].

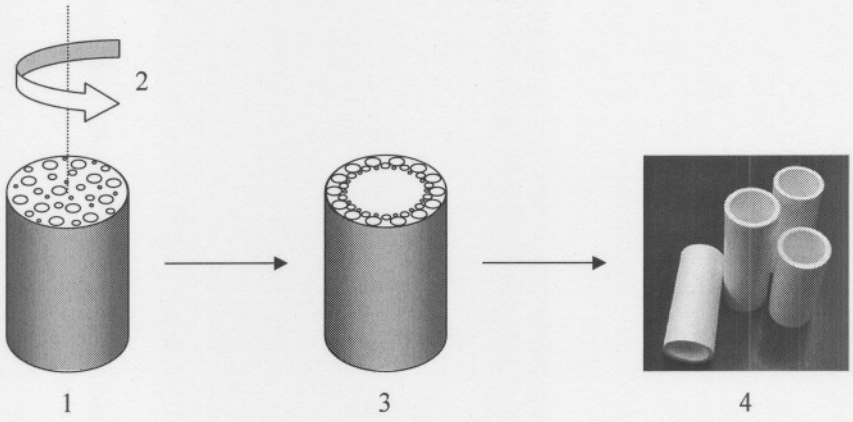

Figure 4.1: Centrifugal casting of α-Al_2O_3 membrane supports.
1: Stainless steel mould filled with colloidal suspension
2: Axisymmetrical centrifugation (around the vertical axis); 17×10^3 rpm
3: Tubular cast with radial asymmetry (smallest particles inside)
4: Final supports after mould release, drying and sintering

Two commercial α-Al_2O_3 powders, AKP-15 and AKP-30 (Sumitomo Chemical Co. Ltd, Japan), having mean particle sizes of 0.61 and 0.31 μm respectively, were used to produce two different support types. The repeatability of the manufacturing process was within acceptable limits, with typical pore diameters for identically prepared supports deviating by no more than 5% (within a 95% confidence interval). The average (micro)structural properties for the supports are depicted in Table 4.1. The narrow particles size distributions in the starting powders were translated into similarly narrow pore size distributions in the sintered supports, validating the use of average pore sizes for later calculations on the effect of support resistance.

Table 4.1: Structural properties of tubular membrane supports

Support type	Sintering temperature, T_{sinter} (°C)	Average pore diameter[a], Φ_p (nm)	Porosity[a], ε (%)	Inner diameter, i.d.(mm)	Wall thickness (mm)
1 (AKP-15)	1200	163	34.8	18.0	1.3
2 (AKP-30)	1050	101	40.8	17.9	1.5

[a] Measured by mercury intrusion (Autopore III, Micromeritics)

Finally prepared tubes were cut to 60 mm in length and then sonicated for 10 min in a solution comprising H_2O_2 (35%):NH_4OH (25%):H_2O in a volume-to-volume ratio of 1:1:5. This was done to remove all particle residues that resulted from the machining step and to clean handling contamination.

4.3.2 ZEOLITE MEMBRANE SYNTHESIS

NaA-type zeolite layers were crystallised directly on supports in a batch hydrothermal procedure at 85 °C, using a clear solution with a molar composition ratio of Na_2O:Al_2O_3:SiO_2:H_2O = 49:1:5:980. Reagent chemicals included sodium metasilicate pentahydrate ($Na_2SiO_3 \cdot 5H_2O$: 28% Na_2O, 27% SiO_2; BDH, technical grade), sodium aluminate ($NaAlO_2$: 41% Na_2O, 54% Al_2O_3; Riedel-de Haën) and sodium hydroxide (NaOH; 97%, Aldrich). Deionised water (MilliQ) was used throughout. Details on the complete synthetic procedure are described in Ref. [15] and were followed accordingly, except that in this study the finally mixed synthesis solution was aged for 30 min directly on the support prior to hydrothermal treatment. The cumulative time of aging however, remained unchanged at 2 h.

Five morphologically different membrane structures were obtained by varying only the duration of synthesis. This was done at 0.5 h intervals to isolate membranes corresponding to synthesis times of 2.0, 2.5, 3.0, 3.5 and 4.0 h. To optimise membrane intergrowth, we applied two-stage syntheses (double zeolite layers) in all cases, unless stated otherwise. Synthesis parameters for the respective secondary zeolite layers were duplicated from the first, except that all secondary solutions were aged externally. Membranes were used as-synthesised, the only post-synthesis treatment being a cleaning step in an ultrasonic water bath for 20 min (4 × 5 min), and drying at 30 °C for 24 h.

All the membranes were initially screened for cracks or handling-induced defects by individually fitting them in a dead-end filtration reactor, filling the tube (zeolite) side with an absolute EtOH feed, and pressurising this feed with N_2 gas to reach a 200 kPa pressure drop. Any visible permeation of EtOH indicated laminar flow of fluid through the membrane, thereby negating its use in further permeation tests.

4.3.3 MEMBRANE CHARACTERISATION

4.3.3.1 Morphology and crystallinity

The microstructure (morphology) and thickness, as well as a qualitative measure of the continuity of the membrane layers, were examined using scanning electron microscopy (SEM). Layer thicknesses were taken as the average of ten scattered measurements in each case. The zeolite phase, its purity and an estimated measure of crystallinity were determined by X-ray diffraction analysis (XRD; Siemens D-501).

4.3.3.2 Pervaporation

Composite membranes were evaluated by their total pervaporation flux (Q, in $kg.m^{-2}.h^{-1}$) and mixture selectivity (α_{WE}) in a H_2O/EtOH binary system. Fig. 4.2 shows the standard experimental set-up used. To prevent bypass leakage, the tubular membrane ends were sealed by dip-coating in a 5 wt.% solution of polysulfone (Sigma-Aldrich) in chloroform. (The integrity of the seals was tested beforehand – the polysulfone film remained stable after exposure to an absolute EtOH solution under refluxing conditions, at 75 °C, over a period for 24 hours.) After drying the seals overnight, the membranes were secured into a cross-flow stainless steel module (3; Fig. 4.2), using elastomeric Viton® O-rings. The effective membrane areas were 2.84×10^{-3} m^2 and 2.69×10^{-3} m^2 for support types 1 and 2 respectively.

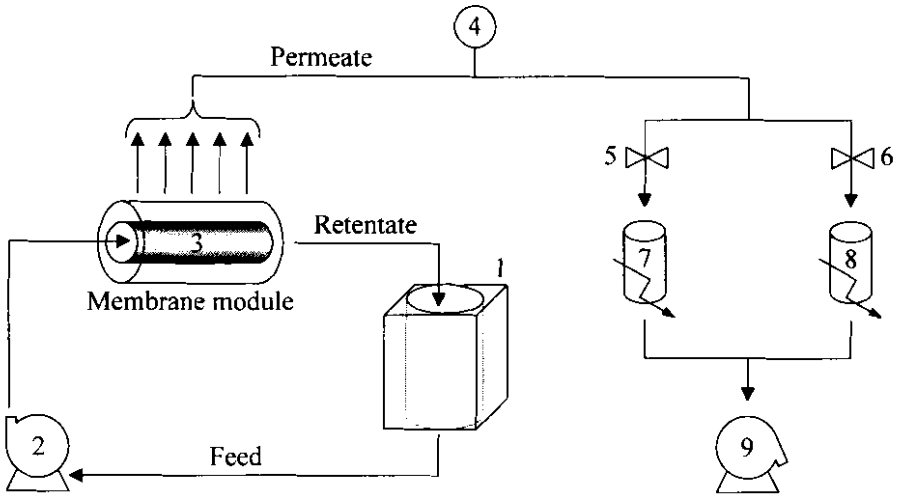

Figure 4.2: Schematic illustration of the pervaporation set-up for H_2O/EtOH separation. Feed streams consisted of 95 wt.% EtOH at 45 °C, while permeate pressures were maintained at 0.4 kPa.

A feed solution of 95 wt.% EtOH (prepared from EtOH AR, 99.5 vol.% min.; Merck) was heated in a thermally regulated sleeve reservoir (1) and circulated under ambient pressure (90 kPa) through the tube side (zeolite side) of the membrane using a magnetic pump (2). The continuous circulation inhibited concentration polarisation at the feed-membrane interface. Unless stated otherwise, the temperature was held constant at 45 °C, as measured by a thermocouple (type K) fitted at the feed/membrane interface. The retentate solution was re-dispersed into the feed mixture, forming a continuous upstream loop. In addition to the use of a relatively large volume of feed solution (~1.5 dm^3), sampling volumes were kept low (~1 cm^3) to minimise changes in feed composition during experimental runs.

A rotary vane vacuum pump (9) evacuated the shell side of the membrane to 0.4 kPa (measured by a downstream pressure gauge, 4). The total transmembrane pressure was 90 kPa. Permeate vapour was collected and condensed by two liquid nitrogen impingers in parallel (cold traps 7 and 8, controlled with valves 5 and 6). The pervaporation unit was allowed to reach steady-state permeation over a period of 90 min (using cold trap 7) before collecting experimental data samples in cold trap 8.

Permeate samples were accurately weighed and analysed by gas chromatography (GC, HP series 6985; manual injection). The instrument was equipped with a flame ionisation detector (FID) and a polyethylene glycol column (HP-FFAP, 30 m × 0.53 mm i.d., 1.0 μm film thickness; J&W Scientific), using nitrogen as carrier. The column head pressure was fixed at 32 kPa, oven temperature constant at 87 °C and injector (splitless) and detector temperatures 230 and 220 °C respectively.

Sample composition was based on EtOH concentration. Acetonitrile (CH_3CN, 99.8 %; Riedel-de Haën) was used as internal standard at a fixed concentration of 1.2 wt.%. For each set of experiments a new calibration curve was drawn up, and the regression coefficients (R^2) for these analyses always exceeded 0.993. The EtOH fractions in feed and permeate samples were determined directly, while the H_2O fractions in these samples were calculated by subtraction. H_2O/EtOH selectivity was expressed as

$$\alpha_{W,E} = \frac{(z_W / z_E)_{\text{Permeate}}}{(x_W / x_E)_{\text{Feed}}} \qquad (4.11)$$

with $z_{W,E}$ representing the permeate and $x_{W,E}$ the feed mole fractions of H_2O ($_W$) and EtOH ($_E$) respectively.

For each membrane, the selectivity and flux values are reported as the average of three independent measurements. Within these individual measurements, selectivity values deviated by less than 5 %, while flux measurements were all within a standard deviation range of 2 %.

4.3.3.3 Calculations

Fugacity calculations for the mixture components were based on the theoretical formulas as indicated; the saturated vapour pressures were computed by means of the extended Antoine equation, while the respective activity coefficients were generated by modeling software (Aspen Plus® version 10.1, using the UNIQUAC module). All other calculations involved the actual experimental values for pressure, concentration and layer thicknesses as set out in each section.

4.4 RESULTS AND DISCUSSION

4.4.1 MEMBRANE FORMATION

4.4.1.1 Time-dependent layer morphology

Morphological features of the membrane layers are shown as a function of synthesis time (t_c) in Fig. 4.3. The micrographs present a top view of each membrane after a single stage synthesis. (Note that the layer at t_c 1.5 h, Fig. 4.3**a**, was discontinuous even after a two-stage synthesis and was thus not regarded as a separation layer, but is included here for illustrative purposes.) The synthesis of these layers was based on our previous work [15] where we described how supported NaA layer formation from a clear solution occurs over time. This time-dependent layer growth can be subdivided into two distinct, consecutive morphologies. Firstly, the formation of a homogeneous layer of hemisphere-shaped grains (Fig. 4.3**b**, t_c = 2.0 h) and secondly, a densely intergrown layer of cubic morphology (Fig. 4.3**f**, t_c = 4.0 h). The intermittent layers at t_c = 2.5, 3.0 and 3.5 h represent, in order, a transformation event from the first into the second morphology type.

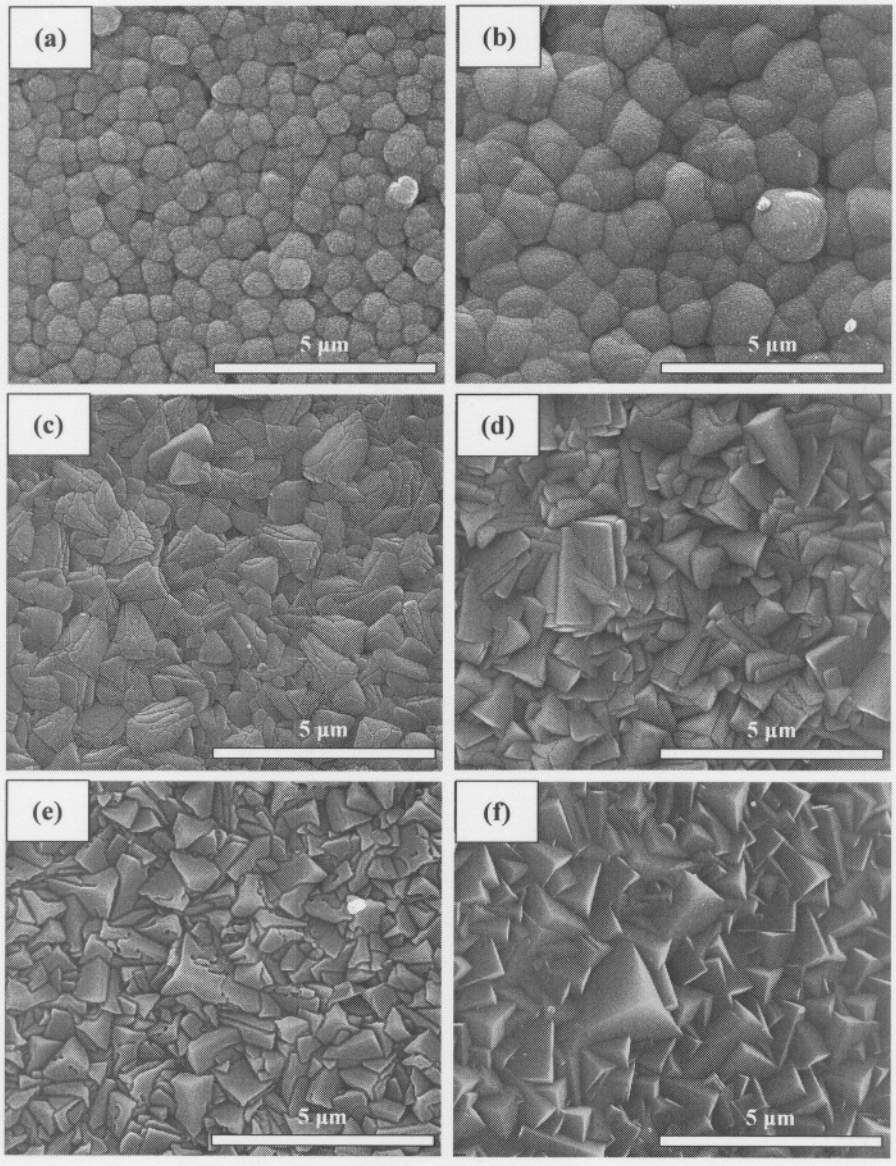

Figure 4.3: SEM imaging of NaA membrane formation over time, t_c. Top views of single layered membranes after t_c = 1.5 h **(a)**, 2.0 h **(b)**, 2.5 h **(c)**, 3.0 h **(d)**, 3.5 h **(e)** and 4.0 h **(f)**.

The chronological order of the formation events can be briefly summarised as follows [15]:

- t_c 1.0 h (not shown): An amorphous gel layer, consisting of colloidal aluminosilicate species, is deposited on the support surface, during which nucleation occurs mainly by way of the autocatalytic mechanism.

- t_c 1.5 h: Small clusters of nuclei start to coalesce and crystallise to form a matrix of crystallite clusters in close proximity to each other.

- t_c 2.0 h: The intergrowth of neighbouring crystallite clusters leads to the development of hemisphere-shaped grains. Amorphous material is still occluded between the grains, indicating high levels of supersaturation.

- t_c 2.5 h: The crystal surfaces become fractionised into additional growth planes, marking a change in the layer morphology. This change is related to a drop in supersaturation levels as well as the lateral pressure developing between neighbouring crystals.

- t_c 3.0 h: The additional growth planes on each crystal start to fuse together to form larger, defined crystal faces. The round edges show that fusion and growth proceeds rapidly.

- t_c 3.5 h: The fractionised crystal surfaces are still prominent, but the fusion process is drawing to an end.

- t_c 4.0 h: Crystal faces are now well-defined into the cubic morphology. Sharp edges indicate that nutrients are depleted and growth has ended.

The formation of the polycrystalline NaA layer over time can thus be regarded as a gradual solid-phase transformation, where morphology transition and intergrowth between adjacent crystallites leads to larger, shape-defined crystals.

4.4.1.2 Zeolite crystallinity

The XRD assessments revealed that all growth layers (t_c 1.5-4.0 h) contained zeolite NaA without any preferred orientation of the individual crystallites and/or crystals. No crystalline impurities were detected within the membrane layers over the time range investigated. The crystallinity of

the hemispheric layer at t_c 2.0 h was estimated at ~70 %, based on the spectral peak-to-noise-height ratio (see Ref. [15] for more detail on the calculation). No specific crystallinity values were assigned to the intermediate layers from t_c 2.5-3.5 h, but an increasing degree of crystallinity over time was presumed here. The layer with cubic morphology at t_c 4.0 h represented a fully crystalline membrane. These estimations were supported by the cross-sectional SEM images, especially for the 2.0 h layer (Fig. 4.4**a**) where the fractured surface did not show the clean-break resolution typical for crystalline material. In contrast, the 4.0 h layer showed a sharply-edged break surface (Fig. 4.4**b**).

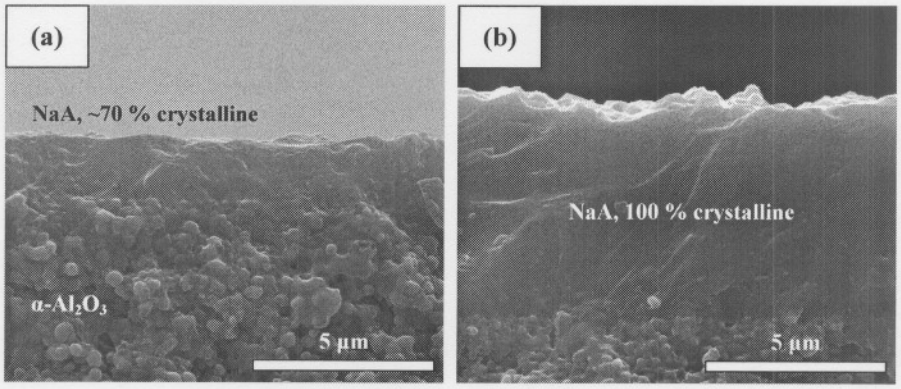

Figure 4.4: Cross-sections through the double layered zeolites corresponding to synthesis times of 2.0 h **(a)** and 4.0 h **(b)** respectively.

4.4.2 PERVAPORATION

4.4.2.1 Choice of operating conditions and support types

Experimental feed streams for pervaporation were maintained at a fixed concentration of 95 wt.% EtOH. At this feed composition the adsorption site occupancy of H_2O on the feed side of the zeolite is expected to be marginally incomplete and the separation selectivity would give a good qualitative indication of the extent of intercrystalline diffusion through the zeolite layer. Furthermore, since diffusion is an activated process, a standard operating temperature of 45 °C was chosen to provide fluxes high enough for meaningful comparison between the different growth layers, while ensuring that the feed streams remained in liquid form. In addition, the operating conditions offered a convenient platform for easily benchmarking the performance of our membranes to those published in literature.

The two support types used in this study were selected to investigate the influence of contrasting support structures on the integrity of the zeolite layer. Surface roughness and porosity can influence not only the zeolite crystal size, but more importantly, also the layer thickness needed for achieving layer continuity. Fig. 4.5 shows the structural difference between the experimental supports.

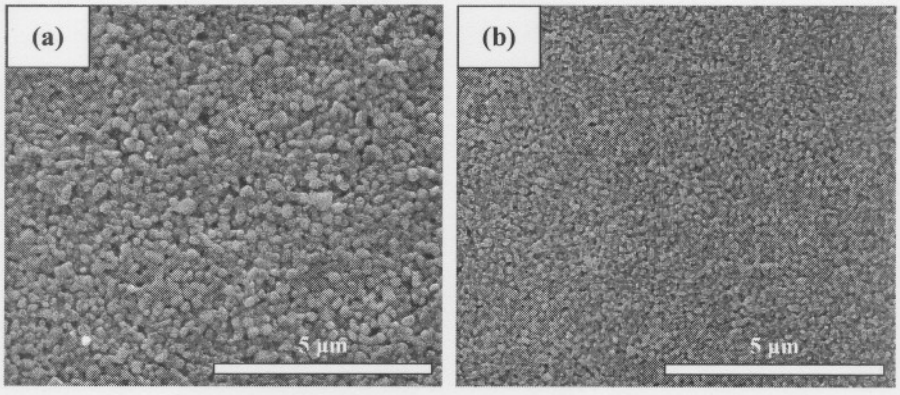

Figure 4.5: Top view electron micrographs for the surfaces of support type 1 **(a)** and support type 2 **(b)**. The microstructural properties are given in Table 4.1.

Due to the difference in particle sizes, support type 1 provided a coarser surface with deeper porosity and indentations than support type 2. In theory one would expect the smoother surface of support type 2 to facilitate more uniform intergrowth between zeolite crystals and therefore, membrane layers with higher selectivity qualities. The only disadvantage of these casted supports is that the packing density and microstructure extends through the bulk of the support, meaning that support type 2, despite offering clear benefits for zeolite growth, poses a stronger resistance to mass transfer. In terms of permeation flux, support type 1 should then allow a higher through-put rate or productivity than type 2.

Keeping these factors in mind, we initially synthesised the whole series of NaA layers (t_c 2.0-4.0 h) on support type 1, followed by a selection of the best performing membranes thus obtained, on support type 2. In this way, the basic repeatability of the different zeolite growth layers could also be confirmed. Details of all the samples prepared for pervaporation testing are listed in Table 4.2.

Table 4.2: Properties for experimental pervaporation membranes

Membrane no.	Support type	t_c (h)	Zeolite layers	Estimated crystallinity (%)	Layer thickness, *lz* (μm)
JZM_09	1	2.0	2	70	1.7
JZM_10	1	2.5	2	>70	3.0
JZM_11	1	3.0	2	>>70	5.3
JZM_12	1	3.5	2	near 100	5.7
JZM_06	1	4.0	1	100	2.8
JZM_07	1	4.0	2	100	6.3
JZM_13	2	2.0	2	70	2.0
JZM_14	2	3.5	2	near 100	5.0
JZM_15	2	4.0	2	100	5.7

4.4.2.2 Separation through growth layers on support type 1

All double layered membranes prepared on support type 1 were highly selective towards H_2O with $\alpha_{W/E}$ values ranging between 4 600 (for t_c 3.0 h) and 12 500 (for t_c 3.5 h). Fig. 4.6 presents the selectivity and total pervaporation flux as time-dependent functions of zeolite synthesis.

The selectivity of the 2.0 h layer was relatively high at 9 000, followed by a decreased separation trend in the intermediate 2.5 and 3.0 h layers ($\alpha_{W/E}$ of 4 700 and 4 600 respectively). The layer at t_c 3.5 h exhibited the highest separation capability with $\alpha_{W/E}$ = 12 500, while the 4.0 h layer ($\alpha_{W/E}$ = 8 300) was comparable in selectivity to the 2.0 h layer.

Many authors agree that high selectivity values should be interpreted with discretion, since the expression of selectivity (Eq. 4.11) is a calculated ratio of ratios. Small changes in feed or permeate compositions can therefore translate into relatively large differences in selectivity values. Despite thereof, we found that the selectivity trend observed in Fig. 4.6 could be rationalised in terms of the morphological and crystallinity variations between the progressively synthesised layers as described in the previous section.

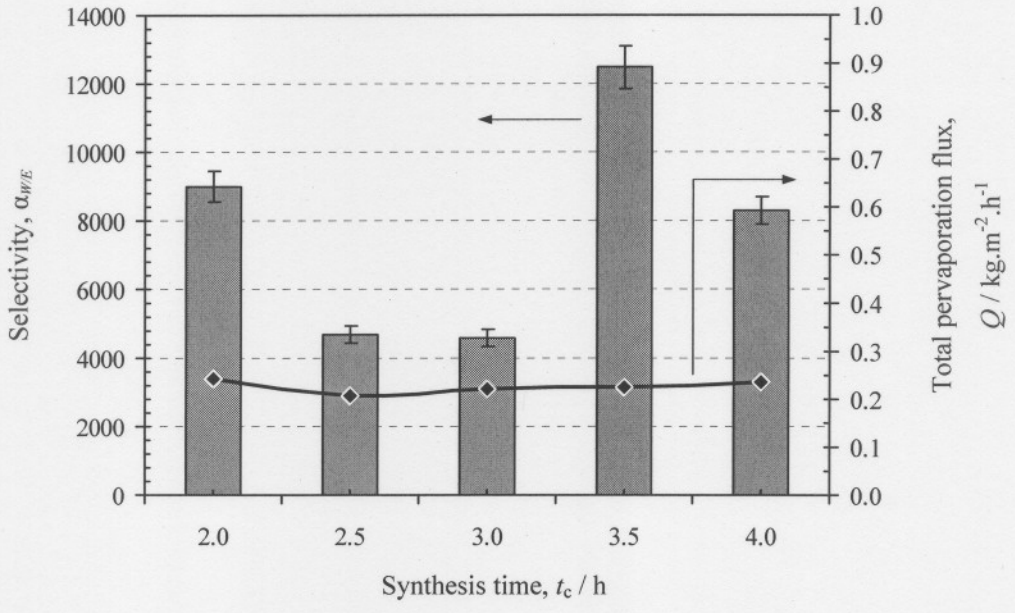

Figure 4.6: Influence of synthesis time on the H_2O/EtOH separation performance of individual NaA membranes after a two-stage synthesis each, using support type 1. Selectivity (columns) is related to the left ordinate and total pervaporation flux (♦, solid line) to the right.

After a 2.0 h synthesis the relative crystallinity of the hemisphere-shaped layer was only ~70%. This layer could therefore be regarded as a collection of growing NaA crystals embedded in an amorphous gel matrix. The gel phase comprises precursor species of aluminosilicate from which nutrients are provided for crystal growth [38]. The development of the NaA layer over time is therefore associated with the dissolution of the amorphous material, and hence an increase in overall crystallinity (see Table 4.2). Furthermore, the amorphous material is mainly located at the perimeter of the growing crystals, implying that neighbouring crystals can only intergrow completely when all amorphous material is disseminated. For the 2.0 h layer this meant that the intercrystalline voids and grain boundaries were still filled with amorphous (gel) material acting as a non-crystalline membrane sealant. This probably afforded the membrane with high selectivity, despite the fact that the polycrystalline component of the zeolite layer was not fully intergrown yet.

Whether the amorphous phase is completely impermeable to the feed components is not known at this stage. It is however known that the adsorption capacity of this material (for H_2O and EtOH) is far less than that of purely crystalline NaA, because the zeolitic microporosity has not been

fully established yet [39]. Due to its ionic strength, the gel phase should also be preferentially hydrated. If a certain degree of diffusion through the amorphous material is therefore assumed to occur, it is reasonable to accept that such permeation is H_2O-selective and takes place much slower than through the crystalline phase.

Based on these observations, the decreased selectivity in the layers at t_c 2.5 and 3.0 h was related to the progressive dissolution of the amorphous material in these layers, leaving the intercrystalline porosity and non-intergrown grain boundaries exposed. The contribution of non-zeolitic diffusion to the total transmembrane diffusion was therefore higher in these layers than in the semi-amorphous layer at t_c 2.0 h. After synthesis times of 3.5 and 4.0 h however, the polycrystalline boundaries had begun to intergrow and the selectivity trend increased as a result of lowered intercrystalline diffusion. The difference in $\alpha_{W/E}$ values between the 3.5 and 4.0 h layer was partially attributed to the morphological difference between the layers. After 3.5 h the crystal surfaces were still prominently fractionised, leading to a higher zeolitic surface area-to-volume ratio than for the fully developed 4.0 h layer with complete cubic morphology (see Fig. 4.3**e** & **f**). Since H_2O is preferentially adsorbed, the higher membrane surface area could have lead to a marginally higher feed side coverage of H_2O which, to a certain degree, could account for the selectivity maximum in the 3.5 h layer. A more likely explanation, though, would be that an incremental quantity of amorphous gel was still present after 3.5 h, selectively sealing the grain boundaries during the final stages of crystallisation. Judging from the selectivity drop from 3.5 to 4.0 h, this final fraction of amorphous material is probably consumed without further tightening of the intercrystalline boundaries as they had been formed after 3.5 h.

While observing a defined interdependence between selectivity and synthesis time, Fig. 4.6 shows that the pervaporation flux was mainly independent of synthesis time. Total flux values remained fairly constant at $Q \sim 0.23$ kg.m^{-2}.h^{-1} over the whole duration of synthesis, bearing no clear relation to the increasing zeolite thickness indicated in Table 4.2 (for support type 1). Since flux is a known function of zeolite layer thickness, results showed that the support's resistance to the total transmembrane diffusion was significantly high for support type 1. Further discussions on support resistance will follow in section 4.4.2.5.

4.4.2.3 Separation through growth layers on support type 2

Based on the separation results for support type 1, the three best performing zeolite layers were repeated on support type 2, that is, double layers at t_c 2.0, 3.5 and 4.0 h. This was done to

determine whether a similar selectivity trend could be observed. Fig. 4.7 illustrates the results for the time-dependent layers on support type 2.

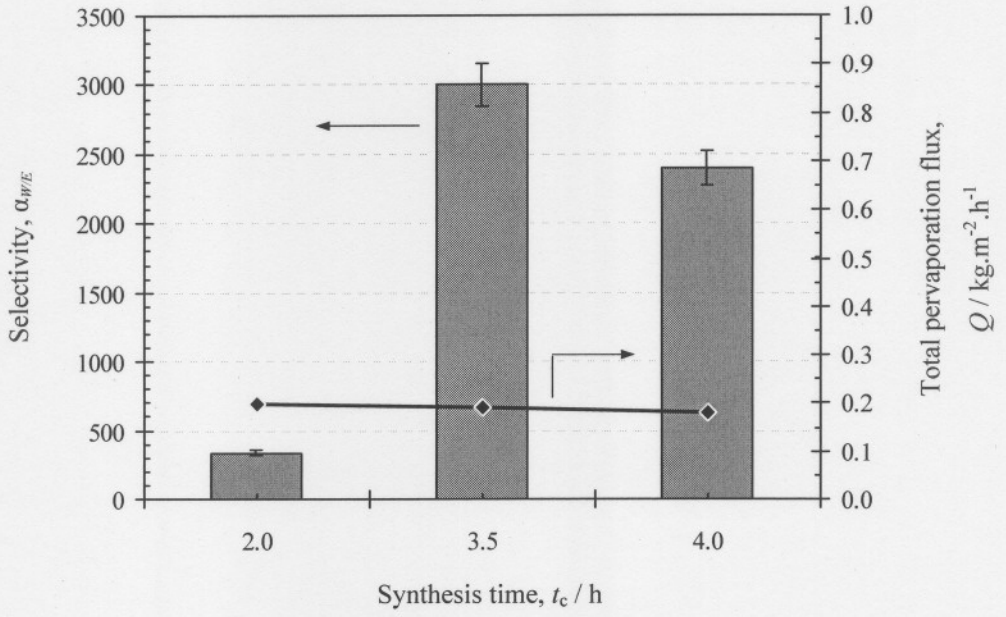

Figure 4.7: H_2O/EtOH separation as a function of synthesis time on support type 2. Selectivity (columns) is presented on the left ordinate and total pervaporation flux (♦, solid line) on the right.

The general selectivity trend on support type 2 remained the same, with the 3.5 h layer still achieving the highest selectivity ($\alpha_{W/E}$ = 3 000), followed by a slightly decreased separation capability for the 4.0 h layer ($\alpha_{W/E}$ = 2 400). The semi-crystalline 2.0 h layer though, performed rather worse than either these membranes with $\alpha_{W/E}$ = 340, indicating that considerable non-selective, intercrystalline diffusion occurred. Despite their different selectivities and layer thicknesses (Table 4.2), average fluxes for all three membranes remained comparable at $Q \sim 0.19$ kg.m^{-2}.h^{-1}, showing that the type 2 support also imparted a significant resistance to permeation. Flux values were somewhat lower than for support type 1, as to be expected from the smaller support pore diameter.

4.4.2.4 Support type 1 versus support type 2

Contrary to our expectations, all separation factors for the type 2 membranes were distinctly lower than for their counterparts synthesised on support type 1. Table 4.3 gives a comparative summary of the performance characteristics for the two sets of experiments.

Table 4.3: Summary of the results obtained for different growth layers (two-stage syntheses for t_c 2.0, 3.5 and 4.0 h) relative to the two support types used

Support type	l_z (μm)			$\alpha_{W/E}$ (-)			Q (kg.m^{-2}.h^{-1})		
	t_c 2.0	t_c 3.5	t_c 4.0	t_c 2.0	t_c 3.5	t_c 4.0	t_c 2.0	t_c 3.5	t_c 4.0
1	1.7	5.7	6.3	9 000	12 500	8 300	0.24	0.23	0.23
2	2.0	5.0	5.7	340	3 000	2 400	0.20	0.19	0.18

The fact that the basic selectivity trends for the growth layers on each support type were consistent (Figs. 4.6 & 4.7), confirmed the fundamental repeatability of the zeolite layers with regard to their individual performances. The reason for the universal drop in separation selectivity for the type 2 membranes therefore had to be related to a structural difference between the two support types. All material properties being equal, the only difference between the two types was their porosity and pore sizes. Nevertheless, no crack formation or poor zeolite adhesion to the support was visible under SEM in either instance. Also, no meaningful difference in the penetration depth of the zeolite layers into the different support porosities could be observed. These observations discarded the possibility that mechanical discrepancies between the two supports could have caused the variation in zeolite performance.

If we assumed that both supports were completely inert to the highly alkaline solution used for zeolite synthesis, theory would suggest a better layer integrity (and selectivity) on the smoother support surface of type 2, but this was not the case judging from the respective separation factors (Table 4.3). The difference between individual zeolite layers synthesised on the different support types is thus ascribed to the difference in chemical stabilities of the two supports; more specifically, the relative degrees of leaching of the alumina surface.

The dissolution of alumina at high alkalinity is a well-known phenomenon [40]. Even for α-Al_2O_3, which is expected to be more stable than other alumina phases (such as γ-Al_2O_3), it has

been demonstrated that a certain amount of aluminium-containing ions are released from the support during the hydrothermal treatment with alkaline solutions [41,42]. These "exogenous" ions can affect the local chemistry at the support surface during zeolite synthesis, and hence the composition of the zeolite layer itself.

Desset et al. [43] have shown that the α-Al_2O_3 surface partially transforms into aluminium hydroxides, such as gibbsite [$Al(OH)_3$], under the hydration conditions of hydrothermal treatment. Due to the high NaOH content of the synthesis solution, a plausible dissolution of this surface would then simply occur via the well-known Bayer extraction process [44]:

$$Al(OH)_{3(s)} + NaOH_{(aq)} \longrightarrow Na^+_{(aq)} + Al(OH)_4^-{}_{(aq)} \quad \text{(i)}$$

The consequence of leaching is therefore the discharge of soluble $Al(OH)_4^-$ ions into the synthesis gel, thereby changing the chemical composition of the synthesis mixture, particularly near the support surface. Interesting to note is that these tetrahedral aluminium ions can act as nutrients in the process of zeolite formation, since zeolite growth is mainly associated with the incorporation of monomeric silicate and aluminate anions into the growing crystal surfaces [45]:

$$[Zeo{\equiv}Al{-}OH]^- Na^+ + {}^-O{-}Si{\equiv} \rightleftharpoons [Zeo{\equiv}Al{-}O{-}Si{\equiv}]^- Na^+ + OH^- \quad \text{(ii)}$$

and

$$Zeo{\equiv}Si{-}O^- Na^+ + Al(OH)_4^- \rightleftharpoons [Zeo{\equiv}Si{-}O{-}Al(OH)_3]^- Na^+ + OH^- \quad \text{(iii)}$$

For high silica zeolites like MFI, the excess of $Al(OH)_4^-$ ions can merely be built into the zeolite framework in accordance to reaction (iii), changing the Si/Al ratio of the corresponding zeolite layer. For NaA with its Si/Al ratio of 1 however, the situation is not so straightforward. Since the NaA synthesis gel already contains an ample amount of $Al(OH)_4^-$ ions, the excess ions cannot be absorbed into the zeolite structure because the condensation-linkage of two adjacent aluminium-tetrahedra in the LTA framework is not possible (Loewenstein's rule [46]):

$$[Zeo{\equiv}Al{-}OH]^- Na^+ + Al(OH)_4^- \longrightarrow \text{no reaction} \quad \text{(iv)}$$

The leaching of alumina thus creates an over-supply of $Al(OH)_4^-$ ions and upsets the balance of alternating silicate and aluminate species reacting with each other. As a result, the growth of the zeolite layer is retarded, and it would be fair to presume that poor intergrowth occurs between crystals in the later stages of layer formation, leaving wider intercrystalline regions open to non-zeolitic diffusion.

Based on this theory, support leaching had its most detrimental effects on the type 2 layers. That is not to say that leaching did not occur on the type 1 support, only that the degree of leaching was more intense on the second type. The subordinate layer thickness of the type 2 layers confirms this statement. Although we were unable to express the exact crystallinity values for the zeolites relative to the two support types, it is also likely that the crystallinity of the type 2 layers were slightly less than their type 1 counterparts.

The difference in chemical stabilities is simply related to the pore surface areas of the respective supports. For support 1 we calculated a total pore surface of 42 m^2 per membrane, while support 2 exposed a total of 86 m^2 of pore surface to the synthesis solution. Since the dissolution of alumina is a surface-related process, the exaggerated leaching of $Al(OH)_4^-$ ions from the type 2 support is obvious.

Finally, we might add that a set of control experiments was conducted where both supports were subjected to a synthesis solution similar to the one used for membrane synthesis, but with the aluminium source omitted. Although the conditions of temperature (85 °C) and pH (13.5) were replicated, no zeolite formation on either of the two support types was observed after 2.0 h of hydrothermal treatment. The leaching effects were therefore assumed strong enough to restrict crystallisation from an aluminosilicate solution, but, at the same time, too weak to induce NaA formation in the absence of an external aluminium source.

4.4.2.5 Influence of support resistance

For low-resistance supports, the permeate side fugacity downstream ($z_i p^P$) corresponds to the fugacity at the zeolite/support interface (p_i^{zs}), because the resistance in the support layer is negligible. This means that increasing the driving across the composite (by increasing the temperature for example) relates linearly to an increased driving force over the zeolite layer. Where the support resistance is substantial however, a certain pressure-drop exists over the thickness of the support, so that the fugacity at the zeolite/support interface is somewhat higher than the permeate side fugacity.

For comparison, we determined the fugacity profiles for H_2O and EtOH across both support types, involving the zeolite layers at t_c 2.0, 3.5 and 4.0 h under the same testing conditions described above (i.e. ~95 wt.% EtOH feed at 45 °C). For simplicity, vapour flow through the supports was assumed to follow the Knudsen regime, and fugacities at the zeolite/support

interface were calculated using Eq. 4.9. Table 4.4 gives the fugacity values for the respective permeants at three locations on the pervaporation route – the liquid feed, the zeolite/support interface and the downstream permeate vapour.

Table 4.4: Permeant fugacities for pervaporation across different growth layers (two-stage syntheses for t_c 2.0, 3.5 and 4.0 h) relative to the two support types used, all at 45 °C

Support	Fugacity (kPa)					
	Feed, f^f		Zeolite/support interface, p^{zs}		Permeate, $(z.p^p)$	
Type 1	H_2O	EtOH	H_2O	EtOH	H_2O	EtOH
t_c 2.0	2.45	20.71	1.66	2.1×10^{-3}	0.39	3.5×10^{-4}
t_c 3.5	3.00	20.13	1.57	1.1×10^{-3}	0.39	1.9×10^{-4}
t_c 4.0	2.45	20.71	1.60	3.3×10^{-3}	0.39	5.7×10^{-4}
Type 2						
t_c 2.0	2.71	20.43	1.93	5.9×10^{-2}	0.39	8.1×10^{-3}
t_c 3.5	2.62	20.53	1.96	0.7×10^{-2}	0.39	1.0×10^{-3}
t_c 4.0	2.53	20.62	1.88	0.9×10^{-2}	0.39	1.3×10^{-3}

For all three zeolite layers the permeate side fugacities for H_2O, for both support types, remained constant at approximately 0.4 kPa. This was found in spite of the small experimental variations in the feed concentration, showing that H_2O adsorption on the zeolite surface is highly competitive, even at low activities in the liquid phase. The individual feed and permeate fugacities for EtOH, on the other hand, showed a resemblance to the selectivity values obtained for each membrane layer (compare Table 4.3). On average, the permeate fugacities of EtOH were higher for the type 2 membranes, which is to be expected from their lower separation performances described earlier.

The fugacity values at the zeolite/support interface confirm that the resistances from both support types were significant for pervaporation across all the membrane layers. For support type 1, the interfacial H_2O fugacities were about 4 times higher than the corresponding permeate values, while this ratio increased to about 5 for the type 2 membranes. Considering that the interfacial

fugacities for EtOH were about three orders of magnitude smaller than that of H_2O, the support resistance primarily influenced the flow of H_2O through the membranes.

To point out the difference between the supports, we normalised the fugacity for each component by expressing it as a fraction of the feed fugacity. Fig. 4.8 displays the relative fugacities (f / f^f) for the 4.0 h double layer across the respective support types. (Note that these profiles purely reflect the fugacity values at the different membrane interfaces, and not the actual concentration of species within each membrane section.)

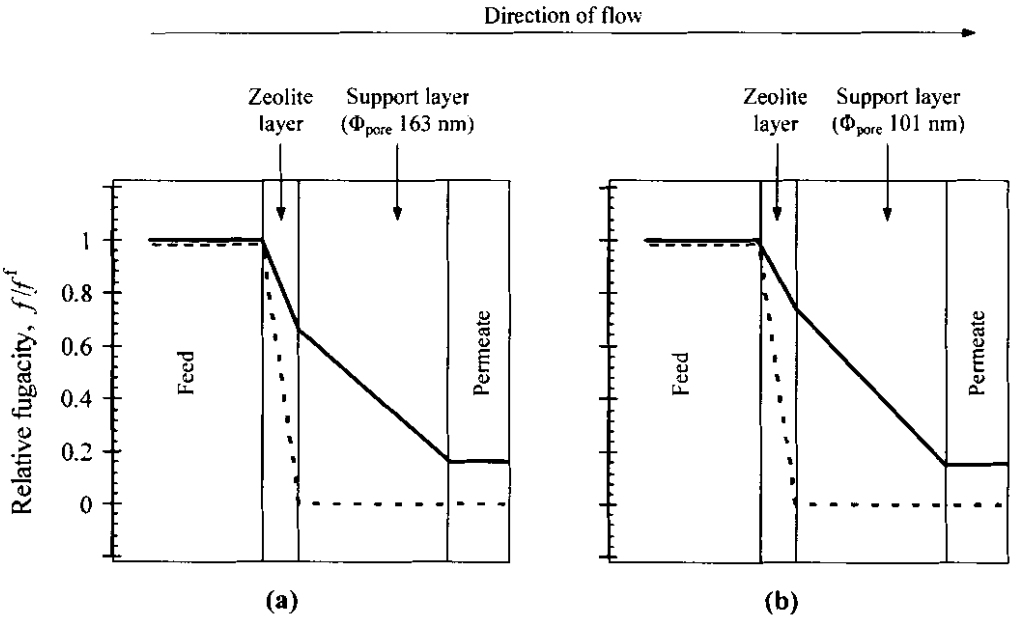

Figure 4.8: Relative fugacity profiles for mixture pervaporation through the 4.0 h double layered zeolite on support type 1 **(a)** and support type 2 **(b)**: ——H_2O; - - -EtOH. Feed concentration (95 wt.% EtOH), temperature (45 °C) and permeate total pressure (0.4 kPa) were similar in both instances. Knudsen flow was assumed through the supports and concentration polarisation was considered negligible.

Since all membranes were subjected to the same testing conditions, the total fugacity gradient for H_2O across both 4.0 h composites was similar at $\left(x_W \gamma_W p_W^\circ - z_W p^P\right) \approx 2.1$ kPa. For EtOH the total fugacity gradient was somewhat higher at $\left(x_E \gamma_E p_E^\circ - z_E p^P\right) \approx 20.6$ kPa, because the feed-side activity and saturated vapour pressure for EtOH under these conditions were higher. On the lower resistance support (Fig. 4.8**a**) the zeolite/support fugacity for H_2O decreased to a 0.65

fraction of its original value in the feed solution, while on the type 2 support (Fig. 4.8**b**) the relative H_2O fugacity at the zeolite/support interface was still 0.74. For the H_2O component of the mixture, these values indicated a clear decrease in the driving force over the selective zeolite layer, going from the lower to the higher resistance support. According to the resistance-in-series model, support type 1 contributed 59 % of the total resistance to H_2O permeation across the 4.0 h composite, while the resistance from the type 2 support was even higher at 69 %.

It is of interest to note that the relative fugacity profiles for EtOH were similar across both support types due to the high H_2O selectivity of the membranes. Since the interfacial and permeate fugacities for EtOH were so small relative to the feed values (see Table 4.4), the support influence on EtOH flow could actually be neglected, again showing that the support resistance mainly influenced the driving force for H_2O across these hydrophilic composite membranes.

4.4.2.6 Driving force limitation

The previous section clearly demonstrated how the two different supports exerted different limitations on the driving force over the selective zeolite layer, under fixed conditions of feed concentration, temperature and permeate pressure (i.e. a fixed driving force). To examine the level of support resistance as a function of an increasing driving force, we conducted a series of pervaporation experiments over a temperature range of 30-60 °C. For this purpose we chose a single membrane – the 3.5 h zeolite layer (double synthesis) prepared on the higher resistance support, type 2 (sample JZM_14, Table 4.2). The feed composition (95 wt.% EtOH) and permeate vacuum were the same as for the previous experiments so that the driving force was manipulated only by increasing the temperature. Pertaining to H_2O permeation, Fig. 4.9 portrays the molar flux, as well as the effective driving force over the zeolite layer, as functions of the applied driving force (fugacity gradient) over the composite membrane.

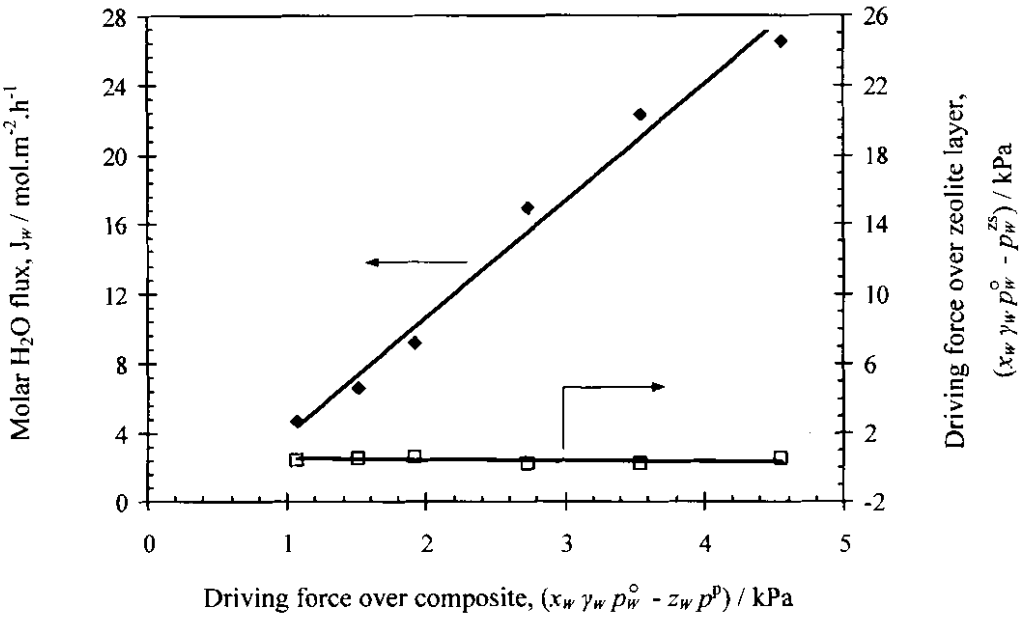

Figure 4.9: Influence of the applied driving force for H_2O on the molar flux (♦) and the effective driving force over the zeolite layer (□), using pervaporation across the 3.5 h double layered zeolite on support type 2.

As to be expected from Eq. 4.8, the experimental H_2O flux through the composite responded linearly to the applied driving force, increasing from 4.7 mol.m^{-2}.h^{-1} at 30 °C to about 22.4 mol.m^{-2}.h^{-1} at 60 °C. This relation seems simple enough, but the origins of the increased H_2O flux have to be considered carefully, because Fig. 4.9 shows that the effective driving force over the zeolite layer remained more or less unchanged over the temperature range investigated. Since the permeate pressure remained constant, this means that the fugacity gradient over the support layer had to increase; in other words, the fugacity of H_2O at the zeolite/support interface had to increase in reply to the rising fugacity gradient over the composite membrane. At 30 °C the experimental feed-side fugacity was ~1.4 kPa, with a corresponding interfacial fugacity of 1.1 kPa. At 60 °C, the feed-side fugacity had increased to 4.0 kPa, while the interfacial fugacity at this temperature was calculated at ~3.7 kPa. The support resistance therefore limited the driving force achievable over the zeolite layer.

4.4.2.7 *Layer permeance and the influence of temperature*

Keeping in mind that temperature influences not only the driving force, but also the permeability dynamics of the membrane [32], the relation between flux and driving force in Fig. 4.9 could only describe the H_2O flux through the composite membrane as a resultant effect of the changing driving force and membrane permeability. It also failed to express the fundamental driving force and permeability differences that exist between the zeolite and support layer.

A simple way to isolate the contribution of permeability from that of driving force is to divide the flux by the driving force (see Eq. 4.8), so that the membrane permeance is obtained. Since the flux-force relation is generally linear, the permeance is usually independent of the driving force. Exploring the influence of temperature on the permeance then provides insight into the permeability properties of the membrane. If the permeance remains a constant (equal to the slope of the flux-driving force function) it means that the membrane permeability is also constant, but if the permeance changes with temperature, it signifies a change in the membrane permeability at different temperatures. In such a case the permeance is no longer independent of the driving force.

Considering that the fugacity gradients over both the zeolite and the support layers were known, we could separately determine the permeance of the zeolite layer, by rearrangement of Eq. 4.8, as

$$\text{Permeance}_{i(\text{zeolite})} = \frac{J_i}{(x_i \gamma_i p_i^{\circ} - p_i^{zs})} = \frac{P_{Bi(\text{zeolite})}}{lz} \tag{4.12}$$

Similarly, the permeance of the support layer was determined by rearrangement of Eq. 4.10, as

$$\text{Permeance}_{i(\text{support})} = \frac{J_i}{(p_i^{zs} - z_i p^{p})} = \frac{\varepsilon D_{Kn}}{lsRT} \tag{4.13}$$

The relation between the individual H_2O permeances of the zeolite and support layer of the exemplary JZM_14 membrane, and temperature, is given in Fig. 4.10.

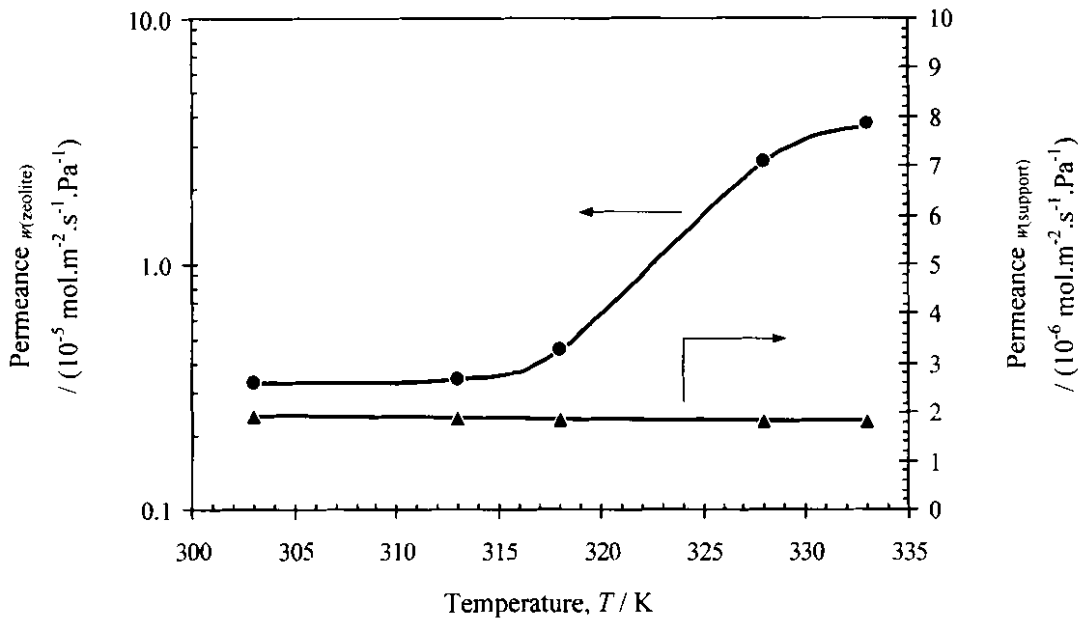

Figure 4.10: Influence of temperature on the H_2O permeance of the zeolite layer (●, left ordinate) and the H_2O permeance of the support layer (▲, right ordinate), using pervaporation across the 3.5 h double layered zeolite on support type 2.

Generally speaking, the H_2O permeance in the zeolite layer increased as a function of temperature, ranging about ten-fold from 0.33×10^{-5} mol.m^{-2}.s^{-1}.Pa^{-1} at 30 °C, to 3.73×10^{-5} mol.m^{-2}.s^{-1}.Pa^{-1} at 60 °C. Seeing that the fugacity gradient over the zeolite remained fairly constant and the zeolite thickness was invariable, it meant that the permeability of H_2O in the zeolite increased correspondingly (cf. Eq. 4.12). However, permeability at a given temperature is determined by the adsorption and diffusion coefficients for H_2O at that temperature. Although we have not determined these coefficients experimentally, it is unlikely that the adsorption of H_2O on the zeolite changed significantly over the temperature range depicted here. While it is true that elevated temperatures would theoretically decrease the adsorption of H_2O on the zeolite, the feed solution was still completely liquid and the temperatures tested were probably too low to significantly alter the adsorption behaviour. The important factor is the strong H_2O affinity of the NaA zeolite, stabilising the adsorption coverage of H_2O at near-saturated conditions across the whole temperature series. As mentioned before, the fugacity gradient across the zeolite did not change much with temperature either, keeping the driving force for adsorption practically constant. This argument is supported by literature where the separation factors for zeolite-based H_2O/EtOH pervaporation were correlated to the fugacity ratios of these components in the liquid feed [24]. It was suggested that competitive adsorption depended on these ratios, in other words

the relative coverages of H_2O and EtOH at the feed-side of the zeolite depended on their fugacity ratio in the feed. As the feed concentration was kept constant (i.e. a constant fugacity ratio), we also found the separation factor for the membrane under discussion to remain fairly constant with rising temperature (results not shown), showing that the feed-side coverage of H_2O probably remained constant during these low-range changes in temperature.

The increase in permeance, for the zeolite layer, is therefore largely attributed to an increased diffusivity of H_2O through the zeolite at higher temperatures. The shape of the curve in Fig. 4.10 supports this notion, showing that the permeance is not linearly related to temperature but roughly follows the Arrhenius-type exponential relation, which is eminent for diffusion through zeolite membranes. Accordingly, Fig. 4.10 implies that a certain maximum will exists for the mixture diffusivity of H_2O in the zeolite, even though it still remains an activated process over the depicted temperature range. Such a maximum seems reasonable, because the mobility of species within the zeolite framework can only increase up to the saturation capacity of the zeolite, and from there only to a point where frictional forces and molecule-wall interactions become limiting. Earlier work by Okamoto et al. [23] strengthens this view, suggesting that the diffusion of H_2O, rather than adsorption, is the rate-determining step for H_2O permeation through the zeolite.

It is important not to regard the suggested maximum as the true maximum permeance achievable for this membrane. In the current situation, the build-up of pressure at the zeolite/support interface limited the coverage gradient of H_2O across the zeolite. The diffusivity, and thus permeance, was therefore also restricted by the driving force limitation across the zeolite.

Contrary to the surface diffusion through the zeolite, which is preceded by an adsorption step, the major mode of transport through the support is Knudsen diffusion. Adsorption in the support is insignificant and the main determinant of transport is the mean free pathlength traversed by the permeating molecules before bumping into the wall of the support pore. Since molecule mobility (kinetic energy) is a direct function of temperature, the temperature also plays a fundamental role in determining the overall diffusion kinetics through the support. In this regard, Fig. 4.10 might be somewhat misleading in showing that the permeance through the support remained largely independent of temperature, varying only slightly from 1.92×10^{-6} $mol.m^{-2}.s^{-1}.Pa^{-1}$ at 30 °C to about 1.83×10^{-6} $mol.m^{-2}.s^{-1}.Pa^{-1}$ at 60 °C. Considering the mechanism of Knudsen diffusion (Eqs. 4.9 & 4.10), the increase in temperature on one level should have enhanced the Knudsen diffusivity in a square root-type fashion. Our calculations showed an incremental increase in D_{Kn} from 0.178 $cm^2.s^{-1}$ at 30 °C, to about 0.187 $cm^2.s^{-1}$ at 60 °C, which should influence the

Knudsen flux in a positive way. On another level, the Knudsen flux is inversely proportional to the permeation temperature itself [47], implying a drop in permeation with rising temperature. Yet the overall flux through the composite membrane, and therefore also the support, increased as a function of temperature.

The logic here seems contradictory, but in fact it only shows that temperature influences the permeation process through the support on opposing levels and the observed flux is merely a nett effect of these balancing forces. For the tested membrane sample, the inhibitory effect of temperature was merely overridden by the increasing driving force across the support, as demonstrated earlier. As a result, the Knudsen flux increased almost linearly with the rising driving force, which means that the support permeance remained more or less constant.

Although it has been established that the total measured flux, and therefore also the permeance, for the composite membrane was mainly related to the flow of H_2O, it is interesting to outline the influence of temperature (driving force) on the shared permeation of EtOH. For the same JZM_14 sample, Fig. 4.11 shows the molar EtOH flux, as well as the effective driving force over the selective zeolite layer, as functions of the applied driving force across the composite membrane.

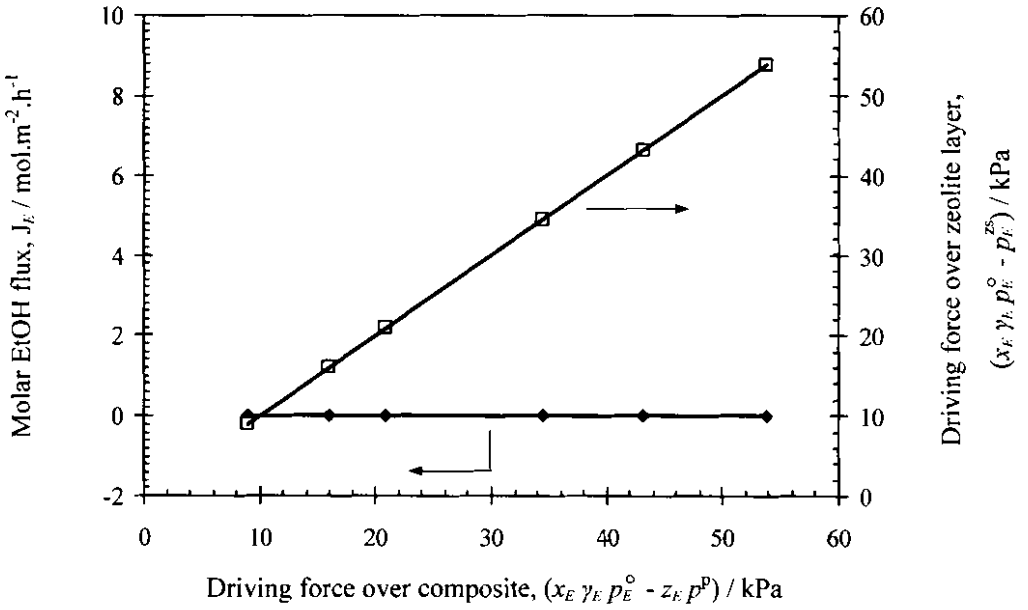

Figure 4.11: Influence of the applied driving force for EtOH on the molar flux (♦) and the effective driving force over the zeolite layer (□), using pervaporation across the 3.5 h double layered zeolite on support type 2.

The driving force for EtOH over the zeolite increased proportionally to the increasing driving force over the composite – the exact opposite of what has been observed for H_2O (compare Fig. 4.9). Due to the extreme selectivity of the zeolite, however, the flux for EtOH remained practically negligible at $\sim 3 \times 10^{-3}$ mol.m^{-2}.h^{-1}, across the whole temperature range.

In summary we may infer that the resistance exerted by the support strongly depends on the flux of the permeating species through the membrane; this resistance increases as the flux increases. In turn, the species in the separation mixture which is affected most, is mainly determined by the zeolite layer selectivity.

4.4.2.8 Layer permeability

The adsorption coverage of species on the zeolite depends on the relative fugacities in the feed solution. As long as this adsorption obeys Henry's law, the coverage is expected to increase linearly with fugacity, but as the adsorption behaviour transgresses from the Henry into the Langmuirian region, the coverage becomes limited by the saturation capacity of the zeolite. Since we assumed that the feed-side coverage for H_2O under the given conditions were already near-saturated, the preceding section showed that the permeability of a single NaA membrane then probably becomes a strong function of the diffusivity of H_2O. For the morphologically different zeolite layers used in this study, however, one has to consider that the diffusivities for the different layers at a certain temperature may be different, due to the amorphous content in the intermediate layers. In addition, the saturation capacities of these semi-crystalline layers should also be different.

To gain some insight into these essential differences between the respective morphology types, we determined the permeability constants for the entire series of double layered zeolites with regard to both permeants, and both supports, all at 45 °C (Fig. 4.12). The permeability constant is simply given by the product of the permeance and the zeolite thickness (see Eq. 4.12) and provides a normalised basis for comparing the intrinsic material differences between the morphology types [19].

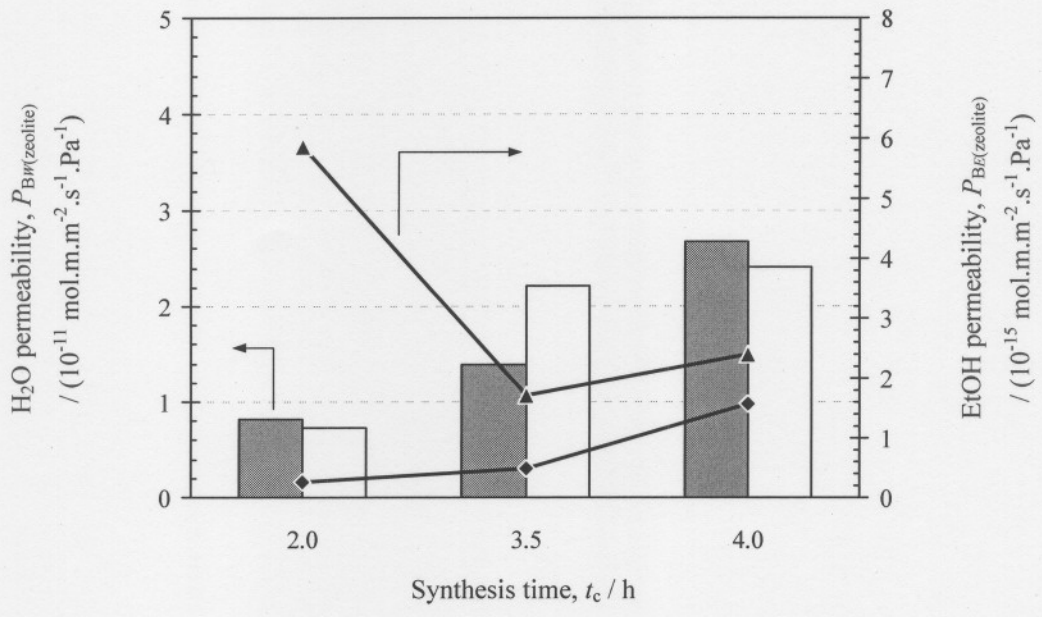

Figure 4.12: Zeolite layer permeability at 45 °C as a function of synthesis time (t_c 2.0, 3.5 and 4.0 h). H_2O permeability is related to the left ordinate and is shown by columns – dark columns represent the respective layers on support type 1, while the clear columns depict layers on support type 2. EtOH permeability is associated with the right ordinate, also for support type 1 (♦) and type 2 (▲).

Fig. 4.12 shows that the H_2O permeabilities of the zeolite layers increased as a function of synthesis time. For the type 1 layers, the values varied between 0.8×10^{-11} mol.m.m^{-2}.s^{-1}.Pa^{-1} for the 2.0 h zeolite, and 2.7×10^{-11} mol.m.m^{-2}.s^{-1}.Pa^{-1} for the 4.0 h zeolite. For the equivalent layers on support type 2, the H_2O permeabilities ranged from 0.7-2.4 $\times 10^{-11}$ mol.m.m^{-2}.s^{-1}.Pa^{-1}. The increasing tendencies, for both types, confirmed that the permeability through the zeolite layers was affected by their relative degrees of crystallinity, with the more crystalline layers exhibiting the higher permeabilities. This justifies our earlier assumption that the amorphous component in the 2.0 and 3.5 h layers has an inhibiting effect on the adsorption capacity and diffusivity of H_2O in these layers.

The permeability values of EtOH in the type 2 layers were distinctly higher than those on support type 1. The former values ranged from 5.9×10^{-15} mol.m.m^{-2}.s^{-1}.Pa^{-1} for the 2.0 h zeolite, to 2.4×10^{-15} mol.m.m^{-2}.s^{-1}.Pa^{-1} for the 4.0 h layer, while the EtOH permeabilities of their counterparts on support type 1 only ranged from 0.3-1.6 $\times 10^{-15}$ mol.m.m^{-2}.s^{-1}.Pa^{-1} for the

equivalent synthesis times. The generally increasing tendency for the layers on support 1 was in line with their increasing crystallinities, as was the case for H_2O, showing the same inhibitory effect of the amorphous component on the permeation of EtOH. However, the same scenario was not true for the type 2 layers. Here the 2.0 h zeolite had a much higher EtOH permeability than either the 3.5 or 4.0 h layers, referring back to the poor selectivity achieved by this membrane compared to all the other layers (see Table 4.3). Comparing the permeability values for the 2.0 h layer with respect to the two support types not only reaffirms that considerable intercrystalline diffusion took place across the type 2 membrane, but shows that this non-zeolitic permeation mainly increased the flow of EtOH, since the H_2O permeabilities for both support types were very similar.

4.4.2.9 Membrane performance – a literature comparison

As a benchmarking exercise, the separation capabilities of the membranes presented in this paper were compared to those published in literature. Table 4.5 provides a brief survey of the current state of the art for the NaA based pervaporation of H_2O/EtOH mixtures.

Table 4.5: Literature summary for the pervaporative separation of H_2O/EtOH mixtures, using NaA composite membranes under relatively similar conditions

Support material	Layer thickness, l_z (μm)	EtOH in feed (wt.%)	T_{pv} (°C)	Q (kg.m^{-2}.h^{-1})	α_{WE} (-)	Reference
SS[a]	5	95	40	0.11	150	[48]
Ceramic[b]	10	95	50	0.40	4 800	[49]
Mullite	NA	95	25	0.45	>10 000	[50]
α-Al_2O_3	30	95	75	1.10	16 000	[51]
α-Al_2O_3	5.7	95	45	0.23	12 500	This study
α-Al_2O_3	1.7	95	45	0.24	9 000	This study
TiO_2	3.5	95	45	0.5-0.80	<10 000	[52]

[a] Stainless steel
[b] Mullite/α-Al_2O_3/cristobalite
NA: not available

The selectivity of our membranes measured up well to NaA layers crystallised on other alumina-based materials. Considering the average zeolite thicknesses, this comparison shows that the direct in situ crystallisation technique produces favorable results when it comes to synthesising thin, continuous layers, especially when a reactive synthesis solution is used. With the exception of the TiO_2 based layers, all other membranes cited in Table 4.5 were produced by using seeding assisted methods. An important factor to remember is the general integrity of the support surface – the highly regular surface produced by the centrifugal casting technique also contributes to attaining layer continuity by direct synthesis, whereas seeding might be more beneficial when the support surface has an appreciable roughness, or the reactivity of the synthesis mixture is low [53].

Unfortunately the biggest drawback for our membranes was their low productivity rates (fluxes), due to the considerable support resistance as explained earlier. De Bruijn et al. [54] illustrated that for supports with pore diameters around 500 nm and smaller, the support resistance on pervaporation separations reported in literature became significant when the total flux exceeded ~80 $mol.m^{-2}.h^{-1}$ (~1.4 $kg.m^{-2}.h^{-1}$). The results from our work show that, for supports with pore diameters in the region of 100-200 nm, the resistance can become important even at fluxes as low as 11 $mol.m^{-2}.h^{-1}$ (0.2 $kg.m^{-2}.h^{-1}$), which is probably lower than what is normally expected.

4.5 CONCLUSIONS

This paper provided an extensive description of the H_2O/EtOH pervaporation differences between time-dependent layers of zeolite A supported on porous α-Al_2O_3 tubes. The influence of the support on the pervaporation process was also investigated by comparing similar zeolite layers synthesised on two structurally different supports (with pore diameters of 163 nm, type 1; and 101 nm, type 2, respectively).

Membrane selectivity was strongly correlated to the occlusion of amorphous material in each time-related layer. For the type 1 membranes, the selectivity of the initial 2.0 h layer (70 % crystallinity) was high at 9 000, due to the filling of intercrystalline regions with amorphous aluminosilicate. Lower selectivity in the intermediate layers (2.5 and 3.0 h) was explained by the progressive dissolution of this amorphous component, which exposed the grain boundaries to non-selective transport. Maximum selectivity was achieved after 3.5 h (α_{WE} = 12 500) where the crystals were firmly intergrown, but a small amount of gel was still trapped between crystals. At full crystallinity (4.0 h), α_{WE} again decreased to 8 300, showing that the transition between the

3.5 and 4.0 h layers only removed the final fraction of gel material, without further tightening of the intercrystalline junctions. The same general tendency was true for the type 2 layers, but the overall selectivity values (especially for the 2.0 layer) were lower than for the type 1 membranes. This was attributed to the accentuated dissolution of the type 2 supports during synthesis, causing an over-supply of liquid-phase $Al(OH)_4^-$ ions that inhibit zeolite intergrowth and intercrystalline pore filling.

Under fixed conditions of feed concentration (95 wt.% EtOH) and temperature (45 °C), the permeability of H_2O in the zeolite (for both membrane types) was a direct function of the crystallinity, due to the increasing microporosity and sorption capacity over time. It confirmed the strong preferential adsorption of H_2O in both the crystalline and amorphous phases, as well as in the intercrystalline pores. Despite their increasing permeabilities, the average fluxes within the two membrane types remained constant, showing that both support types exerted a significant resistance to the flow of H_2O.

Under conditions of increasing temperature (30-60 °C), it was shown that an increased driving force over a given composite (type 2, 3.5 h synthesis) did not necessarily translate into an increased driving force over the zeolite layer itself, due to the build-up of pressure at the zeolite/support interface. The increasing flux in such a situation was shown to probably depend on the increased diffusivity of H_2O in the zeolite layer at higher temperatures.

The given results should provide a foundation for the further development of pervaporation through composite zeolite membranes in general. More comprehensive research is needed on the relation between the intrinsic properties of the zeolite and the support layer, but also their combined influence on the performance of a given membrane.

4.6 ACKNOWLEDGEMENTS

The financial assistance of the Department of Labour (DoL), South Africa, towards this research is hereby acknowledged. Opinions expressed and conclusions arrived at, are those of the authors and are not necessarily to be attributed to the DoL. The authors wish to thank Dr. L. Tiedt (NWU, South Africa) for taking the SEM images, and Dr. S. Verryn (UP, South Africa) for the XRD analyses. We also thank Mr J. Kroeze (Technical Advisory - SST, NWU, South Africa) for crafting the membrane reactors and preparing the permeation setup.

4.7 REFERENCES

[1] H. Suzuki, Composite membrane having a surface layer of an ultrathin film of cage-shaped zeolite and processes for production thereof, US Patent 4,699,892 (1987).

[2] M. Noack, P. Kölsch, R. Schäfer, P. Toussaint, I. Sieber, J. Caro, Preparation of MFI membranes of enlarged area with high reproducibility, Micropor. Mesopor. Mater. 49 (2002) 25.

[3] G.T.P. Mabande, G. Pradhan, W. Schwieger, M. Hanebuth, R. Dittmeyer, T. Selvam, A. Zampieri, H. Baser, R. Herrmann, A study of Silicalite-1 and Al-ZSM-5 membrane synthesis on stainless steel supports, Micropor. Mesopor. Mater. 75 (2004) 209.

[4] M.P. Bernal, J. Coronas, M. Menéndez, J. Santamaria, Characterization of zeolite membranes by measurement of permeation fluxes in the presence of adsorbable species, Ind. Eng. Chem. Res. 41 (2002) 5071.

[5] Y. Hasegawa, K. Kusakabe, S. Morooka, Effect of temperature on the gas permeation properties of NaY-type zeolite formed on the inner surface of a porous support tube, Chem. Eng. Sci. 56 (2001) 4273.

[6] Y. Hasegawa, K. Watanabe, K. Kusakabe, S. Morooka, Influence of alkali cations on permeation properties of Y-type zeolite membranes, J. Membr. Sci. 208 (2002) 415.

[7] K. Weh, M. Noack, I. Sieber, J. Caro, Permeation of single gases and gas mixtures through faujasite-type molecular sieve membranes, Micropor. Mesopor. Mater. 54 (2002) 27.

[8] H. Kita, K. Fuchida, T. Horita, H. Asamura, K. Okamoto, Preparation of Faujasite membranes and their permeation properties, Sep. Purif. Technol. 25 (2001) 261.

[9] S. Li, V.A. Tuan, J.L. Falconer, R.D. Noble, X-type zeolite membranes: preparation, characterization, and pervaporation performance, Micropor. Mesopor. Mater. 53 (2002) 59.

[10] X. Chen, W. Yang, J. Liu, L. Lin, Synthesis of zeolite NaA membranes with high permeance under microwave radiation on mesoporous-layer-modified macroporous substrates for gas separation, J. Membr. Sci. 255 (2005) 201.

[11] M. Pera-Titus, J. Llorens, F. Cunill, R. Mallada, J. Santamaria, Preparation of zeolite NaA membranes on the inner side of tubular supports by means of a controlled seeding technique, Catal. Today 104 (2005) 281.

[12] J.C. Jansen, D. Kashchiev, A. Erdem-Senatalar, Preparation of coatings of molecular sieve crystals for catalysis and separation, in J.C. Jansen, M. Stöker, H.G. Karge, J. Weitkamp (Eds.), Advanced Zeolite Science and Applications, Stud. Surf. Sci. Catal. Vol. 85, Elsevier, Amsterdam, 1994, pp. 215-250.

[13] F. Kapteijn, J.A. Moulijn, R. Krishna, The generalized Maxwell-Stefan model for diffusion in zeolites: sorbate molecules with different saturation loadings, Chem. Eng. Sci. 55 (2000) 2923.

[14] Y. Morigami, M. Kondo, J. Abe, H. Kita, K. Okamoto, The first large-scale pervaporation plant using tubular-type module with zeolite NaA membrane, Sep. Purif. Tech. 25 (2001) 251.

[15] J. Zah, H.M. Krieg, J.C. Breytenbach, Layer development and growth history of polycrystalline zeolite A membranes synthesised from a clear solution, Micropor. Mesopor. Mater. 93 (2006) 141.

[16] J. Caro, M. Noack, P. Kölsch, R. Schäfer, Zeolite membranes – state of their development and perspective, Micropor. Mesopor. Mater. 38 (2000) 3.

[17] D. Shah, K. Kissick, A. Ghorpade, R. Hannah, D. Bhattacharyya, Pervaporation of alcohol-water and dimethylformamide-water mixtures using hydrophilic zeolite NaA membranes: mechanisms and experimental results, J. Membr. Sci. 179 (2000) 185.

[18] T. C. Bowen, R. D. Noble, J. L. Falconer, Fundamentals and applications of pervaporation through zeolite membranes, J. Membr. Sci. 245 (2004) 1.

[19] M. Mulder, Basic Principles of Membrane Technology, 2nd ed., Kluwer, Dordrecht, 1996.

[20] D.W. Breck, Zeolite Molecular Sieves: Structure, Chemistry, and Use, R.E. Krieger Publishing, Malabar, Florida, 1984.

[21] S.G. Izmailova, S.S. Khvoshchev, M.A. Shubaeva, Adsorption properties of low-silica zeolite ZK-5, Bull. Russ. Acad. Sci. – Div. Chem. Sci. 41 (1992) 1960.

[22] W. Zhu, L. Gora, A.W.C. van den Berg, F. Kapteijn, J.C. Jansen, J.A. Moulijn, Water vapour separation from permanent gases by a zeolite-4A membrane, J. Membr. Sci. 253 (2005) 57.

[23] K. Okamoto, H. Kita, K. Horii, K. Tanaka, M. Kondo, Zeolite NaA membrane: preparation, single-gas permeation, and pervaporation and vapour permeation of water/organic liquid mixtures, Ind. Eng. Chem. Res. 40 (2001) 163.

[24] T.C. Bowen, S. Li, R.D. Noble, J.L. Falconer, Driving force for pervaporation through zeolite membranes, J. Membr. Sci. 225 (2003) 165.

[25] J.G. Wijmans, R.W. Baker, A simple predictive treatment of the permeation process in pervaporation, J. Membr. Sci. 79 (1993) 101.

[26] J.G. Wijmans, R.W. Baker, The solution-diffusion model: a review, J. Membr. Sci. 107 (1995) 1.

[27] H. Jobic, J. Karger, M. Bee, Simultaneous measurement of self- and transport-diffusivities in zeolites, Phys. Rev. Lett. 82 (1999) 4260.

[28] R. Krishna, Diffusion of binary mixtures across zeolite membranes: entropy effects on permeation selectivity, Int. Comm. Heat Mass Transfer 28 (2001) 337.

[29] E.A. Mason, A.P. Malinauskas, Gas Transport in Porous Media: The Dusty Gas Model, Elsevier, Amsterdam, 1983.

[30] R. Krishna, J.A. Wesselingh, The Maxwell-Stefan approach to mass transfer, Chem. Eng. Sci. 52 (1997) 861.

[31] T.Q. Gardner, A.I. Flores, R.D. Noble, J.L. Falconer, Transient measurements of adsorption and diffusion in H-ZSM-5 membranes, AIChE J. 48 (2002) 1155.

[32] X. Feng, R. Y. M. Huang, Liquid separation by membrane pervaporation: a review, Ind Eng. Chem. Res. 36 (1997) 1048.

[33] E.L. Cussler, Diffusion Mass Transfer in Fluid Systems, 2nd ed., Cambridge University Press, Cambridge, UK, 1997.

[34] G.A. Steinlage, R.K. Roeder, K.P. Trumble, K.J. Bowman, Centrifugal slipcasting of components, Am. Ceram. Soc. Bull. 75 (1996) 92.

[35] A. Nijmeijer, C. Huiskes, N.G.M. Sibelt, H. Kruidhof, H. Verweij, Centrifugal casting of tubular membrane supports, Am. Ceram. Soc. Bull. 77 (1998) 95.

[36] P.M. Biesheuvel, V. Breedveld, A.P. Higler, H. Verweij, Graded membrane supports produced by centrifugal casting of a slightly polydisperse suspension, Chem. Eng. Sci. 56 (2001) 3517.

[37] K. Kim, S. Cho, K. Yoon, J. Kim, J. Ha, D. Chun, Centrifugal casting of alumina tube for membrane application, J. Membr. Sci. 199 (2002) 69.

[38] B. Subotić, J. Bronić, Theoretical and practical aspects of zeolite crystal growth, in S.M. Auerbach, K.A. Carrado, P.K. Dutta (Eds.), Handbook of Zeolite Science and Technology, Marcel Dekker Inc., New York, Basel, 2003, pp. 129-203.

[39] Ö Andaç, M. Tather, A. Sirkecioğlu, I. Ece, A. Erdem-Şenatalar, Effects of ultrasound on zeolite A synthesis, Micropor. Mesopor. Mater. 79 (2005) 225.

[40] A.S.T. Chiang, K. Chao, Membranes and films of zeolite and zeolite-like materials, J. Phys. Chem. Solids 62 (2001) 1899.

[41] E.R. Geus, M.J. den Exter, H. van Bekkum, Synthesis and characterization of zeolite (MFI) membranes on porous ceramic supports, J. Chem. Soc., Faraday Trans. 88 (1992) 3101.

[42] M. Noack, P. Kölsch, V. Seefeld, P. Toussaint, G. Georgi, J. Caro, Influence of the Si/Al-ratio on the permeation properties of MFI-membranes, Micropor. Mesopor. Mater. 79 (2005) 329.

[43] S. Desset, O. Spalla, P. Lixon, B. Cabane, Variation of the surface state of α-alumina through hydrothermal treatments, Colloids Surf., A 196 (2002) 1.

[44] A.R.Hind, S.K.Bhargava, S.C. Grocott, The surface chemistry of Bayer process solids: a review, Colloids Surf., A 146 (1999) 359.

[45] T. Lindner, H. Lechert, Influence of fluoride on the crystallization kinetics of zeolite NaY, Zeolites 14 (1994) 582.

[46] H. van Bekkum, E.M. Flanigen, P.A. Jacobs, J.C. Jansen, Introduction to Zeolite Science and Practice, 2nd ed., Stud. Surf. Sci. Catal. Vol. 137, Elsevier, Amsterdam, 2001.

[47] R.J.R. Uhlhorn, A.J. Burggraaf, Gas separations with inorganic membranes, in R.R. Bhave (Ed.), Inorganic Membranes: Synthesis, Characteristics and Applications, Van Nostrand Reinhold, New York, 1991, pp. 155-176.

[48] S.M. Holmes, M. Schmitt, C. Markert, R.J. Plaisted, J.O. Forrest, P.N. Sharratt, A.A. Garforth, C.S. Cundy, J. Dwyer, Zeolite A membranes for use in alcohol/water separations. Part I. Experimental investigation, Chem. Eng. Res. Des. 78 (2000) 1084.

[49] M. Kondo, M. Komori, H. Kita, K-I. Okamoto, Tubular-type pervaporation module with zeolite NaA membrane, J. Membr. Sci. 133 (1997) 133.

[50] M. Kazemimoghadam, A. Pak, T. Mohammadi, Dehydration of water/1,1-dimethylhydrazine mixtures by zeolite membranes, Micropor. Mesopor. Mater. 70 (2004) 127.

[51] K. Okamoto, H. Kita, K. Horii, K. Tanaka, M. Kondo, Zeolite NaA membrane: preparation, single-gas permeation, and pervaporation and vapour permeation of water/organic liquid mixtures, Ind. Eng. Chem. Res. 40 (2001) 163.

[52] A.W.C. van den Berg, L. Gora, J.C. Jansen, M. Makkee, T. Maschmeyer, Zeolite A membranes synthesized on a UV-irradiated TiO_2 coated metal support: the high pervaporation performance, J. Membr. Sci. 224 (2003) 29.

[53] X. Xu, Y. Bao, C. Song, W. Yang, J. Liu, L. Lin, Synthesis, characterization and single gas permeation properties of NaA zeolite membrane, J. Membr. Sci. 249 (2005) 51.

[54] F.T. de Bruijn, L. Sun, Z. Olujic, P.J. Jansens, F. Kapteijn, Influence of the support layer on the flux limitation in pervaporation, J. Membr. Sci. 223 (2003) 141.

CHAPTER 5

ENHANCED SELECTIVITY OF A ZEOLITE A MEMBRANE BY PRETREATING THE ALUMINA SUPPORT WITH UV RADIATION

ABSTRACT

Thin layered zeolite membranes rely on the use of effective carrier materials to provide mechanical support. A particularly suitable material is α-Al_2O_3, due to its intrinsic stability under harsh environments and its thermal expansion compatibility with different zeolite types. The chemical nature of the α-Al_2O_3 surface is determined by the presence of terminal hydroxyl (–OH) groups, which also favour the attachment of the zeolite layer to the support. The surface density of these functional groups, however, depend on the treatment history of the support.

Using a standard zeolite NaA membrane as model, the influence of ultraviolet (UV) radiation on the α-Al_2O_3 support surface prior to synthesis was examined, specifically in terms of the resultant effects on membrane integrity. Water/ethanol pervaporation under fixed conditions (95 wt.% EtOH; 45 °C) indicated a significant improvement in the selectivity of the NaA layer after pre-exposing the support to UV radiation (α_{WE} = 25 500 for the pretreated membrane versus α_{WE} = 3 000 for the control). A simple hypothesis for the selectivity enhancement was described in terms of the UV-induced increase in the number of -OH groups on the α-Al_2O_3 surface, which improves the wettability of the support, particularly in the macroscopic defect sites. As a result, the initially formed precursor gel is spread uniformly over the surface, leading to a high integrity zeolite layer with reduced intercrystalline porosity.

Keywords: zeolite NaA, UV radiation, α-Al_2O_3 support, pervaporation, hydroxyl (OH)

5.1 INTRODUCTION

The synthesis of effective zeolite membranes has relied strongly on the use of ceramic carriers. Support materials of α-Al_2O_3, TiO_2 and ZrO_2 are particularly suited due to their relative stability under given conditions of membrane synthesis and application, as well as their thermal expansion compatibility with various zeolite types [1]. The natural surface properties of these oxide materials also favour the nucleation and attachment of zeolite crystals, especially when direct synthesis is used. Different approaches have been suggested to further improve these surface properties in terms of membrane growth, such as acid etching and functionalisation with pH-controlled surfactants [2], prior to synthesis. The most notable approach, however, has been described by Van den Berg et al. [3,4], who used ultraviolet (UV) radiation to drastically increase the selectivity of their TiO_2 supported NaA membranes. Applying H_2O/EtOH pervaporation at 45 °C, separation factors in excess of 5×10^4 were reported for zeolite layers on UV-treated supports. The mechanism for the enhanced membrane performance was explained in terms of the UV-induced increase in terminal hydroxyl (—OH) groups on the lattice surface of the TiO_2 support. Since these —OH groups (mainly dissociated into the $—O^-$ form) act as zeolite anchors by condensation with precursor molecules such as $Si(OH)_4$, the treated supports induced higher nucleation densities in the NaA layers subsequently synthesised on them. As a result, the NaA crystals in the membrane layers were more densely intergrown and the bases of the crystals were more firmly attached to the support surface, affording membranes with superior separation qualities.

It is the aim of this paper to report for the first time the UV-facilitated enhancement of a NaA membrane specifically supported on α-Al_2O_3. While an attempt is made to explain the observations, further work will be required to verify and quantify these explanations, which fall beyond the scope of the current investigation. Although the effects of UV radiation on α-Al_2O_3 have been studied widely in the physical sciences, e.g. in terms of its dielectrical and optical properties [5], the application of such effects to zeolite membrane science constitutes a novel approach in optimising membrane performance.

5.2 EXPERIMENTAL

Tubular supports of α-Al_2O_3 (60 mm in length; 1.5 mm wall thickness) were produced in-house from AKP-30 powder (0.31 μm; Sumitomo Chemical Co. Ltd, Japan), using the centrifugal casting technique [6,7]. The average pore diameter was 101 nm and the total porosity was 41 %.

The manufacturing process was highly repeatable, with pore sizes of identically prepared supports deviating by less than 5 %. Prior to synthesis, an experimental support was pretreated with UV radiation under atmospheric conditions, using a 400 W high pressure mercury vapour lamp (HOK 4/120, UV+IR Engineering). The tube was placed vertically at an arbitrary distance of 200 mm from the overhead lamp surface, fully submerged in deionised water and continuously irradiated for 10 h. It was then turned over (180°) and irradiated for another 10 h to ensure full UV exposure of the inside surface. For the control support, no specified treatment was performed other than rinsing the tube with deionised water in an ultrasonic bath for 10 minutes. Both supports were dried for 3 h at room temperature and wrapped in Teflon tape to leave only the inside surface (tube side) exposed to zeolite crystallisation.

Zeolite NaA membranes were crystallised directly at 85 °C, using a clear solution with a molar composition of $Na_2O:Al_2O_3:SiO_2:H_2O$ = 49:1:5:980. A detailed description of the synthesis procedure can be found in Ref. [8]. The reagent chemicals comprised deionised water (MilliQ), sodium metasilicate pentahydrate ($Na_2SiO_3 \cdot 5H_2O$: 28% Na_2O, 27% SiO_2; BDH), sodium aluminate ($NaAlO_2$: 41% Na_2O, 54% Al_2O_3; Riedel-de Haën) and sodium hydroxide (NaOH; 97%, Aldrich). Each reaction was carried out in a Teflon-lined, rotating steel autoclave for 3.5 h. Two-stage syntheses (double zeolite layers) were used in all cases to increase selectivity, but the UV radiation was assumed to influence the formation of the first layer only.

The identity of the zeolite membranes was confirmed using XRD (Siemens D-501), while the morphological features and layer thicknesses were examined with SEM (FEI Quanta 200 ESEM). The separation performance was evaluated using H_2O/EtOH pervaporation under fixed conditions of temperature (45 °C), feed concentration (95 wt.% EtOH) and transmembrane pressure (90 kPa). Permeate concentrations were determined using gas chromatography (HP series 6985; $R^2 = 0.9998$). The H_2O/EtOH selectivity (α_{WE}) was expressed as

$$\alpha_{WE} = \frac{(z_W / z_E)_{\text{Permeate}}}{(x_W / x_E)_{\text{Feed}}}$$

with z_{WE} representing the permeate and x_{WE} the feed mole fractions of H_2O ($_W$) and EtOH ($_E$) respectively. The reported values were averaged from three independent measurements on each membrane.

5.3 RESULTS AND DISCUSSION

We recently described the morphological development of NaA layers on the untreated α-Al_2O_3 support [8]. It was shown that after 3.5 h of synthesis, a near-crystalline membrane of well-intergrown, cubic crystals is obtained, where the surface of each crystal is fractionised into smaller growth planes. By extending the crystallisation time to 4.0 h, these fractionised surfaces consolidate into flat, low-index crystal faces. This investigation was based on the fractionised morphology (3.5 h), since it represented membranes with a higher surface area-to-volume ratio. In addition, any morphological changes caused by the UV-treatment could be better detected from this irregular surface.

5.3.1 MEMBRANE PERFORMANCE

UV radiation had a pronounced effect on the pervaporation features of the experimental membrane. The H_2O/EtOH selectivity increased dramatically from $\alpha_{W/E}$ = 3 000 (control membrane) to $\alpha_{W/E}$ = 25 500 (for the UV-pretreated membrane). Fig. 5.1 shows that the selectivity difference can be mainly ascribed to an increased permeability of ethanol in the untreated sample, suggesting a substantial contribution of non-selective, intercrystalline transport. The permeability of water was similar in both membranes, probably due to the adsorptive retention of water in the larger, intercrystalline pores of the untreated membrane.

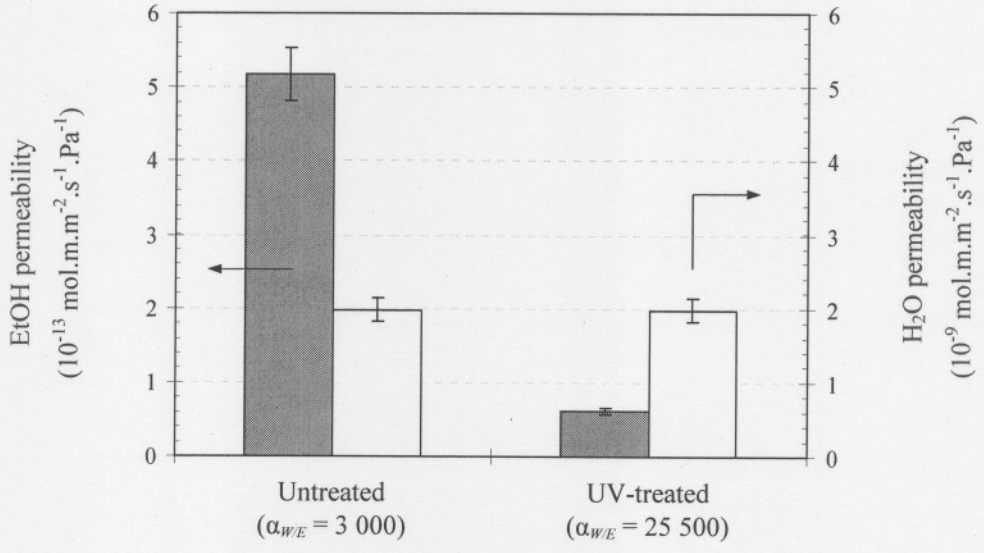

Figure 5.1: Mixture permeability of the NaA membranes on the untreated and UV-treated supports, at 45 °C. EtOH permeability is related to the left ordinate (dark columns) and H_2O permeability to the right (clear columns).

5.3.2 MORPHOLOGY

The crystallisation process in the UV-treated sample was slightly advanced, in other words, the fusion of the fractionised crystal faces into flat surface planes was closer to completion than in the untreated sample (Fig. 5.2). Likewise, the treated membrane was more homogeneous in thickness and the average crystal size seemed larger, as confirmed by the increased layer thickness for the treated membrane - an average of 5.6 μm versus the 5.0 μm of the non-treated membrane.

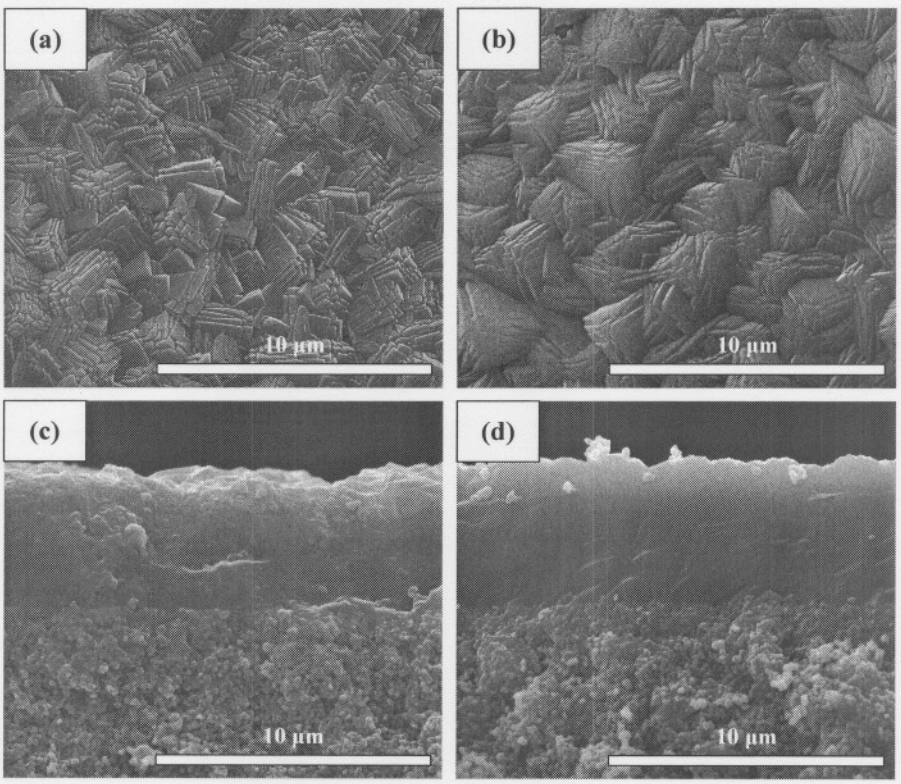

Figure 5.2: Top-view and cross-sectional features of the NaA membrane synthesised on the non-treated support **(a** and **c)**, compared to the UV-treated support **(b** and **d)**.

Since all the synthesis parameters (mixture composition, synthesis time and temperature) were identical, it is unlikely that the growth rates for the two membranes were different, because the growth rate is kinetically related to the concentration of nutrients in the liquid phase [9]. It is

therefore postulated that the crystallisation process had to start earlier in the UV-treated membrane, that is, a shorter induction time was necessary for crystal growth to start.

We also found a striking difference regarding the presence of surface defects. Due to common shortcomings in the experimental preparation procedures, one would realistically expect certain microstructural defects to exist on the surface of the support. Since the zeolite layers were very thin, these defects are usually expected to translate into small imperfections in the NaA layers themselves. The non-treated membrane therefore exhibited certain voids where the thickness of the zeolite layer could not compensate for the defects in the support. Fig. 5.3 shows such an example.

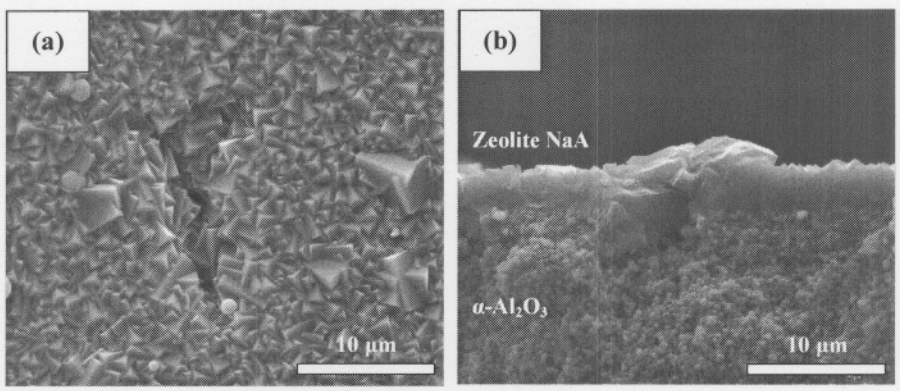

Figure 5.3: Example of a macroscopic defect in the support surface translating into a growth imperfection in the subsequently synthesised zeolite layer. Top view **(a)** and cross-section **(b)** of a non-treated membrane sample.

A contributing factor to the formation of these defects may be the relatively slow wetting of the α-Al_2O_3 material by the viscous synthesis solution [10]. As a result, small pockets of air could easily become trapped within the defects when the dried support is exposed to the synthesis solution. Since the given solution is fairly reactive, crystal growth could then commence before these air-filled cracks are completely wetted, culminating in poor growth of NaA crystals within the cracks.

In contrast to the untreated sample, we found no observable defects in the UV-treated membrane, showing that the UV radiation also improved the wettability of the support surface with the synthesis solution, especially in the macroscopic defect sites.

5.3.3 HYPOTHESES FOR ENHANCED SELECTIVITY

While appreciating the complexity of oxide surface chemistry, a fundamental understanding for the enhancing effect of UV-pretreatment could be proposed in terms of the photo-induced changes in the surface properties of the α-Al_2O_3 support.

Like all crystalline metal oxides, α-Al_2O_3 has certain structural defects inherently built into its crystallographic lattice structure [11]. One such defect is the so-called F-center, which is basically an oxygen vacancy in the atomic α-Al_2O_3 grid that holds two electrons trapped inside it. The F-center as such is neutral in nature and cannot bind (or trap) new electrons [5]. When exposed to UV radiation though, electrons throughout the atomic grid are excited to higher energy levels and become mobile throughout the bulk of the α-Al_2O_3 crystal. An important result of this electronic mobility is the rearrangement of the charge distributions within the defect sites, leading to the modification of F-centers. The net result is an oxygen vacancy with the acquired ability to trap new electrons or electrical charges [5].

If we assume that those original, "unreactive" F-centers, situated at the edge of the support surface, were chemically stable to the environment under ambient conditions, the photo-induced cascade of events can then be seen as a process of creating "new" (or active) oxygen vacancies at the Al_2O_3 surface. These new oxygen vacancies will dissociatively adsorb water (i.e. chemisorption by splitting water into H^+ and OH^- ions) from its surroundings to form additional —OH groups at the support surface [12]. The simplified assumption is therefore that the UV-treatment increases the surface coverage of —OH groups on the α-Al_2O_3 support, facilitating the nucleation and adhesion of the zeolite layer. Whether the actual nucleation density is increased, remains a matter of dispute, since one would expect a higher nucleation density to manifest into a zeolite layer with more, but smaller crystals [3]. Clearly this is not the case here (cf. Fig. 5.2**a** and **b**). In fact, if the assumed difference in induction times for the two membranes was to be ignored, their crystal sizes would appear very similar.

In contrast to the generally assumed mechanism of heterogeneous nucleation [1], the formation of NaA layers on the α-Al_2O_3 support rather seems to follow the pathway of autocatalytic nucleation [8]. The nuclei for crystal growth are formed within an aluminosilicate gel precipitated on the support surface during the initial stages of hydrothermal treatment. The number (or density) and distribution of nuclei within this gel act as a "fingerprint" for the crystal size distribution in the following stages of crystal growth, and depend primarily on the chemical composition of the synthesis mixture (i.e. the gel memory effect [13]). It is thus doubtful that the nucleation

densities in the two membranes were significantly different, because both were prepared from a fixed synthesis mixture. A more comprehendible explanation would be that the increased concentration of –OH groups improves the hydrophilicity of the alumina surface and speeds up the formation of the precursor gel layer, and therefore the critical rate of nucleation, by lowering the interfacial energy between gel and support [14]. As a consequence, the induction time for membrane growth would be shorter in the UV-treated sample, as presumed earlier, although the actual number of nuclei would remain similar in both membranes [13].

Based on these arguments, the enhanced selectivity of the UV-treated membrane could be simply explained by the initial, improved interaction between the gel and the support, which would lead to a more uniform and continuous spreading of gel on the surface and result in a more densely intergrown membrane with reduced intercrystalline porosity.

As a final remark, one might consider that the UV-treatment could also reduce the possible leaching of the support surface. In addition to the surface –OH groups acting as anchoring sites for zeolite adhesion, they may serve as reaction centers for chemical attack by the alkaline synthesis solution:

$$Al(OH)_{3(s)} + NaOH_{(aq)} \longrightarrow Na^{+}_{(aq)} + Al(OH)_4^{-}{}_{(aq)}$$

The important effect of leaching entails the release of aluminium-containing ions from the support, particularly during the initial period of zeolite formation. This process would theoretically disturb not only the growth of zeolite, but also the attachment of crystals to the support, thereby decreasing the integrity (selectivity) of the membrane. While it has been established that the -OH groups at different locations on the α-Al_2O_3 surface exhibit different local energies [15], an increase in the surface coverage of these OH species, in the presence of water, has been shown to reduce the energy differences [16]. Could it be possible that this energetically homogeneous surface, despite there being more -OH groups, becomes less reactive and therefore less prone to chemical attack? However interesting, this question remains currently unanswered, and will be the subject of future research in this field.

5.3.4 LITERATURE COMPARISON

To put the significance of UV-pretreatment in perspective, Table 5.1 summarises the current performance of NaA membranes reported in literature. With the exception of the TiO_2 based membranes, the selectivities of all other alumina-based membranes, tested under similar

conditions, were inferior to that of the UV-treated membrane discussed here. Likewise, the untreated TiO_2 based membranes performed similarly to those in literature, while the UV-treated layers exhibited unequalled selectivities. The difference in performance between the UV-enhanced layers on TiO_2 and Al_2O_3 could possibly be related to the intrinsic material differences between these supports. In its natural state, the TiO_2 surface has a higher density of surface hydroxyls (1-2.5 $OH.nm^{-2}$) compared to that of α-Al_2O_3 (<1 $OH.nm^{-2}$) [10]. This implies that the UV radiation probably induced a higher density of hydroxyls on the TiO_2 support than on the α-Al_2O_3 support, leading to more improved membranes.

Table 5.1: Literature summary for the pervaporative separation of H_2O/EtOH mixtures, using NaA composite membranes under relatively similar conditions

Support material	Layer thickness (μm)	EtOH in feed (wt.%)	Temp. (°C)	Flux ($kg.m^{-2}.h^{-1}$)	α_{WE} (-)	Reference
Ceramic[a]	10	95	50	0.40	4 800	[17]
Mullite	NA	95	25	0.45	>10 000	[18]
α-Al_2O_3	30	95	75	1.10	16 000	[19]
α-Al_2O_3	5.0	95	45	0.19	3 000	This study
α-Al_2O_3[b]	5.6	95	45	0.17	25 500	This study
TiO_2	3.5	95	45	0.5-0.80	<10 000	[4]
TiO_2[c]	3.5	95	45	0.86	54 000	[4]

[a] Mullite/α-Al_2O_3/cristobalite
[b,c] Pretreated with UV radiation
NA: not available

5.4 CONCLUSIONS

Ultraviolet (UV) radiation was presented as a simple pretreatment method in optimising the surface properties of an α-Al_2O_3 support for the growth of a highly selective zeolite A membrane. For a given synthesis regimen (batch composition, synthesis time and temperature), it was shown that pre-exposure of the support to UV radiation radically improved the separation properties of the subsequent membrane. Using H_2O/EtOH pervaporation at 45 °C, the separation factor increased from 3 000 to 25 500, representing a near-tenfold increase in selectivity. A simple hypothesis for the selectivity enhancement was described in terms of the UV-induced increase in

the number of –OH groups on the α-Al_2O_3 surface, which improves the interaction between the support and the synthesis mixture, particularly in the macroscopic defect sites. As a result, the initially formed precursor gel is spread uniformly over the surface, leading to a high integrity zeolite layer with reduced intercrystalline porosity.

The observed effect of improved selectivity, as well as its proposed mechanism, definitely warrants further investigation into the use of UV radiation for improving the quality of supported zeolite membranes in general. The approach is simple, non-invasive and easy to reproduce, but most importantly, highly effective.

5.5 REFERENCES

[1] M. Noack, J. Caro, Zeolite membranes, in F. Schüth, K.S.W. Sing, J. Weitkamp (Eds.), Handbook of Porous Solids, vol. 4, Wiley-VCH, Weinheim, 2002, pp. 2433-2507.

[2] J.L.H. Chau, C. Tellez, K.L. Yeung, K. Ho, The role of surface chemistry in zeolite membrane formation, J. Membr. Sci. 164 (2000) 257.

[3] A.W.C. van den Berg, L. Gora, J.C. Jansen, T. Maschmeyer, Improvement of zeolite NaA nucleation sites on (001) rutile by means of UV-radiation, Micropor. Mesopor. Mater. 66 (2003) 303.

[4] A.W.C. van den Berg, L. Gora, J.C. Jansen, M. Makkee, T. Maschmeyer, Zeolite A membranes synthesized on a UV-irradiated TiO_2 coated metal support: the high pervaporation performance, J. Membr. Sci. 224 (2003) 29.

[5] J. Vallayer, C. Jardin, D. Tréheux, Optical and dielectric behaviors of alumina after an electromagnetic irradiation, Opt. Mater. 16 (2001) 329.

[6] G.C. Steenkamp, H.W.J.P. Neomagus, H.M. Krieg, K. Keizer, Centrifugal casting of ceramic membrane tubes and the coating with chitosan, Sep. Purif. Technol. 25 (2001) 407.

[7] G.C. Steenkamp, K. Keizer, H.W.J.P. Neomagus, H.M. Krieg, Copper(II) removal from polluted water with alumina/chitosan composite membranes, J. Membr. Sci. 197 (2002) 147.

[8] J. Zah, H.M. Krieg, J.C. Breytenbach, Layer development and growth history of polycrystalline zeolite A membranes synthesised from a clear solution, Micropor. Mesopor. Mater. 93 (2006) 141.

[9] S. Bosnar, T. Antonić, J. Bronić, B. Subotić, Mechanism and kinetics of the growth of zeolite microcrystals. Part 2: Influence of sodium ions concentration in the liquid phase on the growth kinetics of zeolite A microcrystals, Micropor. Mesopor. Mater. 76 (2004) 157.

[10] J.C. Jansen, J.H. Koegler, H. van Bekkum, H.P.A. Calis, C.M. van den Bleek, F. Kapteijn, J.A. Moulijn, E.R. Geus, N. van der Puil, Zeolitic coatings and their potential use in catalysis, Micropor. Mesopor. Mater. 21 (1998) 213.

[11] J. Valbis, N. Itoh, Electronic excitations, luminescence and lattice defect formation in α-Al_2O_3 crystals, Radiat. Eff. Defects Solids 116 (1991) 171.

[12] M. Harju, T. Mäntylä, K. Vähä-Heikkilä, V. Lehto, Water adsorption on plasma sprayed transition metal oxides, Appl. Surf. Sci. 249 (2005) 115.

[13] T. Antonić-Jelić, S. Bosnar, J. Bronić, B. Subotić, M. Škreblin, Experimental evidence of the "memory" effect of amorphous aluminosilicate gel precursors, Micropor. Mesopor. Mater. 64 (2003) 21.

[14] J.C. Jansen, D. Kashchiev, A. Erdem-Senatalar, Preparation of coatings of molecular sieve crystals for catalysis and separation, in J.C. Jansen, M. Stöker, H.G. Karge, J. Weitkamp (Eds.), Advanced Zeolite Science and Applications, Stud. Surf. Sci. Catal. Vol. 85, Elsevier, Amsterdam, 1994, p. 219.

[15] C.E. Nelson, J.W. Elam, M.A. Cameron, M.A. Tolbert, S.M. George, Desorption of H_2O from a hydroxylated single-crystal α-Al_2O_3 (0001) surface, Surf. Sci. 416 (1998) 341.

[16] H. Tamura, A. Tanaka, K. Mita, R. Furuichi, Surface hydroxyl site densities on metal oxides as a measure for the ion-exchange capacity, J. Colloid Interface Sci. 209 (1999) 225.

[17] M. Kondo, M. Komori, H. Kita, K-I. Okamoto, Tubular-type pervaporation module with zeolite NaA membrane, J. Membr. Sci. 133 (1997) 133.

[18] M. Kazemimoghadam, A. Pak, T. Mohammadi, Dehydration of water/1,1-dimethylhydrazine mixtures by zeolite membranes, Micropor. Mesopor. Mater. 70 (2004) 127.

[19] K. Okamoto, H. Kita, K. Horii, K. Tanaka, M. Kondo, Zeolite NaA membrane: preparation, single-gas permeation, and pervaporation and vapour permeation of water/organic liquid mixtures, Ind. Eng. Chem. Res. 40 (2001) 163.

CHAPTER 6

OVERVIEW

6.1 GENERAL

In this thesis a study of different aspects of a ceramic supported NaA membrane was presented. The aim was to provide an improved fundamental understanding of the composite NaA membrane as a whole, including structural and permeation related aspects, under the auspices of optimising and broadening the application potential of supported zeolite membranes in general.

The main areas of research included a study of the morphological and compositional development of the polycrystalline zeolite layer during its direct synthesis from a clear solution, and an evaluation of the relation between the intrinsically different layers thus obtained, and their (selective) permeation properties. In addition, the role of the α-Al_2O_3 support was scrutinised, both in terms of liquid (pervaporation) and gas based permeation resistance, as well as its surface-related facilitation of zeolite growth. In each case the results were evaluated by correlating the observed tendencies to relevant literature works and theories dealing with similar matters. The specific conclusions of each subject were discussed in detail at the end of the respective chapters.

6.2 COMPARISON OF PERVAPORATION AND GAS PERMEATION

To view the individual results within a broader, more generalised framework, we return to the two main application fields envisaged for NaA membranes, namely pervaporation and gas permeation. With specific reference to the semicrystalline (2 h synthesis) and fully crystalline (4 h synthesis) layers, the following distinctive similarities and differences became apparent:

- *Crystallinity.* The relative crystallinity had a significant effect on the permeability (zeolite layer only) of both pervaporation and gas permeation components, confirming that the possible permeation of components through the amorphous phase was negligible compared to zeolitic (both intra- and intercrystalline) diffusion. However, the degree to

which the amorphous component in the semicrystalline layer (70 %) inhibited the total permeation, depended strongly on the adsorptive and diffusive differences between the different permeants under the applied conditions in each case.

- *Intercrystalline porosity.* The relative permeance and ideal selectivity results obtained from the single gas measurements, suggested a smaller contribution from non-zeolitic diffusion to the total permeation through the semicrystalline membrane. There seems to be a qualitatively closer contact between the crystal/amorphous phase in the boundary regions of the semicrystalline membrane, compared to the crystal/crystal interface in the fully crystalline membrane. Existing theories on the electrostatic and hydration repulsion between two hydrophilic surfaces could explain the observed phenomenon in terms of a possibly attenuated intergrowth barrier presented by the amorphous interface, where Si/Al > 1. The same argument could also explain the selectivity trends in the time-dependent layers in pervaporation. However, the contribution of intercrystalline porosity was much more significant for gas permeation, where the selectivity of the semicrystalline layer (*PS* H_2/SF_6 = 63.8, at 23°C) exceeded that of its crystalline counterpart considerably (*PS* H_2/SF_6 = 11.4). In contrast, the pervaporation selectivities for the two membrane types were comparable (α_{WE} = 9000 for the semicrystalline membrane versus α_{WE} = 8 300 for the fully crystalline layer), due to the high affinity of water for the intercrystalline pore walls.

- *Support resistance.* A fundamental difference between pervaporation and gas permeation is the applied pressure conditions under which each permeant migrates through the support structure. In pervaporation the pressures are low (vacuum conditions), and within the support pore size regimes tested, the flow consisted mainly of Knudsen diffusion (~98 % for water at room temperature). In the single gas measurements, permeation occurred under atmospheric pressure, and the flow regime through the support contained a stronger contribution of Poiseuille flow (~10 % for H_2 at room temperature). Although the essential mechanistic difference seemed small, it translated into significant changes in the relative resistances presented to the permeance in pervaporation compared to gas permeation. Based on the fugacity calculations for the zeolite/support interface, it was shown that the support exerted a staggering contribution (~60 %) to the total membrane resistance in pervaporation, while the same support contributed less than 10 % of the single gas resistance at similar temperature (25 °C). As a result, the support resistance can be viewed as a limiting factor on the temperature-induced driving force in

pervaporation, while the permeance through the zeolite layer still remains the rate-determining step in single gas permeation, in relation to the applied driving force.

3.1 EVALUATION

From the combined results from various sections of the work (chapter 2-5), it became clear that the individual performances of the different ceramic supported NaA layers (in terms of selectivity, permeance and thermal stability) were highly condition-specific. It thus shows that favourable results under certain conditions do not necessarily imply favourable results under differently applied conditions.

The given performances of the time-dependent NaA layers in terms of their permeance and selectivity, depended predominantly on two dynamic factors – the internal or intrinsic identity of the membrane, and the external or application-related conditions.

The internal identity consisted of the specific layer composition. This composition could be evaluated on two levels. Firstly, the microporosity as determined by the relative crystallinity of the zeolitic phase, which establishes the pore filling (sorption) capacity and therefore the physical permeance limits of the given layer under the applied conditions. Secondly, the chemical composition (Si/Al ratio), where the overall composition of the layer integrates the compositions of both the crystalline and amorphous NaA phases. The crystalline composition (Si/Al = 1) directly influences the membrane permeance and selectivity by determining the fundamental interaction of the zeolitic framework with the specific permeants under given conditions; and indirectly, by establishing the crystal/crystal boundary phase limits for non-zeolitic diffusion. The amorphous composition (Si/Al > 1) mainly exerts an indirect influence on the permeance and selectivity, by establishing the crystal/amorphous boundary phase limits for non-zeolitic diffusion through the semicrystalline layers.

The external influences on the layer performance mainly consisted of the physicochemical nature of the permeants used, the fundamental mode of transport (pervaporation or gas permeation) and the applied temperature and driving force conditions. It was shown that the support and its contribution to resistance largely constitutes an external factor, because the membrane performance under given conditions changes in relation to the particular support's structural properties, while the intrinsic character of the zeolite layer remains unchanged. In the same context, the UV pretreatment of the support can be viewed as an external influence exerted by the

support surface onto the zeolite layer, influencing membrane selectivity without changing the fundamental compositional qualities of the zeolite layer.

The very nature of the composite membrane causes the internal and external factors to function dependently, by relating to a complicated interdependence in their influences on membrane performance. Such interdependence exists even within the respective internal and external aspects themselves, and herein lies the complexity of controlling the ultimate membrane performance. In some instances the different factors influence each other in a positive way. For example, the optimised surface chemistry of the support (UV) contributes to the high separation qualities of a given zeolite layer. Also, the chemical nature of the mixture permeants in pervaporation supplements the existence of intercrystalline porosity in the zeolite layer, where water selectively condenses in, and blocks the boundary regions from ethanol. On the other hand, many opposing influences are also observed. A certain degree of intercrystalline closure would benefit the performance in pervaporation, but render dry gas separations ineffective. A meaningful amount of amorphous content increases gaseous selectivity by diminishing the non-zeolitic diffusion through the boundary phase regions, but decreases the overall permeability (productivity) of the membrane. Increased temperature then increases the permeability, but degrades selectivity due to the thermal instability of the amorphous phase. Also, the fundamental mode of transport in pervaporation (vacuum) increases the driving force for permeation through the zeolite layer, but hampers the overall performance by simultaneously increasing the support resistance. In contrast the same support would be more than satisfactory in gas separations under high pressure.

In view of these complexities and in accordance to the described interventions, future advances for the NaA membrane could be realised by applying the fundamental principles gained from their permeation behaviour under certain conditions. Such an approach would entail:

- decreasing the intercrystalline boundary phase barrier during synthesis and thus restraining its detrimental effects on *dry gas permeation*,
- reducing the support's resistance to mass flow, particularly in *pervaporation* applications, and
- tailoring the support surface chemistry to best suit the zeolite-specific layer formation mechanism.

The application value of the zeolite NaA membrane therefore has to be found not in the full optimisation of the respective internal and external factors independently, but in the delicate balance of these factors under given conditions. It seems that the way forward should not be based on a methodology of "one size fits all", but should rather concentrate on finding specific applications for different membranes, and optimise their performance within these condition-specific environments.

3.2 FINAL REMARKS

Zeolite membranes are advanced, high technology materials. Due to the intrinsic variety of framework structures, both existing and still to be discovered, the application potential of these membranes in improving our everyday life is certainly not yet exhausted.

Despite representing a relatively new frontier in the field of membrane separation, a strong information base already exists regarding their synthesis, current industrial exploitation and the fundamental mechanisms of separation upon which these processes rely. However, the apparent simplicity of their functioning, namely size exclusion, selective adsorption and diffusion, and catalysis, can be deceptive. The predominant reason is the mere molecular scale on which these actions occur. This means that true control over the membrane performance, and thus its application, can only be achieved if we can manipulate the membrane structure on molecular level. In essence, this project has shown that this level of control is necessary not only in the synthesis and composition of the zeolite layers (layer development), but also in the workings of the composite membrane as a whole, including the support, its physicochemical interaction with the zeolite and its influence on the actual permeation process (both liquid and gas based). It proves that various aspects of intervention into the production of highly effective zeolite membranes for different applications still remain unexploited. Using NaA as model, the generated results will hopefully contribute to the more fundamental understanding of the composite zeolite membrane in general, and play part in ensuring its future success in industry.

APPENDIX A

Extended abstract of an **oral presentation** delivered at the International Congress on Membranes and Membrane Processes (ICOM), August 2005, Seoul, South Korea.

SYNTHESIS OPTIMISATION OF ZEOLITE A MEMBRANES ON CENTRIFUGALLY CASTED CERAMIC SUPPORTS

Jaco Zah, Jaco C. Breytenbach and Henning M. Krieg

Separation Science and Technology, North-West University, Private Bag X6001, Potchefstroom, 2531, South Africa. Tel. +27-18-299 2360, E-mail: chehmk@puknet.puk.ac.za

Introduction and aim

Zeolite A is a hydrophilic tecto(alumino)silicate with perpendicularly intersected, three-dimensional channels. Due to its high Al-content (Si/Al ratio = 1) and the subsequent susceptibility to ion-exchange, unit cell aperture sizes may be altered from 4.1 Å (NaA) to 3.2 Å (KA) and 4.6 Å (CaNaA). In addition to a well-established role in the field of adsorption [1], LTA-ceramic composite membranes have also recently been commercialised for the pervaporation-based dehydration of organic solvents [2,3]. Combined with the inherent thermal resistance and chemical inertness characteristic of all zeolites, zeolite A membranes have instigated renewed interest as a tool for gas separation in the petrochemical industry, where current emphasis is directed toward process integration and intensification. The removal of water from Fischer-Tropsch mixtures illustrates one example. However, the viability of such a prospective system depends mainly on the selectivity and permeation flux through the composite, which in turn, is governed by the zeolite layer continuity and thickness of not only the zeolite layer, but also the support and its resistance to mass flow. It is a well-known fact that zeolite membranes exhibiting facetted crystal faces, although seemingly fully interlocked, always contain mesoporous defects due to the existence of pinholes. Efforts are therefore directed towards synthesising layers of completely intergrown grain-like crystallites; nevertheless, acquiring such a system in practise is difficult and requires thorough investigation of synthesis parameters like temperature, time, molar oxide nutrient ratios and most importantly, the degree of solution saturation that can be induced under specific conditions on a specific type of support.

This research describes the synthesis optimisation of thin zeolite NaA coatings on centrifugally casted α-Al_2O_3 supports. The influence of increased support permeability on the overall membrane performance was also illustrated.

Experimental

Supports were manufactured *via* centrifugal casting of α-Al_2O_3 powder suspensions stabilised with ammonium polymethacrylate at pH 9.5. Single particle-sized casts (0.6 μm), as well as bimodal casts (1:9 ratio of 0.6 and 1.0 μm particles), were prepared and sintered at 1200 °C to produce tubular supports ~60 mm in length, having an inner diameter of ~18 mm and wall thickness of ~1.5 mm. Water fluxes were recorded for each support in a dead-end filtration mode at pressure differences between 0.2 and 1.0 MPa and permeabilities calculated accordingly. Pore size, porosity and density were measured by means of mercury intrusion (Autopore III, Micromeritics).

Zeolite NaA layers were prepared reproducibly on the inside surface of the support by a batch hydrothermal synthesis procedure at 85 °C from clear solution of molar composition Na_2O:Al_2O_3:SiO_2:H_2O = 50:1:5:1000. Crystal habit and composition were investigated, *inter alia*, as a function of synthesis time (0.5–4.0 h) and characterised with XRD and SEM. Separation properties of composite membranes were rated by the pervaporation flux and

selectivity in a H_2O/EtOH binary mixture. Feed streams consisted of 95 wt.% EtOH at 45 °C, while moderate permeate pressures were maintained at 15 kPa. Mole fractions of EtOH in feed and permeate samples were analysed *via* GC and related to the H_2O-EtOH separation factor ($\alpha_{W/E}$), where

$$\alpha_{W/E} = \frac{(\text{wt.\% } H_2O \text{ / wt.\% EtOH})_{\text{Permeate}}}{(\text{wt.\% } H_2O \text{ / wt.\% EtOH})_{\text{Feed}}}$$

Results and Discussion

Two distinctive types of zeolite coatings were prepared: a homogeneous layer of well-intersected grains/crystallites 1-2 μm in diameter and a monolayer of fully developed and densely intergrown cubic crystals (2-5 μm) with the typical NaA morphology (Fig. 1). Synthesis times for these two systems were 2 h and 4 h respectively and in principle this occurrence would agree with the island (Volmer-Weber) mode of growth describing heterogeneous nucleation and growth of separate island-like crystallites of multiatomic height. However, as the aluminosilicate structure stabilises and more nutrients are consumed, defined crystal faces are usually clearly developed by the time the crystal reaches micron-sized proportions. As depicted in Fig. 1 however, no facetted crystal planes were present at these dimensions after the 2 h hydrothermal treatment. The XRD analysis of this layer (Fig. 2) confirmed zeolite A crystallinity. True grain growth kinetics seems to be operative here and this phenomenon is related to the high supersaturation of nutrient prevailing during growth. The crystal growth roughening as a function of the extremely high supersaturation is based on the formation of a dense precursor layer of aluminosilicate on the support surface from the clear starting solution.

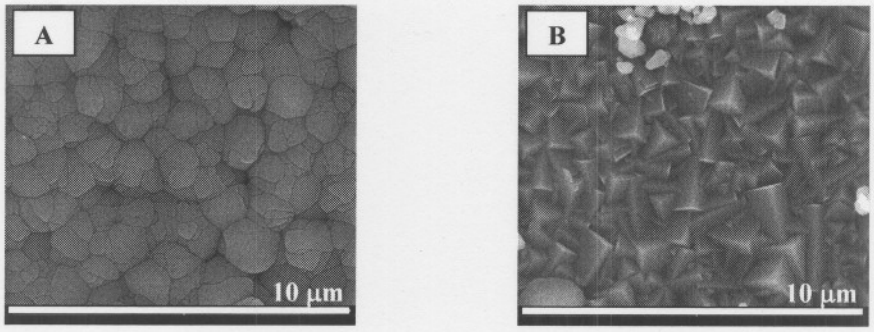

Figure 1: Top view micrographs of thin layer zeolite A membranes obtained on monomodal supports after a 2 h (**A**, membrane thickness = 2 μm) and 4 h (**B**, membrane thickness = 5 μm) hydrothermal treatment.

A double NaA coating (4 h synthesis) on the monomodal support yielded $\alpha_{W/E} \sim 5500$ at a total pervaporation flux of 0.23 $kg.m^{-2}.h^{-1}$, while the same coating on the bimodal support yielded $\alpha_{W/E} \sim 2800$ at a total flux of 0.45 $kg.m^{-2}.h^{-1}$ (Table 1). Fluxes through the zeolite-ceramic composites could thus be improved by increasing the support permeability. Bimodal grading of the centifugally casted supports provided an effective means of achieving this.

Table 1: Pervaporation results for selected composite membranes (two stage zeolite syntheses in each case)

Hydrothermal treatment (h)	Support type	Support pore diameter (μm)	Support H_2O permeability ($kg.m^{-2}.h^{-1}.bar^{-1}$)	$\alpha_{W/E}$	Pervaporation flux ($kg.m^{-2}.h^{-1}$)
2	Monomodal	0.16	45	9000	0.25
4	Monomodal	0.16	45	5500	0.23
4	Bimodal	0.29	146	2800	0.45

The thin layer coating (2 h synthesis) evidently outperformed the former membranes with regard to H_2O/EtOH selectivity ($\alpha_{W/E} \sim 9000$), but further testing at extremely low permeate pressures is necessary to establish the true difference in transmembrane resistance. However, these results are preliminary in nature and studies are ongoing to test repeatability and to ascertain how post-synthesis treatment of membranes influences their final flux-selectivity ratios.

Conclusion

Two types of zeolite A membranes were synthesised on tubular ceramic supports, a homogeneous film of tripod-intersected grains and a monolayer of intergrown crystals. Preliminary pervaporation results indicated justifiable differences in H_2O/EtOH selectivities between these membranes, without significant distinction in flux. Using supports with higher permeabilities increased the total pervaporation flux for all the composite membranes.

References

[1] Jansen, J.C., Kashchiev, D. and Erdem-Senatalar, A. (1994). Preparation of coatings of molecular sieve crystals for catalysis and separation. (*In* Jansen, J.C., Stöker, M., Karge, H.G. and Weitkamp, J., *eds*. Advanced zeolite science and applications. Elsevier, Amsterdam. *Studies in Surface Science and Catalysis*, 85, 215-250.)

[2] Kondo, M., Komori, M., Kita, H. & Okamoto, K. (1997). Tubular-type pervaporation module with zeolite NaA membrane. *Journal of Membrane Science*, 133, 133-141.

[3] Morigami, Y., Kondo, M., Abe, J., Kita, H. & Okamoto, K. (2001). The first large-scale pervaporation plant using tubular-type module with zeolite NaA membrane. *Separation and Purification Technology*, 25, 251-260.

APPENDIX B

Extended abstract of a **poster presentation** delivered at the International Congress on Membranes and Membrane Processes (ICOM), August 2005, Seoul, South Korea.

FLUX OPTIMISATION OF CENTRIFUGALLY CASTED ZEOLITIC MEMBRANE SUPPORTS

Jaco Zah, Jaco C. Breytenbach and Henning M. Krieg

Separation Science and Technology, North-West University, Private Bag X6001, Potchefstroom, 2531, South Africa. Tel. +27-18-299 2360, E-mail: chehmk@puknet.puk.ac.za

Introduction and aim

The functionality of α-Al_2O_3 ceramic supports is well established in the field of composite zeolite membrane technology. Base requirements for such a supporting structure would be a low resistance to mass flow whilst retaining an adequate surface integrity for the deposition of highly selective zeolitic films. Since surface irregularities are translated to subsequently synthesized zeolite layers, homogeneously packed small particles where surface roughness is close to the particle size itself [1], provide the optimal substrate surface for thin, defect-free zeolitic coatings. In addition, cylindrical geometry is often preferred to flat disks due to higher surface area per unit module volume but also the existence of well defined flow profiles within tubular configurations [2]. Axisymmetrical centrifugal casting is a technique that allows the consolidation of a tubular alumina body by means of accelerated differential settling of dispersed particles at the wall of a cylindrical mould. The resulting cast consists of a gradual mean particle size (and thus pore size) gradient along the radial axis, the smallest particles lining the inside surface of the tube. Slight sintering of the compact then provides the necessary reinforcement for handling, mainly keeping the open porosity structure intact without significant grain growth and shrinkage.

This investigation describes the process optimisation of centrifugally casted α-Al_2O_3 supports with specific regard to an increased pore size gradient. Since these substrates are exclusively intended for zeolite-ceramic composites, differently graded supports were coated with a highly reproducible zeolite NaA layer [3]. The influence of increased support permeability on total composite permeation flux could be related to the respective activation energies of pervaporation of a uniform H_2O/EtOH mixture.

Experimental

Two commercial α-Al_2O_3 powders, AKP-15 and AA1 (Sumitomo Chemical Co. Ltd, Japan), having mean particle sizes of 0.6 and 1.0 μm respectively, were used to prepare ~ 40 wt.% suspensions in water. These suspensions were extensively sonicated and electrosterically stabilised with ammonium polymethacrylate at pH 9.5. Single particle-sized compacts (0.6 μm), as well as different bimodal fraction distributions (0.6 and 1.0 μm), were centrifugally casted, dried and horizontally sintered to produce tubular supports ~ 60 mm in length, having an inner diameter of ~18 mm and wall thickness of ~ 1.5 mm. A factorial design was followed in order to investigate graded mixture fractions between 0.1 and 0.9 and sintering regimes between 1100 and 1420 °C for each ratio. Water fluxes were recorded for each support in a dead-end filtration mode at pressure differences between 0.2 and 1.0 MPa and permeabilities calculated accordingly. Pore size, porosity and density were measured by means of mercury intrusion (Autopore III, Micromeritics).

Zeolite NaA layers were prepared on the inside surface of selected supports by a batch hydrothermal synthesis procedure at 85 °C from clear solution of molar composition Na_2O:Al_2O_3:SiO_2:H_2O = 50:1:5:1000. Pervaporation fluxes for composite membranes were

measured from a 95 wt.% EtOH feed stream at increasing temperatures (35-65 °C) and activation energies of pervaporation calculated.

Results and Discussion

The median pore diameter of supports varied between 146 and 332 nm while porosity differed from 14-40 %. Water permeability values ranged between 2 and 170 $kg.m^{-2}.h^{-1}.bar^{-1}$. Table 1 presents an example of support properties for a full range of bimodal mixture ratios, all sintered at 1100 °C, while Fig. 1 illustrates the centrifugal segregation effects for a typically graded support.

Table 1: Bimodal mixtures of 0.6 and 1.0 μm α-Al_2O_3 powders

Fraction 0.61 μm powder	Median pore diameter (nm)	Average pore diameter (nm)	Porosity (%)
0.10	318	298	37.9
0.22	332	268	37.2
0.50	222	210	37.2
0.78	171	165	37.2
0.90	166	163	37.4

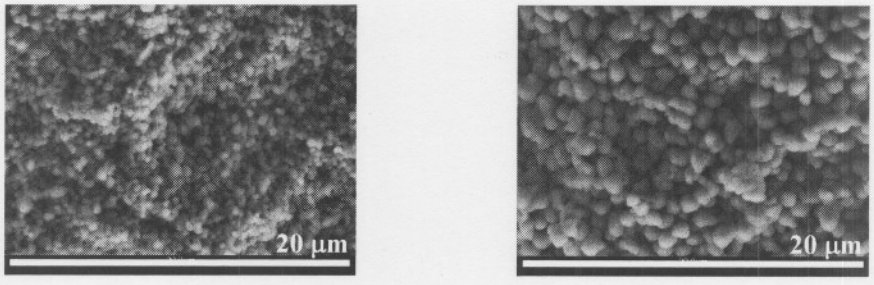

Figure 1: Differential settling leading to a pore gradient between inner (left) and outer (right) sections of a bimodally prepared cast (0.1 fraction 0.61 μm powder).

Although this 0.1 fraction 0.6 μm support exhibited the highest permeability regarding each sintering regimen, Table 2 demonstrates that surface roughness, in comparison to the monomodal 0.6 μm support, is influenced negatively and these irregularities are transferred to the zeolite composite, thus lowering the separation factor α. Total pervaporation fluxes were however increased substantially and calculation of respective activation energies suggested that these increases are mainly due to the lower support resistance, and not to zeolitic defects acquired at the compromised support surface.

Table 2: Pervaporation results for a single (0.61 μm) and bimodal (0.61 and 1 μm) support (T_{sinter} = 1200 °C) coated with the same zeolite A layer

Fraction 0.61 μm powder	Support H_2O permeability ($kg.m^{-2}.h^{-1}.bar^{-1}$)	α (H_2O/EtOH)	Pervaporation flux ($kg.m^{-2}.h^{-1}$)
1.0	45	8200	0.21
0.1	146	2000	0.45

Conclusion

Pervaporation fluxes through zeolite-ceramic composite membranes could be improved by increasing the support permeability. Bimodal grading of centifugally casted supports provided an effective means of achieving this.

References

[1] Nijmeijer, A., Huiskes, C., Sibelt, N.G.M., Kruidhof, H. & Verweij, H. (1998). Centrifugal casting of tubular membrane supports. *American Ceramic Society Bulletin*, 77, 95-98.

[2] Biesheuvel, P. M., Breedveld, V., Higler, A.P. & Verweij, H. (2001). Graded membrane supports produced by centrifugal casting of a slightly polydisperse suspension. *Chemical Engineering Science*, 56, 3517-3525.

[3] Zah, J., Krieg, H.M., Jansen, J.C., Keizer, K., Scholtz, J. & Mulder, H. (2003). The development of zeolite coated ceramic membranes. (Proceedings of the South African Chemical Engineering Congress, 3-5 September 2003, Sun City, South Africa)

ACKNOWLEDGEMENTS

At the end of a particularly long and challenging road I wish to extend my sincerest gratitude to my gracious Lord Jesus. It needs to be said that the final product of work given in this compilation is not the result of days of laborious effort, nights of meticulous planning or years of commitment and effort. No, it is merely a manifestation of the mercy of God in the lives of ordinary people like me. Thank you, Jesus, your grace is truly amazing.

I wish to thank the following people who have enriched both my work and my life:

- My parents, Paul and Christine, for carrying me through all these years, giving me the opportunities they never had, and shaping me into the man I am today;
- My brother Paul, for always supporting me, for taking me on fishing trips and making the tough times seem like just another day at the office;
- Anél, for loving me, for understanding me (which is a tremendously tough job!) and believing in my dreams - I love you dearly;
- Both my and Anél's families, for their prayers and support;
- My promoters, Profs. Krieg and Breytenbach, for continued support and motivation, keeping me on track and providing the means for achieving a good result;
- Prof. Koos Jansen, thank you for sharing such rich experience and expertise with a novice like me;
- Prof. Neomagus and Dr. Lachman, for advice and direction into the fields of chemical engineering and inorganic chemistry respectively;
- Hertzog, Andrew, Lynette, Yolandé and Anriëtte, for your generous assistance whenever I needed it;
- Drs. L. Tiedt, S. Verryn and C. Reinke, for expert inputs and technical contributions;
- Oom Jan, as well as the staff of the Instrumentation Department, Pieter, Hans and Johan, for the highly skilled crafting of the experimental set-ups;
- Prof. Bruinsma, the staff of Chemical Engineering and the SST, for financial support and creating external liaising opportunities;
- Profs. Bergh, Malan and the Department of Pharmaceutical Chemistry, for continued support.

The financial assistance of the Department of Labour (DoL) towards this research is hereby acknowledged. Opinions expressed and conclusions arrived at are those of the author and are not necessarily to be attributed to the DoL.